CONNECTION CAPACITY OF PULTRUDED GFRP CHANNELS IN MULTIDIRECTIONAL LOADING

by

MICHAEL C. WANG

B.S., University of Colorado Denver, 2008

A thesis submitted to the
Faculty of the Graduate School of the
University of Colorado in partial fulfillment
of the requirements for the degree of
Master of Science
Civil Engineering
2013

This thesis for the Master of Science degree by

Michael C. Wang

has been approved

for the Civil Engineering Program

by

Yail Jimmy Kim, Advisor

Kevin Rens, Chair

Frederick Rutz

July 12, 2013

Wang, Michael, C. (M.S., Civil Engineering)

Connection Capacity of Pultruded GFRP Channels in Multidirectional Loading

Thesis directed by Associate Professor Dr. Yail Jimmy Kim

ABSTRACT

Fiber Reinforced Polymer (FRP) composites is a relatively new material that offers unique advantages for many different engineering applications. While there has been plenty of research performed to understand composite fiber failure mechanisms numerically and experimentally, the exact nature of failure based on fiber orientation is unknown. Due to the complex nature of FRP composites, fiber failure mechanisms are not clearly understood and the goal of this study is to gain further knowledge regarding FRP failure, particularly with bolted connections.

The primary objective of this research is to investigate the behavior of bolted Glass Fiber Reinforced Polymer (GFRP) structural channel members subject to cyclic loading. The investigation consisted of testing various channel specimens with different flange geometric configurations. Monotonic loading is performed to determine ultimate strength of the connection in the axial and transverse directions for the first phase. The second phase comprises of how unidirectional cyclic loading effects stiffness and the overall ultimate strength of the connection in the axial and transverse direction. The last phase studies the behavior and the residual connection capacity of the GFRP specimens subject to multidirectional cyclic loading. Various load levels for cyclic loading were established as a fraction of the ultimate strengths obtained from testing.

The testing showed that the absence of the flange did not have a significant impact with respect to the ultimate strengths in the axial and transverse directions. Failure modes observed consisted of initial bearing failure followed by shear-out failure for axial specimens and net tension splitting for the transverse specimens. The GFRP channel specimens undergo a period of nonlinear progressive damage after initial failure. Furthermore, it was found that the residual behavior and strength was affected by unidirectional and multidirectional load cycles.

A probability-based design was adopted to provide design recommendations and guidelines. Resistance factors are determined using the Monte-Carlo simulation for the Load and Resistance Factor Design (LRFD) design method.

The form and content of this abstract are approved. I recommend its publication.

Approved: Jimmy Kim

ACKNOWLEDGMENTS

My sincere gratitude goes to my advisor Dr. Yail Jimmy Kim and co-advisor Dr. Rui Liu. It has been a pleasure to work with both and I thank them for their guidance, support, and time during the preparation of this thesis. They provided me with invaluable knowledge and expertise necessary for completion of the research project. Also I’d like to thank Dr. Kevin Rens and Dr. Frederick Rutz for participating on my thesis defense committee.

The material testing conducted in this research study would not have been possible without the support provided by the following staff and students: Tom Thuis, Jac Corless, Eric Losty, and Dennis Dunn. A special thanks to Shahlaa Alwakeel, for her guidance and assistance in the lab. Your hard work is greatly appreciated. Finally, the author gratefully acknowledges support from International Cooling Towers.

I would also like to express my appreciation to my fellow colleagues and mentors David Blanchette and Jerry Isler, both have been instrumental in the development of my professional and academic career.

Lastly, I would like to thank my friends and family for their support and encouragement along the way.

TABLE OF CONTENTS

Tables x

Figures xi

Chapter

1. Introduction 1

1.1 General 1

1.2 Objectives 2

1.3 Scope 3

1.4 Outline of Thesis 3

2. Literature Review 5

2.1 Introduction. 5

2.2 Overview. 5

2.3 Material Properties of FRP. 6

2.4 Fabrication of FRP Members 7

2.5 Bolted FRP Members 8

2.6 Fasteners 9

2.7 Failure Modes 9

2.7.1 Tension Failure 10

2.7.2 Shear Failure. 11

2.7.3 Bearing Failure 11

2.7.4 Cleavage and Pull-out Failure 12

2.8 Factors Affecting Joint Strength 12

2.8.1 Fiber Orientation 12

2.8.2 Lateral Contraint 13
2.8.3 Stacking Sequence 13
2.8.4 Joint Geometry 14
2.9 Static Behavior of Pultruded GFRP Beams. 14
2.9.1 Experimental Setup and Test Procedure. 15
2.9.2 Results and Conclusions. 15
2.10 Multi-Bolted Joints For GFRP Structural Members 16
2.10.1 Test Parameters 17
2.10.2 Test Setup and Instrumentation 17
2.10.3 Experimental Results 18
2.10.4 Conclusions 19
2.11 Finite Element Modeling of Damage Accumulation 19
2.11.1 Progressive Damage Model 20
2.11.2 Finite Element Modeling 23
2.11.3 Results and Discussions 24

3. Experimental Program 39
3.1 Introduction 39
3.2 Materials used for Test Specimens 39
3.2.1 GFRP Channels 39
3.2.2 GFRP Flat Plates 40
3.3 Experimental Setup and Loading 41
3.3.1 Phase I and Phase II Setup for Axial Tests 41
3.3.2 Phase I and Phase II Setup for Transverse Tests 42
3.3.3 Phase III Testing Procedure 42

4. Finite Element Modeling 48
4.1 Introduction 48
4.2 Modeling and Elements 48
4.3 Failure Criteria 49
4.4 Model Results 50

5. Test Results and Discussion 54
5.1 Introduction 54
5.2 Phase I Testing Results of GFRP Channels 55
5.2.1 Phase I Failure Modes of GFRP Channels. 56
5.2.2 Phase I Testing Results of GFRP Thickened Plates. 57
5.2.3 Phase I Failure Modes of GFRP Thickened Plates. 57
5.3 Phase II Testing Results of GFRP Channels 58
5.3.1 Phase II Failure Modes of GFRP Channels 59
5.4 Phase III Testing Results of GFRP Channels 60
5.4.1 Phase III Failure Modes of GFRP Channels 62
5.5 Comparisons of Phases. 63
5.5.1 Comparison Among Different Flange Geometries in Phase I. 63
5.5.2 Comparison of Post-Cyclic Residual Behavior. 63
5.5.3 Effect of Cyclic Loading on Residual Capacity 64
5.6 Design Recommendations. 64
5.6.1 Monte-Carlo Simulation. 64
5.6.2 Calibration of Resistance Factor. 65

6. Summary and Conclusions. 82

6.1 Summary. 82

6.2 Conclusions. 82

6.3 Recommendations for Future Work 85

Appendix

A Load Displacement Curves for Phase I – Axial and Transverse..........................86

B Load Displacement Curves for Phase II – Residual Capacity 98

C Load Displacement Curves for Phase III – Residual Capacity 101

D Phase I Testing Failure Photos – Axial and Transverse....................................103

E Phase II Testing Photos – Damage From Cyclic Loading 113

F Phase III Testing Photos – Damage From Multi Directional Cyclic Loading 116

G Phase III Testing Failure Photos 118

References...119

LIST OF TABLES

Table

2.1 Comparison of Flexural Rigidity. 26
2.2 Comparison of Shear Rigidity. 26
2.3 Geometrical Data for the Investigated Geometry. 27
2.4 Elastic Properties of HTA/6376 Material. 27
4.1 Material Properties for GFRP Channel Specimens (Extren). 51
4.2 Failure Criteria Strength Values. 51
5.1 Phase I Ultimate Failure Load of GFRP Channel Specimens. 67
5.2 Phase I Ultimate Failure Load of GFRP Thickened Members. 67
5.3 Phase II Residual Connection Capacity of Members Subject to Cyclic Loading.... 68
5.4 Phase III Residual Connection Capacity of Members Subject to Cyclic Loading... 68
5.5 Resistance Factor Calibration. 69

LIST OF FIGURES

Figure

2.1 FRP Pultrusion Process. 28

2.2 Modes of Failure for Bolted Joints in FRP Composities. 28

2.3 Stress Concentration Relief in Fibrous Composites by Delamination 29

2.4 Relation Between Stress Concentration Factors. 29

2.5 Terminology. 30

2.6 Influence of CFRP Fiber Proportion. 30

2.7 Effect of Bolt Torque on Bearing Strength. 31

2.8 Comparison between Bearing Strength with and without Clamping Pressure. 31

2.9 Effect of Grouped 0° Plies on Bearing Strength. 32

2.10 Effects of Stacking Sequence on Bearing Strength for GFRP Laminates. 32

2.11 Variation of Net Tensile Strength with Width of 0°/±45°. 33

2.12 Cross Sections of Test Specimens. 33

2.13 Connection Configuration. 34

2.14 Flowchart of Progressive Damage Model 35

2.15 Geometry of Bolted Single-Lap Joint. 36

2.16 Finite Element Model of Bolted Joint. 36

2.17 Mesh Around Hole and Finite Element Model of Bolt 37

2.18 Comparison of Strains 37

2.19 Illustration of Damage Propagation in Upper Surface of Laminate. 38

2.20 Illustration of Damage Propagation in Lower Surface of Laminate. 38

3.1 Condition #1 43

3.2 Condition #2 43

3.3 Condition #3 44

3.4 Tension Test. 44

3.5 Shear Test 45

3.6 Geometry of Thickened Flat Plate. 45

3.7 Axial Test Setup. 46

3.8 Transverse Test Setup. 46

3.9 Thickened Flat Plate Test Setup. 47

3.10 Thickened Flate Plate Test Setup. 47

4.1 Channel Geometry of ANSYS Model. 52

4.2 Applied Loading of Model 52

4.3 Displacement from 25% of Ultimate Load. 53

4.4 Tsai-Wu Strength Index – 25% of Ultimate Load. 53

5.1 Load-Displacement Curve for Phase I Axial. 70

5.2 Load-Displacement Curve for Phase I Transverse. 70

5.3 Load-Displacement Curve for Phase I Thickened Member Axial 71

5.4 Typical Failure Mode: Monotonic Axial Load. 71

5.5 Typical Failure Mode: Monotonic Transverse Load. 72

5.6 Failure Mode: (a) Monotonic Axial Load; (b) Monotonic Transverse Load 72

5.7 Typical Failure Mode of GFRP Thickened Plate from Axial Loading. 73

5.8 Debonding of GFRP Thickened Plate 73

5.9 Cyclic Unidirectional Load for Phase II Specimens. 74

5.10 Load-Displacement Curve for Phase II Monotonic Axial Loading. 74

5.11 Load-Displacement Curve for Phase II Monotonic Transverse Loading. 75

5.12 Damage Propagation with Load Cycles. 75

5.13 Geometry of GFRP Channel Specimens for Phase III. 76

5.14 Cyclic Multidirectional Load for Phase II Specimens. 76

5.15 Load-Displacement Curve for Phase III Monotonic Axial Loading. 77

5.16 Load-Displacement Curve for Phase III Monotonic Transverse Loading. 77

5.17 Damage Propagation with Load Cycles. 78

5.18 Typical Failure Mode: Monotonic Axial Load for Phase III. 78

5.19 Typical Failure Mode: Monotonic Transverse Load for Phase III. 79

5.20 Failure Mode: Monotonic Transverse Load for Phase III. 79

5.21 Load-displacement of Phase I-Comparison of Various Flange Geometry. 80

5.22 Comparison of Post-Cyclic Residual Behavior. 80

5.23 Effect of Cyclic Loading on Residual Capacity. 81

5.24 Comparison of Strength Reduction Factor (Φ) Based on Phase I. 81

1. Introduction

1.1 General

High cost from repair and maintenance of steel structures damaged from corrosion lead engineers and researchers to search for alternative materials. Fiber Reinforced Polymer (FRP) composites is a relatively new material that offers unique advantages for many different engineering applications. A composite material is formed by the combination of two or more distinct materials to produce a new material with enhanced properties. FRP utilizes a polymer resin matrix that is typically reinforced with glass, carbon, basalt or aramid fibers. The advantages of using FRP are the excellent strength-to-weight ratio and stiffness-to-weight ratio which makes them highly desirable as a building material for structural systems. The composite material has proven to be economical and efficient for new construction and repair and rehabilitation of damaged or deteriorating structures in civil engineering. In addition, they provide favorable corrosion and weathering resistance.

The application of FRP composites in structural engineering involves strengthening of beams, columns, and slabs in existing structures. They can be used for repairing structural members that have been damaged from loading conditions. For example, FRP can be applied to provide flexural and shear strengthening of a damaged beam or column. The strengthening will improve the stiffness and deflection capacity of the member. If flexural strengthening is desired FRP sheets or plates are applied to the bottom or tension face of the beam. When FRP is applied to the web or sides of the beam the shear strength is improved.

FRP composites can also be molded into different structural shapes and is used as an alternative to steel and aluminum due to its benefits. Today manufacturers can produces a variety of structural members including channels, angles, wide flange beams, tubes, and flat-sheets similar to structural steel shapes.

While there has been plenty of research performed to understand composite fiber failure mechanisms numerically and experimentally, the exact nature of failure based on fiber orientation is unknown. Due to the complex nature of FRP composites, fiber failure mechanisms are not clearly understood and the goal of this study is to gain further knowledge regarding FRP failure, particularly with bolted connections. Glass fibers are commonly used for reinforced composites. Glass fiber reinforced polymers (GFRP) channel members with bolted connections will be tested and researched in this study.

1.2 Objectives

The objective of this research is to evaluate GFRP channel members subject to cyclic axial and transverse loading. The components involved in the investigation include the following:

1. Review of previous research and testing conducted on GFRP structural members.
2. Examine the ultimate connection load capacity of the GFRP specimens in the axial and transverse directions.
3. Observe various failure modes based on different loading and geometry conditions.

4. Evaluate the impact of unidirectional and multidirectional loading and unloading cycles and determine the effect it has on the residual strength capacity of the connection. Observe the change in stiffness at various load levels.
5. Develop a finite element model to predict the load-deflection behavior and local stress characteristics of the specimens.
6. Summarize results to provide design recommendations.

1.3 Scope

The scope of the research consists of an experimental program followed by a finite element model to study the behavior of GFRP channel members with bolted connections subject to unidirectional and multidirectional cyclic axial and transverse loading. Testing was performed to determine ultimate strengths and to apply load cycles at different levels. The experimental investigation studies the local deterioration around the bolt holes influenced by high stress concentrations and the reduction of ultimate strength and stiffness caused by repeated loads. A finite element model was developed to validate and predict the deflection response and stress concentrations. The model accounts for change in material properties due to cyclic loading.

1.4 Outline of Thesis

The contents of this thesis include the following:

Chapter 2: presents a review of literature related to previous research conducted on GFRP structural members.

Chapter 3: provides a detailed description of the experimental program, fabrication of test specimens, instrumentation, test setup and procedures. In addition, all ancillary tests required for necessary material properties are discussed.

Chapter 4: provides a detailed description of the finite element model developed to validate and predict the displacement and stress response to cyclic loading of GFRP test specimens.

Chapter 5: discusses the experimental program results, which includes the strength and stiffness degradation due to cyclic loading, various failure modes from different geometric and loading conditions, and results of all ancillary material tests performed. Design recommendations are provided using the results obtained.

Chapter 6: presents the summary and conclusion of the research along with recommendations for further research on GFRP members.

2. Literature Review

2.1 Introduction

The literature presented in this chapter will investigate past research and tests performed on FRP members. The focus of this section will be failure behavior and mechanism from bolted connections and how they are affected by fiber orientation.

This section will discuss the literature available on the subject of GFRP structural members. It is evident based on the study of current literature available that there is a lack of information about how to thoroughly characterize pultruded GFRP members. Currently there is no design standard for FRP.

2.2 Overview

In recent years there has been significant growth of FRP, there usage has spread from aerospace and automotive industry to civil structures. When compared with traditional materials the significant advantages are the resistance to corrosion, lightweight, high strength, and ease of installation. However, negative aspects of FRP would include the high initial cost, durability problems caused by freeze-thaw cycles, moisture, or sustained loading, and the lack of design standards and experience. Their strength and stiffness properties are dependent on the type, quantity, and orientation of the fibers within the member.

2.3 Material Properties of FRP

Material properties of FRP are complex due to the orthotropic nature of the composite material and a clear explanation can be quite difficult. Unlike the American Concrete Institute (ACI) for reinforced concrete design and the American Institute of Steel Construction (AISC) for structural steel design, FRP pultruded structural shapes currently do not have a design code, although two design guides are available for engineers: Structural Plastics Design Manual and Eurocomp Design Code and Handbook (ASCE 1984 and Eurocomp 1996). To complicate matters further, there are many FRP manufacturers in the industry who provide different material properties for their products. Depending on the fiber orientation within the polymer matrix FRP can exhibit different material properties. Other important factors that influence the behavior of FRP materials include the type of fiber and polymer used in the composite (Tibbetts 2008). Common reinforcement fibers used include glass, carbon, aramid, and boron fibers. The unique anisotropic behavior requires special considerations in the manufacturing process and design of FRP materials.

FRP composites pose a high resistance to corrosion regardless of the materials used for the fiber and polymers. However, the durability can be reduced when exposed to harsh environmental conditions which should be avoided for adequate performance, ranging from high temperatures, ultraviolet exposure, and water with high alkalinity levels. The resistance to environmental effects is greatly dependent on the fabrication process along with the material properties of the fibers (Benmokrane et al 2002).

In comparison to steel, FRP structural members have anisotropic properties, low stiffness, and high elastic to shear modulus ratios. From previous experience and tests composite materials must be carefully analyzed due brittle failure modes. FRP differ from metals as typically there is no yielding, strain hardening or elongation prior to failure (Deng 2004). Generally GFPR members have a linear stress-strain relationship to failure. Certain types of GFRP can exceed the strength of conventional steel. A study preformed reported the ultimate strength of GFRP bars at 150 ksi (1,035 MPa) (Pleimann 1987). However, the modulus of elasticity when compared to steel is significantly smaller at approximately 25% of steel which places limitation for the use of GFRP as the main load-carrying element in many types of structures. Graphite reinforcing fibers can be used to increase the modulus of elasticity by up to three times (Saadatmanesh and Ehsani 1991). According to ACI (2006), the tensile strength of GFRP bars can up to twice as large as the tensile strength of steel bars and is even higher for carbon and aramid FRP.

2.4 Fabrication of FRP Members

Fabrication of FRP composites can be completed by the method of pultrusion or by hand layup (Tibbetts 2008). This research uses FRP products that were manufactured through the process of pultrusion. For fabrication by pultrusion, FRP members are formed into different standard structural shapes by an automated process. The manufacturing process produces continuous lengths of various shapes and materials by combining fibers with a polymer resin matrix under heat and pressure and pulled through using a heated steel forming die. Fibers typically used are glass and carbon, although other fibers such as aramid or polyethylene can be used for structural applications (Bank 2006). The basic manufacturing process concept is described in Figure 2.1.

2.5 Bolted FRP Members

Plenty of research has been performed studying the behavior of FRP in the aerospace and automotive engineering industries; however there has been a lack of research conducted for structural engineering applications for FRP materials particularly in the field of bolted connections (Hassan et al. 1994). Similar to steel, FRP structural members utilize bolted connections and although mechanically fastened, FRP joints share the same failure modes as metals. It has been determined that the damage mechanism and propagation is not quite the same. Therefore, the design criteria for steel are not applicable to FRP members (Duthinh 2000). It is important to understand the behavior or FRP members with bolted connections because the strength of the structural member is limited by the strength of the connection.

FRP structural members can be significantly weakened by the presence of bolt holes or cut outs. The strength reduction is attributed to high stress concentrations around discontinuities, damage to the reinforcing fibers and because FRP composites do not yield. The stress concentration value around a hole for isotropic materials is 3 while a uni-directionally FRP sheet can have a value as large as 8 (Collings 1987). Generally isotropic materials exhibit plasticity that relieve high stress concentrations resulting in a small effect on the net failure stress. However, for uni-directional FRP due to the lack of plasticity the material is elastic to failure where the stress concentrations reduce the net failure stress.

2.6 Fasteners

Mechanical fasteners have proven to be an effective method for connecting FRP members. Different types of steel fasteners can be used for connection joints such as nuts, bolts, threaded rods, rivets and self-tapping screws. Self-tapping screws are favorable when it is not possible to access the reverse side of the joint. The use of rivets are appropriate for joining laminates up to 0.1 in (3 mm) thick. However, the installation operation of rivets can potentially damage the laminates due to uncontrollable clamping pressure. In addition to steel fasteners FRP mechanical fasteners are also available which include nut, bolts, threaded rods, and screws. These fasteners present disadvantages when compared to steel due to the high cost and are susceptible to shear failure at low loads. Although there are various options for fasteners Collins (1977) determined that bolted joints were the most efficient and effective method for FRP materials.

2.7 Failure Modes

FRP have similar failure modes to steel member connections by failing in shear, tension, or bearing. The connector can also fracture and pull through the laminates. In addition, FRP can also fail by delamination between layers, debonding, and crack propagation. The different types of failure modes for bolted joints in FRP composites are presented in Figure 2.2. The best performance for shear, tension, and bearing failure is obtained utilizing 0°/±45° fiber orientations.

2.7.1 Tension Failure

When members are subject to a tensile load the average net stress σ_n across a section is:

$$\sigma_n = \frac{P}{(w - nd)t}$$

(2-1)

Where P is the tensile load at the joint having a width w and thickness t. The number of bolts within the section is n having a diameter d. Generally, stress concentration at the hole will initiate failure because FRP does not yield to alleviate high stress concentrations. However, a study by Hart-Smith (1980) showed that slippage between the resin and fibers near bolt holes and cut-outs provide some relief of high stress concentrations (Figure 2.3 and Figure 2.4). When the fibers experience high local stress they pull out of the resin resulting in delamination or debonding of the fibers. Hart-Smith (1980) concluded that around holes improving adhesion between the fibers and resin results in a reduction of joint strength. However, reinforcing fibers near the hole in various directions diminishes the degree of anisotropy allowing minor plastic behavior and softening.

Fiber orientation of the FRP dictates the tensile strength of the composite. The majority of the load is carried by the fibers parallel to the load. Potter (1978) determined that the failure near holes in CFRP occurred at the edge of the hole perpendicular to the loading axis. For GFRP the failure is more complicated and is influenced by both shear and tension. Failure around the hole is initiated by in-plane shearing across the width of the laminate. The shear results in only the 45° plies taking the axial load leading to tension failure immediately after (Godwin et al. 1982).

2.7.2 Shear Failure

The shear stress τ in a FRP joint is calculated by the following equation:

$$\tau = \frac{P}{2et} \tag{2-2}$$

Where *P* is the applied load with thickness *t* and a distance from the bolt hole center to the ends of the connected plates is *e*. See Figure 2.5 for a diagram of the terminology used. It is noted that the shear stress is determined using the same procedure as for isotropic materials. Similar to tensile loading the shear strength around the hole is dependent on the fiber orientation of the member. The in-plane shear strength is significantly lower with 0° fibers when compared with joints that have 45° fibers.

2.7.3 Bearing Failure

The average bearing stress at the cross section of the hole can be calculated by:

$$\sigma = \frac{P}{ndt} \tag{2-3}$$

Where *P* is the load applied, *n* is the number of bolts with diameter *d* and with a material thickness of *t*. Bearing stress is caused by compression of half the bolt hole transferred by the bolt. The compressive strength within the fibers and the clamping pressure are the main parameters that will dictate the bearing strength around the hole (Collins et al.

1977). In a study by Collins (1987) he showed that the shear failure initiated at the hole edge through the fibers and matrix. FRP laminates with a combination of 45° and 90° plies performed well under bolt bearing loads. This discovery contradicted the compressive performance of laminates with 45° and 90° fiber orientations which indicates the failure mechanisms for bearing and compressive loadings are different. The difference can be attributed to the clamping pressure generated by the bolt. The fibers perpendicular to the load and laminates are constrained and fail in constrained transverse compression.

2.7.4 Cleavage and Pull-out Failure

In addition to shear, tension, and bearing failure FRP joints can exhibit cleavage and pull-out failure. Cleavage failure develops only during 0° fiber orientation in a single shear mode and is followed by net section failure occurring on one side of the laminate. Reinforcement should be placed around the bolt holes to prevent cleavage failure. Pull-out failure is initiated by out of plane bending at the joint caused from in plane axial loads which results in peeling at the joint. Typically, they occur with the use of rivets in single shear. Bending or shear failure of the bolt is also possible under extreme loading conditions (Duthinh 2000).

2.8 Factors Affecting Joint Strength

2.8.1 Fiber Orientation

The biggest factor affecting the joint strength of FRP is the fiber orientation. In a study by Collins (1977), concluded that optimum joint performance for CFRP is achieved using a combination of 0° / ±45° plies. It can be seen from Figure 2.6 that shear failure occurs with low levels of ±45° fibers. The shear strength of the joint increases as the ±45° fibers increase in the section, eventually bearing becomes the critical mode of failure. As a result of ±45° fibers being weak in tension, high amounts of ±45° will shift the failure mode to tension.

2.8.2 Lateral Constraint

Lateral constraint caused by clamping pressure from the bolts can significantly affect the joint strength. However, excessive pressure from over-tightening of the bolts can damage the surface of the laminate. The recommended optimum bolt clamping pressure was determined to be 3,190 psi (22 MPa) for CFRP joints (Garbo and Ogonowski 1981). Overtime clamping pressure is decreased by resin creep but does not necessarily reduce the joint strength (Shivakumar and Crews 1982). See Figure 2.7 – Figure 2.8 for the effect that clamping pressure has on the bearing strength of FRP laminates.

2.8.3 Stacking Sequence

In a study performed by Collins (1977) it was shown that there was no change in shear strength for bolted CFRP joints that consisted of 2/3 0° and 1/3 ±45° plies, however there was a difference of 6% in tensile strength when compared with two different stacking sequences. The bearing strength had a substantial drop with laminates grouped together. The highest bearing strength for pin-loaded holes was achieved by using 90°/±45°/0° laminates whereas using 0°/90°/±45° reduced the strength by 30% (Quinn and Mathews

1977). See Figure 2.9 and Figure 2.10 for the effect that the stacking sequence has on the bearing strength of GFRP laminates.

2.8.4 Joint Geometry

The tensile failure stress of FRP members with a hole heavily depend on the width due to no stress relief from lack of plasticity. The width has a significant impact on the strength when the laminates consists of mostly 0° fibers and an opposite effect on 45° fibers. This can be seen in Figure 2.11. Collins (1977) determined that the hole size didn't have a significant impact on the net tensile and shear strength with fiber orientation consisting of 0° / ±45° for CFRP. The same could be said for GFRP laminates (Kretsis and Matthews 1985). The bearing strength of CFRP is not affected by hole size as long as there is sufficient clamping pressure provided by the bolt. On the other hand, because GFRP has low elastic modulus of glass, out-of-plane cracking can occur regardless of clamping pressure for $d/t > 3$. Values of $d/t < 3$ is not recommended due to the possibility of bolt shear failure. It is desirable that the joint geometry selected experiences tension and shear failure simultaneously near the bearing failure stress.

2.9 Static Behavior of Pultruded GFRP Beams (Nagaraj and GangaRao 1997)

A study was performed by Nagaraj and GangaRao (1997) to investigate the experimental and theoretical characterizations of mechanical properties of pultruded GFRP structural members. A total of 187 test were conducted using wide flange and box beams to examine the effects of shear influence, shear lag, warping, and manufacturing quality.

2.9.1 Experimental Setup and Test Procedure

The testing consisted of two different structural shapes with different sizes. The sizes were 102 x 102 x 6 mm (4 x 4 x ¼ in.) for the box section and the wide flange section was 102 x 102 x 6 mm (4 x 4 x ¼ in.) and 152 x 152 x 6 mm (6 x 6 x ¼ in.). See Figure 2.12 for the cross section dimensions of the test specimens. The members were made up with a vinylester matrix reinforced with E-glass fibers. The specimens were testing using a span length of 1,828 mm (72 in.) with simply supported boundary conditions under three-point and four-point bending. Linear variable differential transducers (LVDTs) were used to measure the deflection under the load points at midspan. Electrical resistance strain gauges were placed at a distance of 203 – 305 mm (8 – 12 in.) away from the load point to overcome stress concentration effects. The strain gauges were installed on both the compression and tension face at equal distance from the midspan.

2.9.2 Results and Conclusions

The experimental results were compared using theoretical computations of simplified equations based on classical lamination theory (CLT) (Jones 1975) along with three-dimensional finite-element analysis using ANSYS 1994. Both the flexural and shear rigidities were determined based on the approximate CLT. The finite-element model utilized SHELL 91 elements which had the ability to model the composite material layer by layer and specify the material properties and fiber orientation. The finite-element results compared well with the theoretical calculations and experimental results and were within 0-4%. The comparisons are displayed in Table 2.1 and 2.2.

It was determined that the shear influence on deflection measurements for both three-point and four-point bending was significant. The testing resulted in a shear influence of 36% for three-point bending test and 25% for the four-point bending test. Using 45° layers reduced the shear influence by 9% compared to the specimen with unidirectional fibers in the web. The variation in strain readings was 10-20% and was attributed to interfacial slip between the top layer and the layer beneath it. In addition, variation in strain reading also existed due to asymmetric fiber distribution located in the top and bottom flange laminates. Nagaraj and GangaRao (1997) concluded that the approximate theoretical expressions provided by Jones (1975) could be used to determine the flexural and shear rigidities in a pultruded GFRP beam.

2.10 Multi-Bolted Joints for GFRP Structural Members (Hassan et al. 1997)

An experimental investigation performed by Hassan et al. (1997) at the University of Manitoba studied the behavior of multi-bolted connections using glass fiber-reinforced plastic materials. The study consisted of testing a total of 105 multi-bolted double lap shear connections with various parameters that included the width of the structural member, edge distance, number of bolts, bolt pattern, pitch, thickness of the member, and direction of the fibers with respect to the applied load direction.

The orthotropic composite material used for the tests were EXTREN Flat Sheet Series 500, pultruded glass fiber sheet with alternating stacked layers of E-glass rovings and E-glass continuous strand mat.

2.10.1 Test Parameters

The influence of the placement and number of bolts was investigated by using 5 members with different connection configurations and were designated as Joints A, B, C, D, and E, see Figure 2.13. Various ratios of edge distance to hole diameter (e/d) and side distance to the pitch (s/p) were selected to obtain different failure modes with each bolt patterns. The 105 total specimens tested were 12.7 mm (1/2 in.) thick and had principal unidirectional fibers layers orientated at 0°, 45°, and 90° with respect to the applied load. High-strength structural bolts with a diameter of 19 mm (3/4 in.) and a bolt hole diameter of 20.6 mm (13/16 in.) providing adequate clearance was used for all connections. The bolts were tightened to a constant torque of 32.5 N·m (24 ft·lb).

2.10.2 Test Setup and Instrumentation

The specimens were tested using a 1,000 kN (220,000 lb) MTS closed-loop servo-controlled loading system. The members were loaded axially in tension at a constant stroke rate of 0.001 mm/s (0.0254 in./s). Concentric loading was achieved by a using double-shear configuration thus removing any bending effects. The relative displacements were measured using a linearly variable differential transducer (LVDT) and strain gauges were used to determine the stress distribution in the member along with load distribution of each bolt.

2.10.3 Experimental Results

The results indicated that the ultimate load was within 10% of the identical specimens tested and the main factors effecting strength were the width, edge distance, and fiber orientation with respect to the applied load. Similarly, these factors have a significant effect on the failure mode of the specimens. It was determined that connection type B and D which had smaller edge distances of 38.1 mm (1.5 in.) resulted in cleavage failure and was characterized by crack propagation parallel to the applied load. For connection type E with the same edge distance the section experienced net tension failure located at the inner bolt row without any crack propagation between bolt rows. For the specimens with larger edge distances ranging from 63.5 mm to 152.4 mm (2.5 in. to 6 in.) the resulting failure mode was net tension failure located at the inner row of bolts, which had the highest stress concentrations measured. All connections and tests showed bearing damage after failure around the area adjacent to the loaded section of the hole.

When studying the load distribution among the bolts it was determined the specimens with only one row of bolts (type B and type D) generally experienced equal distribution of the load. However, this was not the case for connection type A, C, and E which had unequal forces at each bolt.

Typically, for mechanically fastened joints with in-plane loading, bearing failure is likely to occur as the width to diameter ratio (w/d) increases. This was not the case for this experimental investigation using composite fiber members as bearing failure did not occur; only localized bearing damage was apparent. Large widths reduced the ultimate net tensile capacity and were relatively low when compared to specimens with smaller widths; this can be attributed to the high stress concentrations for specimens with larger widths. It is concluded that the load of a bolted joint is resisted by the material around the vicinity of the bolt hole and increasing the width of the specimen has no benefits in terms of strength efficiency.

2.10.4 Conclusions

After the experimental investigation performed by Hassan et al. (1997) the following concluding remarks can be made. All connections and specimens tested experienced linear behavior up to failure. The connections with only one row of bolts had equal load distribution whereas, connections with more than one row experienced unequal load distribution. The edge distance to diameter ratio, *e/d*, has a significant impact on the failure mode for connections with either one row or one column of bolts. For small edge distances with *e/d* ratios less than 3 cleavage failure occurred. Large edge distances with *e/d* ratios larger than 3 experienced tension failure. All connections tested with 0°, 45°, and 90° fiber orientation had higher bearing strengths as the *e/d* ratio increased up to a ratio of 5. The ultimate capacities and bearing strengths for all connection types increased as the side distance to pitch *s/p* ratio increased up to a value of 1.2. Having a higher number of bolts is not directly proportional to the increase in ultimate strength capacity in the member.

2.11 Finite Element Modeling of Damage Accumulation (Kermanidis et al. 2000)

A study was performed by Kermanidis et al. (2000) to model the effects of damage accumulation using ANSYS, a finite element analysis program. A three-dimensional model was developed to simulate the progressive damage and predict residual strength and stiffness in single-lap bolted composite joints under in-plane tensile loading.

2.11.1 Progressive Damage Model

The progressive damage model involves an iterative procedure to determine stress analysis, failure analysis, and material degradation. ANSYS has the ability to calculate the stresses between each ply to be used as the model progresses. Due to the complex nature of failure mechanisms in bolted composite laminates, many previous empirical methods are used as failure criteria. The following seven expressions (Shokrieh et al. 1996) below represent stress-based criteria to predict different failure modes. The modes of failure consist of matrix tensile and compressive failure, fiber tensile and compressive failure, fiber-matrix shear-out and delamination of fibers in tension and compression.

Matrix tensile failure for ($\sigma_y > 0$):

$$\left(\frac{\sigma_y}{Y_T}\right)^2 + \left(\frac{\sigma_{xy}}{S_{xy}}\right)^2 + \left(\frac{\sigma_{yz}}{S_{yz}}\right)^2 \geq 1 \tag{2-4}$$

Matrix compressive failure for ($\sigma_y < 0$):

$$\left(\frac{\sigma_y}{Y_C}\right)^2 + \left(\frac{\sigma_{xy}}{S_{xy}}\right)^2 + \left(\frac{\sigma_{yz}}{S_{yz}}\right)^2 \geq 1 \tag{2-5}$$

Fiber tensile failure for ($\sigma_x > 0$):

$$\left(\frac{\sigma_x}{X_T}\right)^2 + \left(\frac{\sigma_{xy}}{S_{xy}}\right)^2 + \left(\frac{\sigma_{xz}}{S_{xz}}\right)^2 \geq 1 \tag{2-6}$$

Fiber compressive failure ($\sigma_x < 0$):

$$\left(\frac{\sigma_x}{X_C}\right)^2 \geq 1 \tag{2-7}$$

Fiber-matrix shear-out for ($\sigma_x < 0$):

$$\left(\frac{\sigma_x}{X_T}\right)^2 + \left(\frac{\sigma_{xy}}{S_{xy}}\right)^2 + \left(\frac{\sigma_{xz}}{S_{xz}}\right)^2 \geq 1 \tag{2-8}$$

Delamination in tension for ($\sigma_z > 0$):

$$\left(\frac{\sigma_Z}{Z_T}\right)^2 + \left(\frac{\sigma_{xz}}{S_{xz}}\right)^2 + \left(\frac{\sigma_{yz}}{S_{yz}}\right)^2 \geq 1 \tag{2-9}$$

Delamination in compression for ($\sigma_z < 0$):

$$\left(\frac{\sigma_Z}{Z_C}\right)^2 + \left(\frac{\sigma_{xz}}{S_{xz}}\right)^2 + \left(\frac{\sigma_{yz}}{S_{yz}}\right)^2 \geq 1 \tag{2-10}$$

Where σ_{ij} are the layer-stress components in the *ij* direction and the denominators are the strengths in the corresponding directions.

Once ply failure occurs, the material properties are disabled from carrying a specific load, this is known as the degradation rule. Therefore, each failure mode has its own corresponding degradation rule. The ply-by-ply degradation rules are based on assumptions and empirical methods from constraints in the composite material properties. The material property degradation rules for failure analysis in this study were taken from Shokrieh et al. (1996) and were believed by Kermanidis et al. (2000) to be best suited for the failure criteria used.

When matrix tensile and compressive failure is observed in a ply, the assumption is that the matrix cannot sustain any load. Therefore, the material properties of the failed ply are reduced to:

$$E_y = \upsilon_{xy} = 0$$

(2-11)

When fiber tensile and compressive failure is observed in a ply, the assumption is that the material cannot sustain any load in the vicinity where the failure has occurred. Therefore, the material properties of the failed play are reduced to:

$$E_x = E_y = E_z = G_{xy} = G_{yz} = G_{xz} = \upsilon_{xy} = \upsilon_{yz} = \upsilon_{xz} = 0$$

(2-12)

When fiber-matrix shear-out failure is observed in a ply, the assumption is that the material can only sustain load in the fiber and transverse to fiber directions. The material does not have the ability to carry shear load, therefore, the material properties of the failed ply are reduced to:

$$G_{xy} = \upsilon_{xy} = 0$$

(2-13)

Delamination failure in tension and compression affect the properties in the z-direction in the delaminated region. This results in the material losing the ability to sustain any load in the z-direction in addition to shear loads. Therefore, the material properties of the failed ply are reduced to:

$$E_z = G_{yz} = G_{xz} = \upsilon_{yz} = \upsilon_{xz} = 0$$

(2-14)

A progressive model is developed in ANSYS using a programmed macro-routine iterative process. The macro-routine is described in the flowchart Figure 2.14 and involves the following steps.

1. Developing a FEM model of the composite joint with initial material properties, specimen geometry, boundary conditions, initial load and load step.

2. Determine the stresses for each ply by performing a non-linear analysis.
3. Perform a failure analysis by implementing the failure criteria.
4. Determine if ply failure exist. If no failure is calculated the applied load is increased. If any failure mode is recognized the program continues to the next step.
5. Apply appropriate material property degradation rules on the failed ply.
6. Determine if final failure is reached. If so, the program is completed. If final failure has not been reached the program returns to step 2 and the analysis is performed again with the same load to compute the redistributed stresses. Final failure is reached when the program converges. Convergence is assumed when no additional failures are detected.
7. Repeat procedure until final failure occurs.

2.11.2 Finite Element Modeling

The study consisted of developing a finite element model of the bolted single-lap joint using ANSYS. The geometry of the member is depicted in Figure 2.15. The model consists of a composite laminate upper plate with fibrous unidirectional layers (0°/90°/±45°) and an aluminum lower plate connected with a bolt. The model utilizes 8-noded SOLID46 3-D ANSYS layered elements with three displacement DOF's per node. The solid element used for the composite material is defined by the orthotropic material properties, the fiber orientation, and layer thickness. For the interaction between two surfaces, 3-D CONTAC49 ANSYS elements were used to model the contact between two plates, between the bolt and the surface of the hole, and between the bolt head and the plate. See Figure 2.16 and Figure 2.17 for the finite element model. The loading conditions for the models consisted of in-plane tensile loading at the ends as well as a pre-tension load at the fastener by applying thermal expansion properties in the axial direction of the bolt. To prevent secondary bending the model was supported laterally in the z-direction.

2.11.3 Results and Discussion

The strains were measured experimentally with an 8 kN (1,798 lbs) tensile load applied to the lap joint. The strains were determined for the global x-direction at the angles of 0, 22.4 and 45° and are displayed in Figure 2.18. Comparisons were made to experimental and numerical values from a study performed by Ireman (1998). The experimental program consisted of installing strain gauges around the hole at angles of 0, 22.4 and 45° to measure the response. The comparison of the numerical to experimental model resulted in sufficient accuracy. The material properties and strengths used for the composite material are shown in Table 2.3 and Table 2.4.

The progressive damage model was subjected to incrementally increasing tensile loading in which the first failure (matrix compressive failure) occurring at a load of 3 kN (674 lbs) near the stress concentrations around the hole. Before the first ply failure the composite material behaved elastically. The damage occurs at an angle of 45° with respect to loading and continues to prorogate due to the pressure from the bolt. Figure 2.19 and Figure 2.20 illustrates the progressive damage at different load steps predicted by the model. The shaded elements in the model represent fiber breakage, which represents the most critical failure mode in the model. Ultimate failure is reached when the composite laminate is unable to carry anymore load and is represented in Figure 2.19(c). The ultimate failure load in the model was determined to be 20.2 kN (4,541 lbs)

Table 2.1. Comparison of flexural rigidity (Nagaraj and GangaRao 1997)

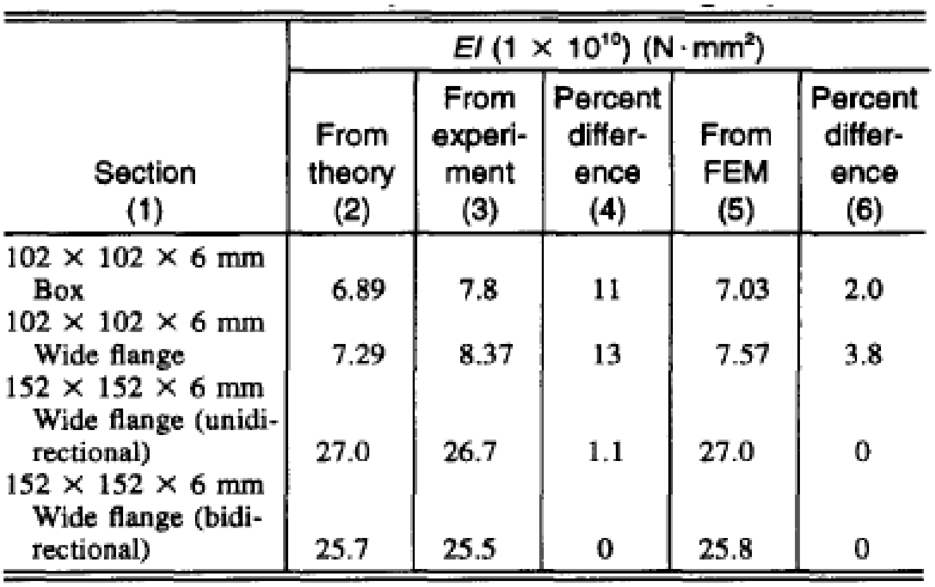

Section (1)	*EI* (1 × 10^{10}) (N·mm^2) From theory (2)	From experiment (3)	Percent difference (4)	From FEM (5)	Percent difference (6)
102 × 102 × 6 mm Box	6.89	7.8	11	7.03	2.0
102 × 102 × 6 mm Wide flange	7.29	8.37	13	7.57	3.8
152 × 152 × 6 mm Wide flange (unidirectional)	27.0	26.7	1.1	27.0	0
152 × 152 × 6 mm Wide flange (bidirectional)	25.7	25.5	0	25.8	0

Table 2.2. Comparison of shear rigidity (Nagaraj and GangaRao 1997)

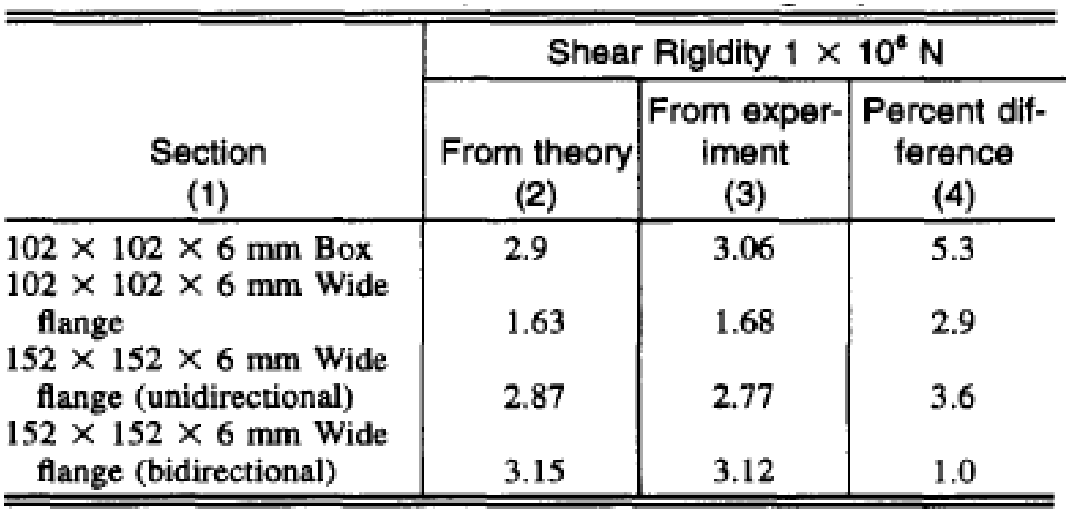

Section (1)	Shear Rigidity 1 × 10^6 N From theory (2)	From experiment (3)	Percent difference (4)
102 × 102 × 6 mm Box	2.9	3.06	5.3
102 × 102 × 6 mm Wide flange	1.63	1.68	2.9
152 × 152 × 6 mm Wide flange (unidirectional)	2.87	2.77	3.6
152 × 152 × 6 mm Wide flange (bidirectional)	3.15	3.12	1.0

Table 2.3. Geometrical Data for the Investigated Geometry (Kermanidis et al. 2000)

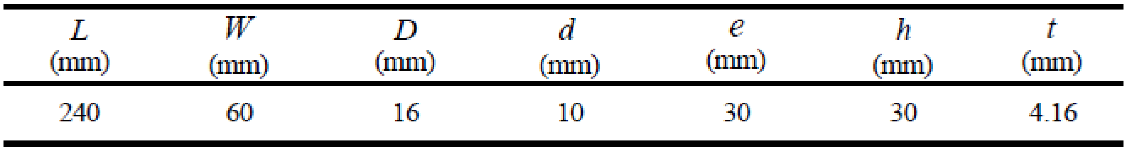

L (mm)	W (mm)	D (mm)	d (mm)	e (mm)	h (mm)	t (mm)
240	60	16	10	30	30	4.16

Table 2.4. Elastic Properties of HTA/6376 Material (Kermanidis et al. 2000)

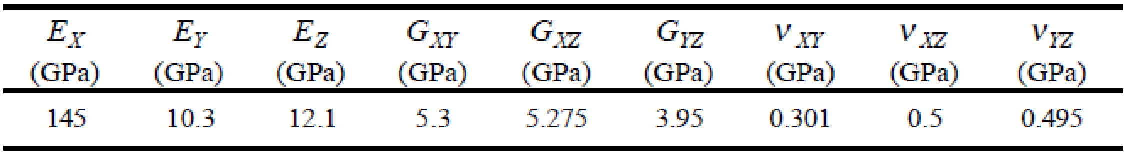

E_X (GPa)	E_Y (GPa)	E_Z (GPa)	G_{XY} (GPa)	G_{XZ} (GPa)	G_{YZ} (GPa)	ν_{XY} (GPa)	ν_{XZ} (GPa)	ν_{YZ} (GPa)
145	10.3	12.1	5.3	5.275	3.95	0.301	0.5	0.495

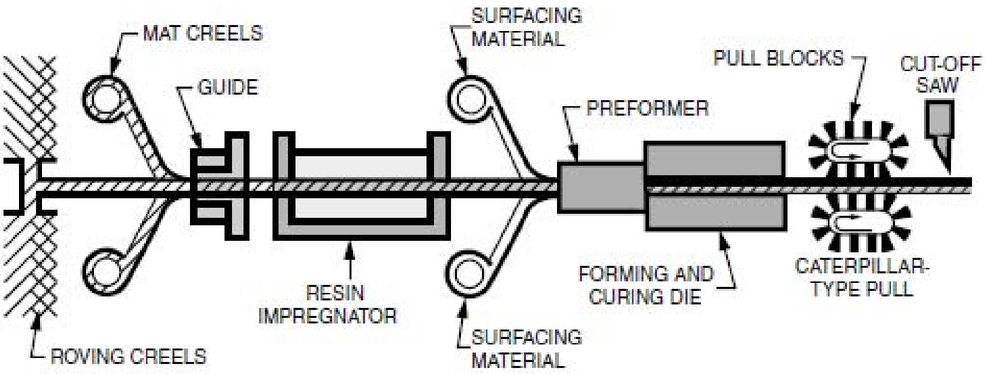

Figure 2.1. FRP pultrusion process (Extren 2003)

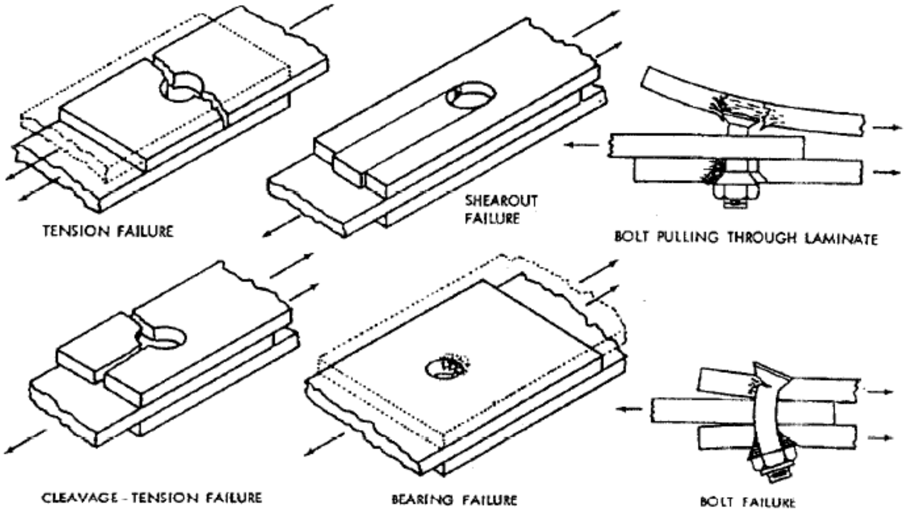

Figure 2.2. Modes of failure for bolted joints in FRP Composites (Hart-Smith 1987)

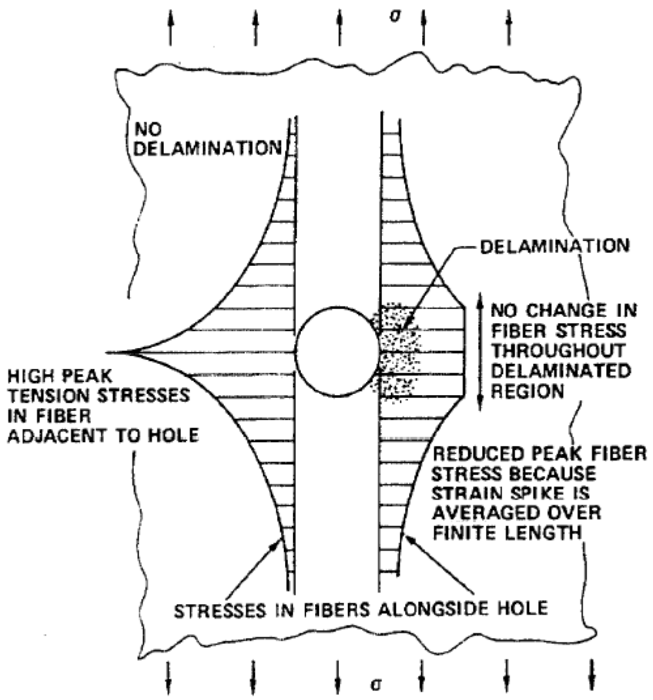
σ
NO DELAMINATION
DELAMINATION
NO CHANGE IN FIBER STRESS THROUGHOUT DELAMINATED REGION
HIGH PEAK TENSION STRESSES IN FIBER ADJACENT TO HOLE
REDUCED PEAK FIBER STRESS BECAUSE STRAIN SPIKE IS AVERAGED OVER FINITE LENGTH
STRESSES IN FIBERS ALONGSIDE HOLE
σ

Figure 2.3. Stress concentration relief in fibrous composites by delamination (Hart-Smith 1977)

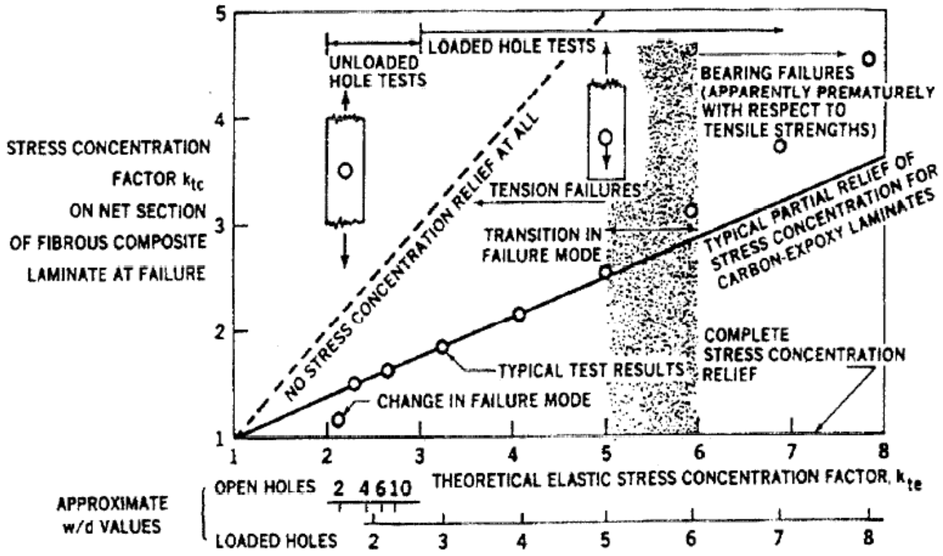

Figure 2.4. Relation between stress concentration factors observed at failure of fibrous composite laminates predicted for perfectly elastic isotropic materials (Hart-Smith 1977)

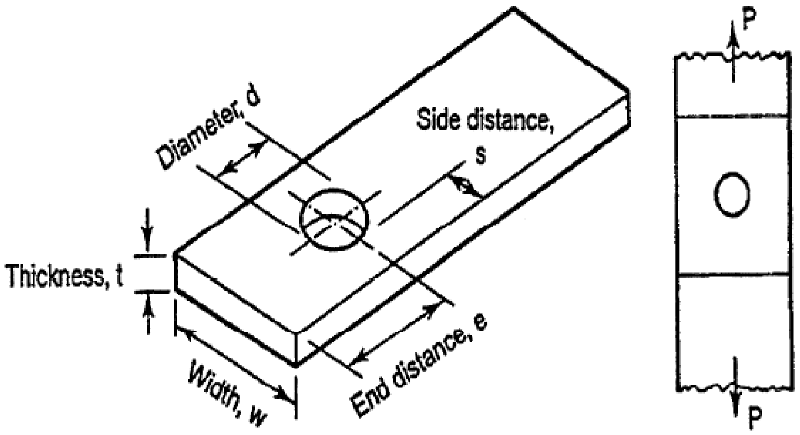

Figure 2.5. Terminology (Duthinh 2000)

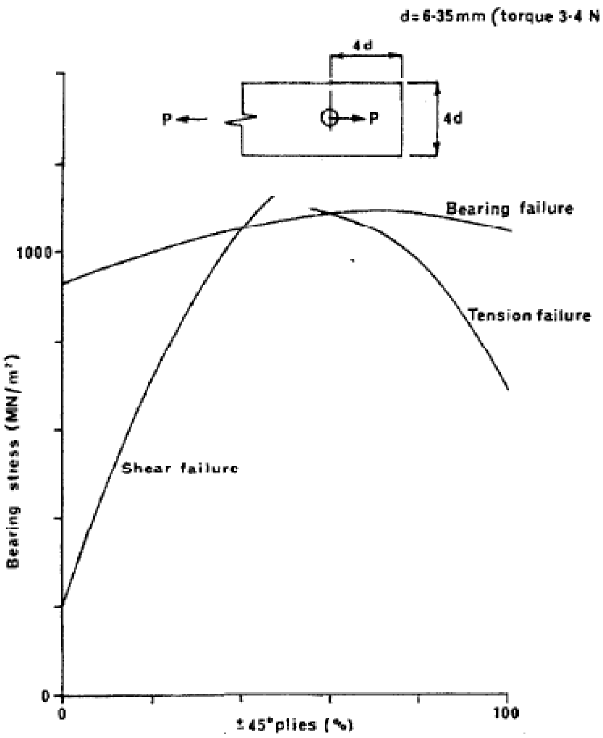

Figure 2.6. Influence of CFRP fiber proportion (0° / ±45°) on failure mode (Garbo and Ogonowski 1981)

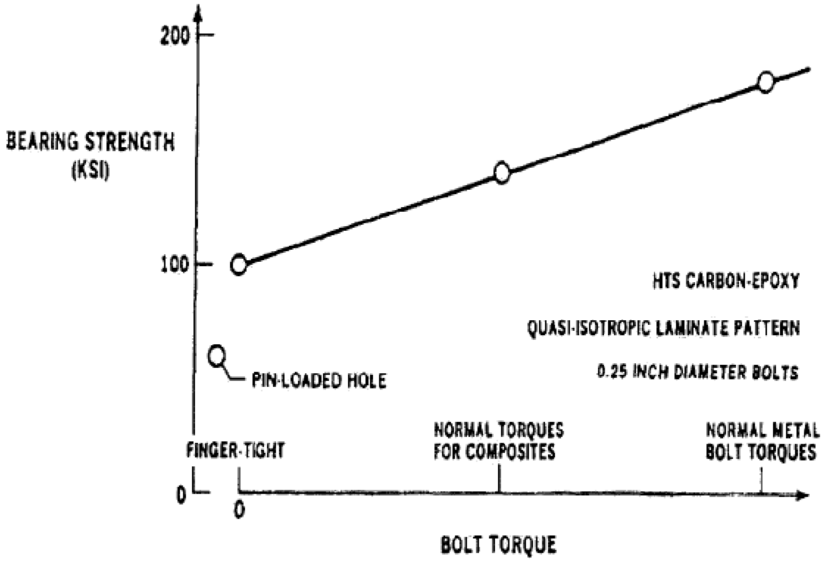

Figure 2.7. Effect of bolt torque on bearing strength of fibrous composite laminates (Hart-Smith 1987)

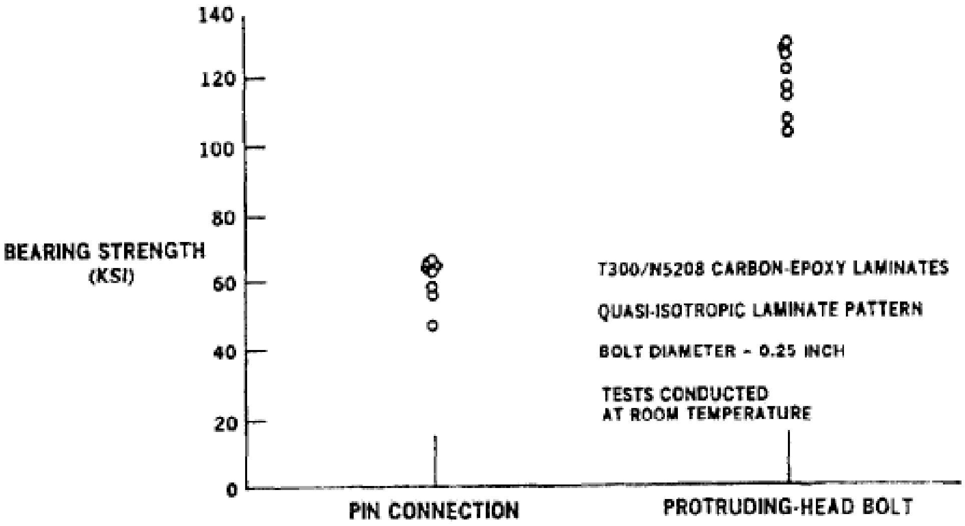

Figure 2.8. Comparison between bearing strengths of connections with and without clamping pressure (Hart-Smith 1987)

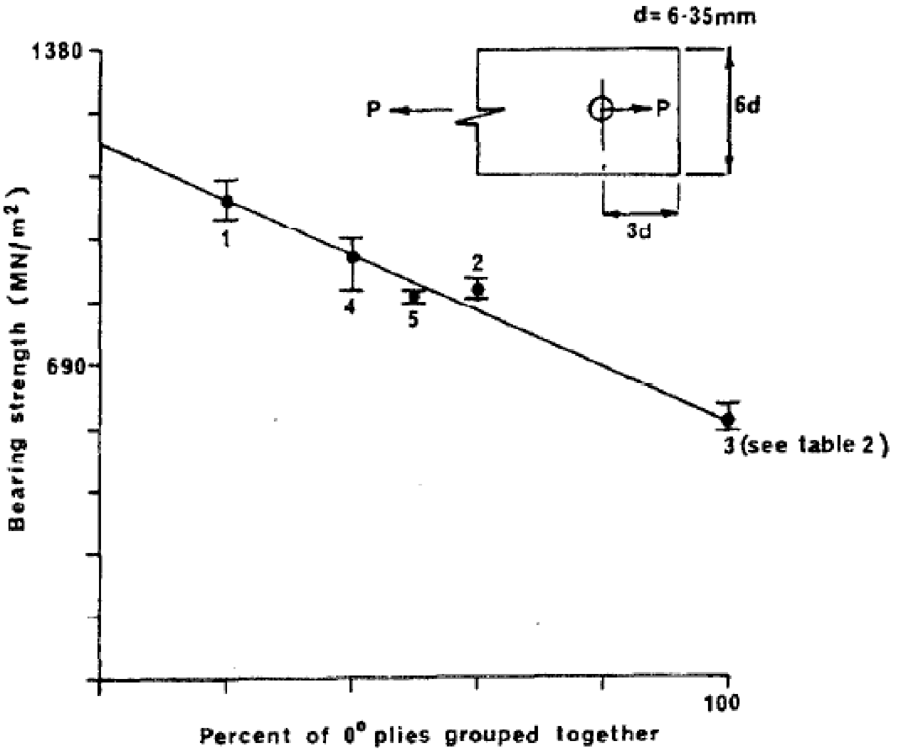

Figure 2.9. Effect of grouped 0° plies on bearing strength (Garbo and Ogonowski 1981)

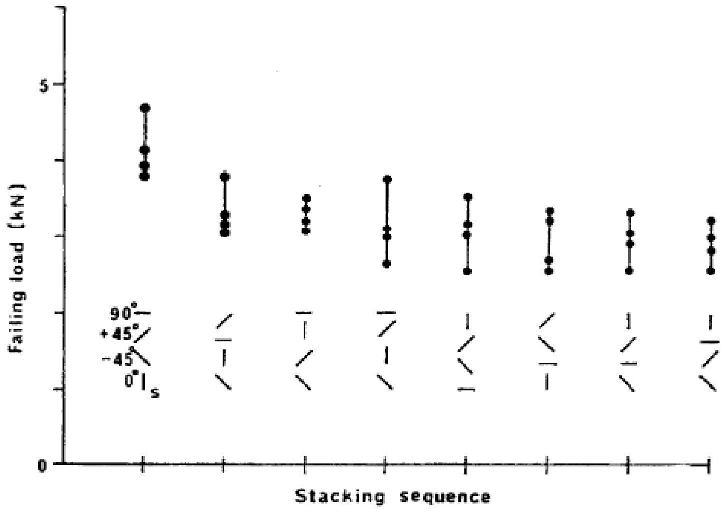

Figure 2.10. Effects of stacking sequence on bearing strength for GFRP laminates (Quinn and Mathews 1977)

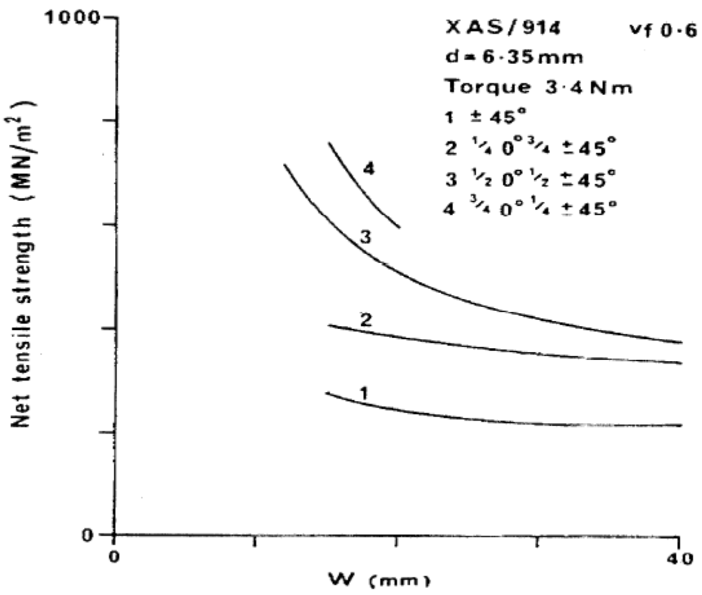

Figure 2.11. Variation of net tensile strength with width of 0°/±45° CFRP composites with 6.35 mm (0.25 in) hole (Collins 1987)

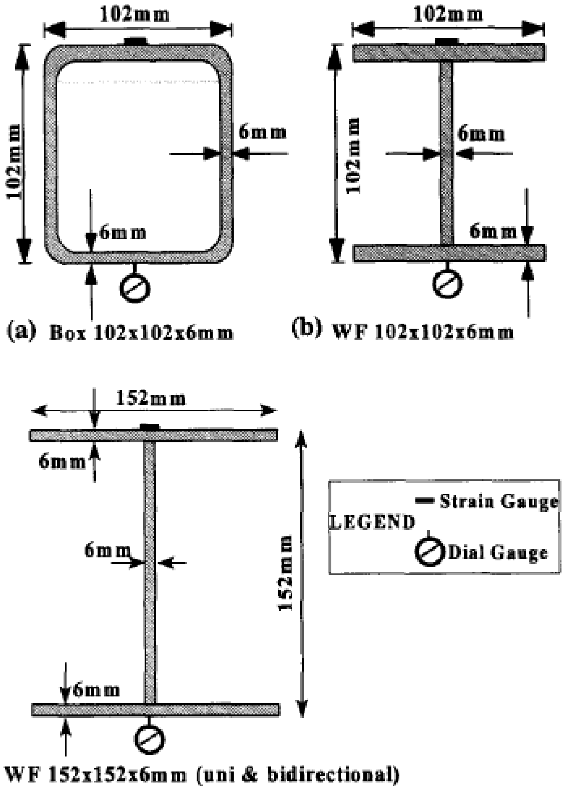

Figure 2.12. Cross sections of test specimens (Nagaraj and GangaRao 1997)

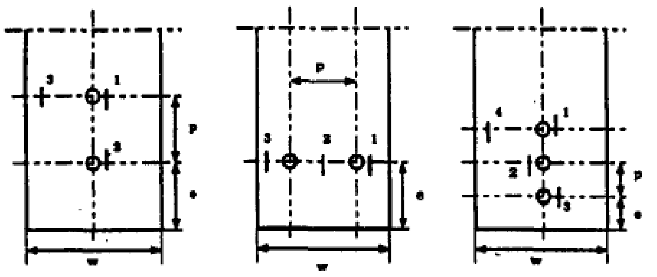

Joint A Joint B Joint C

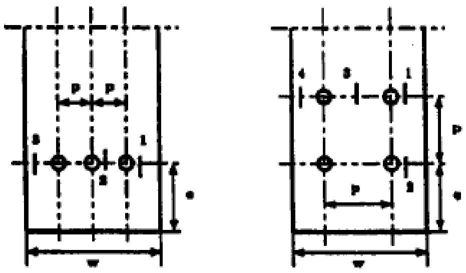

Joint D Joint E

Figure 2.13. Connection configuration (Hassan et al. 1997)

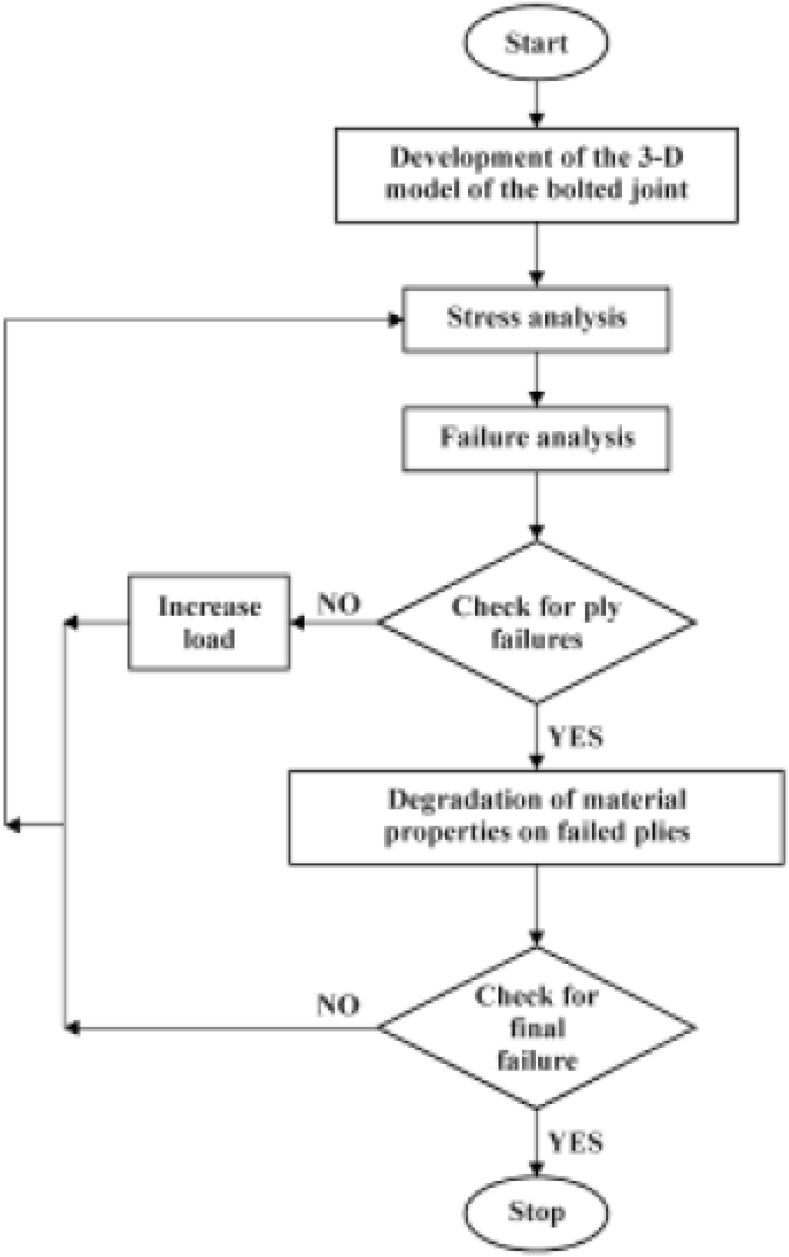

Figure 2.14. Flowchart of the Progressive Damage Model (Kermanidis et al. 2000)

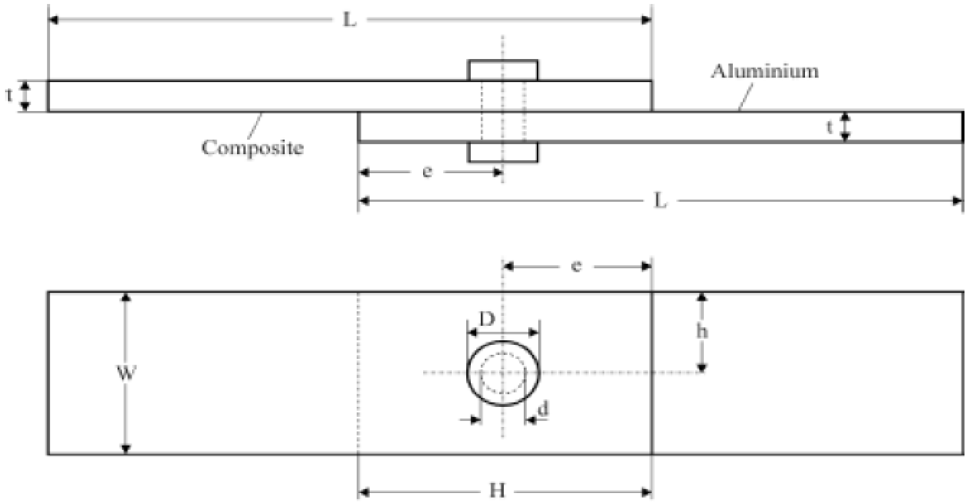

Figure 2.15. Geometry of the Bolted Single-Lap Joint (Kermanidis et al. 2000)

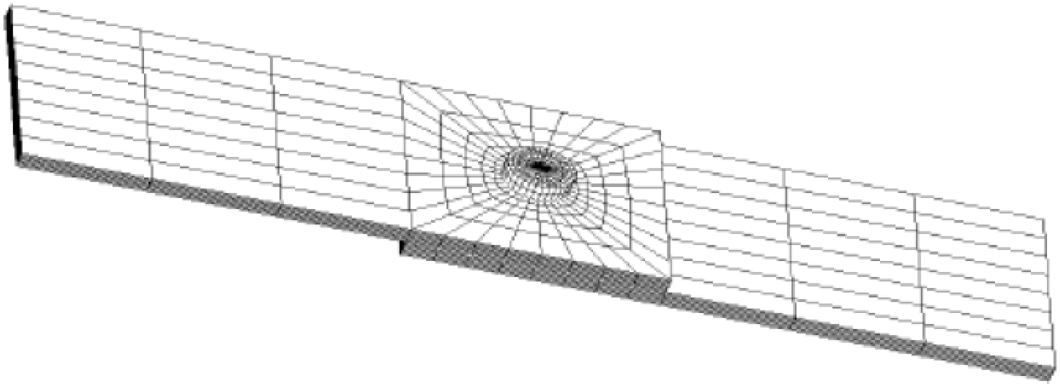

Figure 2.16. Finite Element Model of Bolted Joint (Kermanidis et al. 2000)

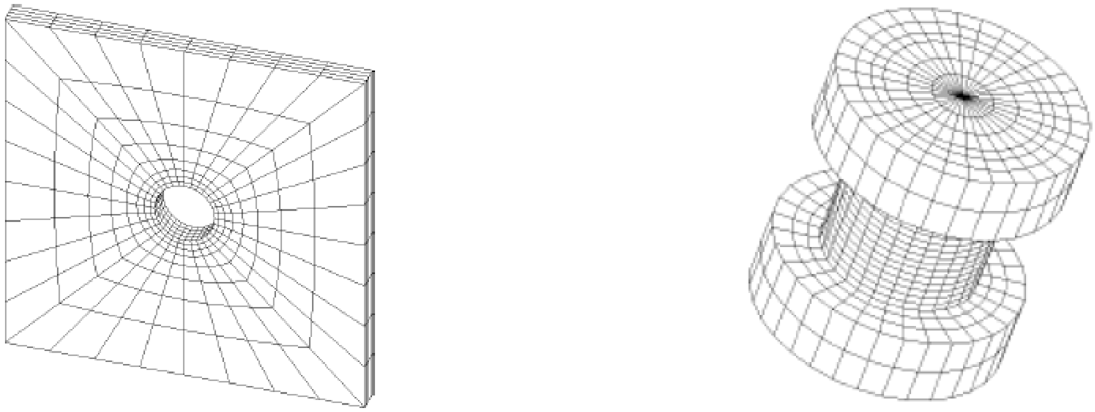

(a) (b)

Figure 2.17. (a) Mesh of Area Around Hole (b) Finite Element Model of Protruding Head Bolt (Kermanidis et al. 2000)

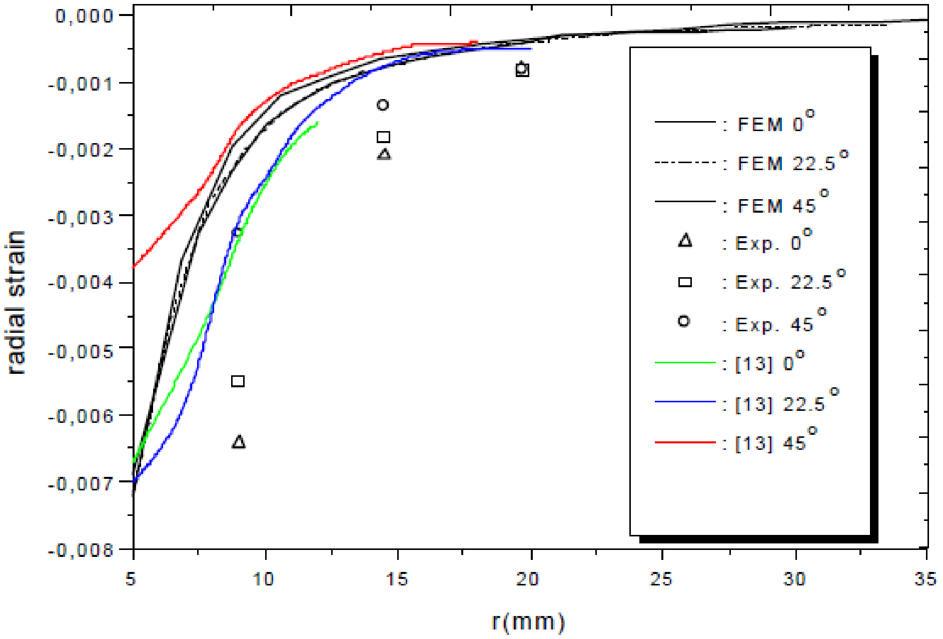

Figure 2.18. Comparison of Calculated Strains with Experimental and Numerical Results (Kermanidis et al. 2000)

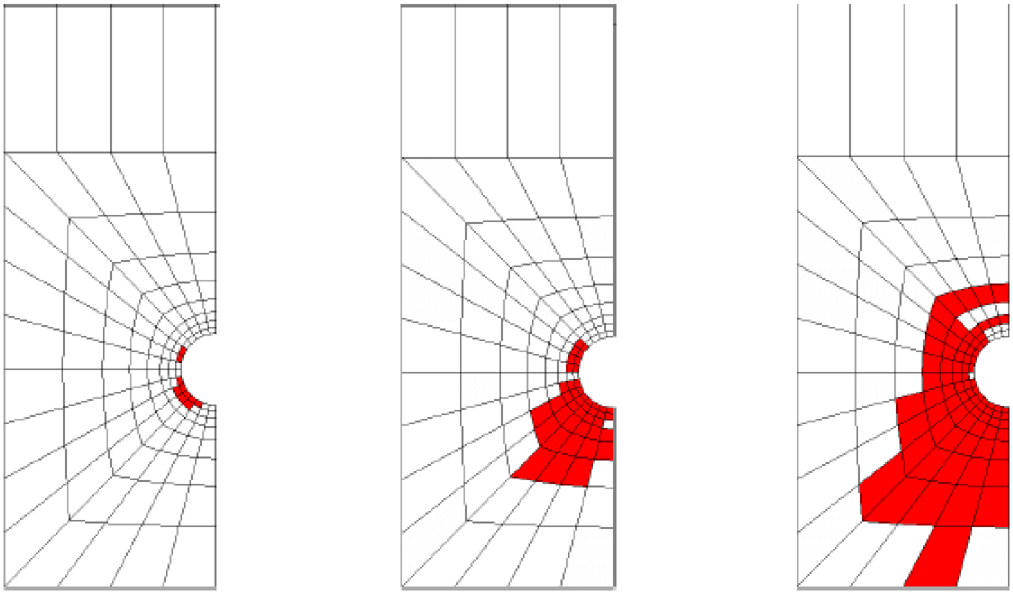

(a) 3kN (b) 12kN (c) 20.2kN

Figure 2.19. Illustration of Damage Propagation Predicted by the Present Model at Different Load Steps. Upper Surface of the Laminate (Kermanidis et al. 2000)

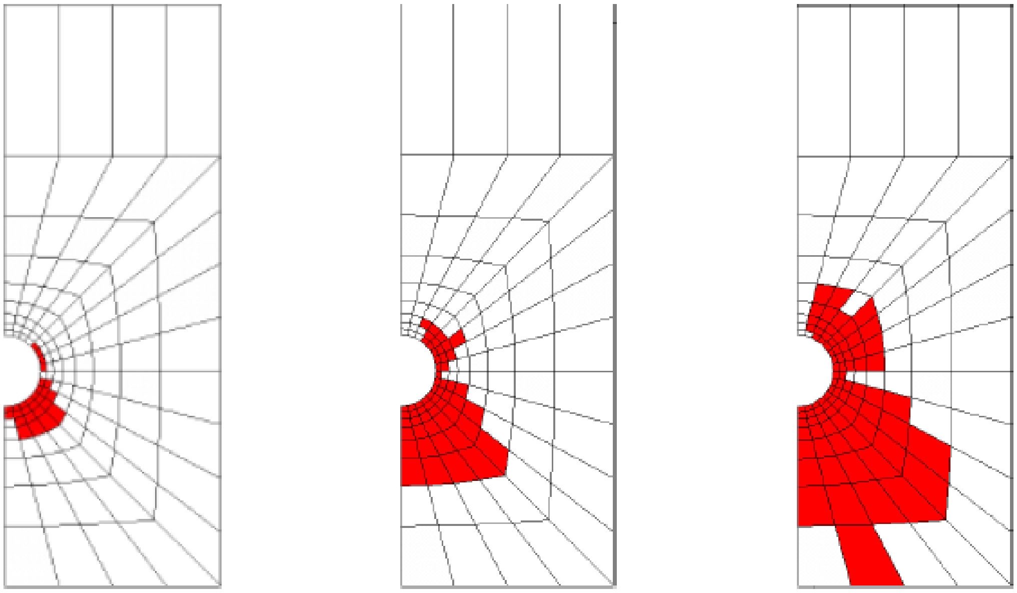

(a) 3kN (b) 12kN (c) 20.2kN

Figure 2.20. Illustration of Damage Propagation Predicted by the Present Model at Different Load Steps. Lower Surface of the Laminate (Kermanidis et al. 2000)

3. Experimental Program

3.1 Introduction

The experimental program examined the axial and transverse strength of GFRP structural channel members with bolted connections using various geometric configurations. The parameters studied included the effects of load cycles at various load levels on the ultimate strength and stiffness. In addition, the effect different flange geometries have on the ultimate strength when loaded in the axial and transverse direction. Phase I consisted of testing a total of 60 specimens with monotonic loading applied in the axial and transverse directions to determine the ultimate strengths of each member (30 axial and 30 transverse). In addition, Phase I tested 10 thickened GFRP members 1 in. (25 mm) thick. Phase II consisted of testing specimens to failure after each specimen underwent unidirectional cyclic loading at various load levels. Phase III tested each member to failure after the specimen underwent multidirectional load cycles in both the axial and transverse directions at different load levels. This chapter will discuss the fabrication process and materials used for the test specimens, instrumentation, test setup, and experimental procedure. All material testing was performed in the Structural Engineering Laboratory at the University of Colorado Denver.

3.2 Materials used for Test Specimens

3.2.1 GFRP Channels

Extren GFRP structural shapes produced by Strongwell (Bristol, Virginia, USA) were used for the experimental testing. Extren is a product line manufactured by Strongwell which consists of more than 100 fiberglass structural shapes. The shapes are made up of long glass fibers intertwined and bound with resin to form a mat. In addition, the glass reinforcements consist of continuous strand rovings containing 800 - 4,000 fiber filaments in each strand. The resins used in Extren are isophthalic polyester and vinyl ester, which provide corrosion resistance and high strength properties. The mechanical properties of the GFRP members were determined through tensile testing of GFRP coupons and using the data provided by the manufacturer.

Channel structural shapes were selected for testing with dimensions of 3 ½” x 1 ½” x 3/16” (90 mm x 38 mm x 5 mm) and 1’-2” (356 mm) in length. Each channel member had a bolt hole with a diameter of 9/16” (14 mm) for loading purposes. The channel members consisted of three different geometric configurations with a portion of the flange cut near the bolt hole. Condition #1 involved the whole section with no flange modifications. For Condition #2 and #3 both the top and bottom flange were cut at a length of 1 5/8” (41 mm) and 3 1/8” (79 mm), respectively. See Figure 3.1 – Figure 3.3 for member dimensions with various flange configurations.

3.2.2 GFRP Flat Plates

The GFRP material testing also included thickened flat plate members that were loaded axially to failure. The GFRP flat plates were ½ in. (13 mm) thick with an additional ½ in. thick plate epoxied at the end where loading occurs. The flat plates had 1 in. chamfers at the corners of both plates. Similar to the channels, a hole with a diameter of 1 9/16” (40 mm) was drilled thru both plates to install a bolt to be loaded. The plates are 3 in. (76 mm) wide and the flat plate that is epoxied has a length of 4 in. (102 mm) See Figure 3.6 for dimensions of the GFRP flat plate.

3.3 Experimental Setup and Loading

3.3.1 Phase I and Phase II Setup for Axial Tests

The tensile testing for each GFRP members consisted of applying a point load through the use of a steel bolt. An MTS closed-loop electro-hydraulic universal testing machine was used for the monotonic axial load application. The loading was performed at a rate of 1 mm/min (0.0394 in./min) and was controlled by the displacement of the actuator. The restraints of the member were provided by fixtures that were connected to the specimen with three ½” (13 mm) diameter bolts. Load was applied at a distance of 1 ½” (38.1 mm) from the end of the specimen using a ½” diameter steel bolt attached to a fixture. The tensile testing was divided into three phases. Phase I consisted of monotonic axial loading to ultimate failure of each channel specimen. The results of Phase I were used to establish various load levels by taking 25%, 50%, and 75% of the ultimate failure to be used for Phase II testing. Phase II testing consisted of axial and transverse loading to failure after the specimens underwent 10 load cycles applied to the specimen using different load levels mentioned above in the axial and transverse directions. Phase III consisted of loading to failure after the specimens were subject to multidirectional cyclic loading. See Figure 3.6 for the axial load experimental testing setup.

3.3.2 Phase I and Phase II Setup for Transverse Tests

The shear tests for each GFRP members were tested in a similar fashion by applying a point load through use of a steel bolt in the transverse direction. The same testing equipment and loading rate of 1 mm/min from the tensile testing was used. Instead of utilizing fixtures with bolted connections, a fixed support was provided by gripping a portion of the channel web with clamps. The restraint required cutting the bottom channel flange to allow for installation of the clamp. The same fixture from the tensile testing was used which applied a transverse concentrated load through the ½" (13 mm) steel bolt. Similar to the axial test the transverse testing was divided into Phase I, Phase II, and Phase III, using the same load levels based on the ultimate failure to be used for the cyclic loading. See Figure 3.7 for the transverse load experimental testing setup.

3.3.3 Phase III Testing Procedure

The channel specimens in Phase III testing are subject to multidirectional loading, which requires the specimen to be loaded in the axial direction at a certain load level followed by loading in the transverse direction at another load level. This procedure constitutes one load cycle and is performed for a total 10 cycles. Phase III requires the fixtures to be alternated for each load cycle to accommodate for loading in the axial and transverse direction. This procedure is different from Phase II, which allows for consecutive unidirectional cyclic loading in one test for all 10 cycles.

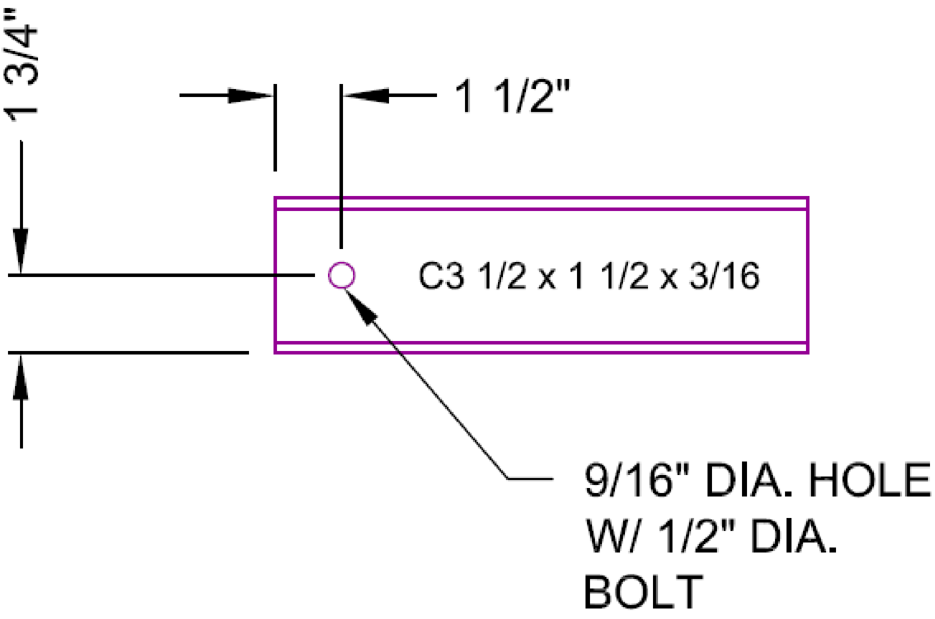

Figure 3.1. Condition #1

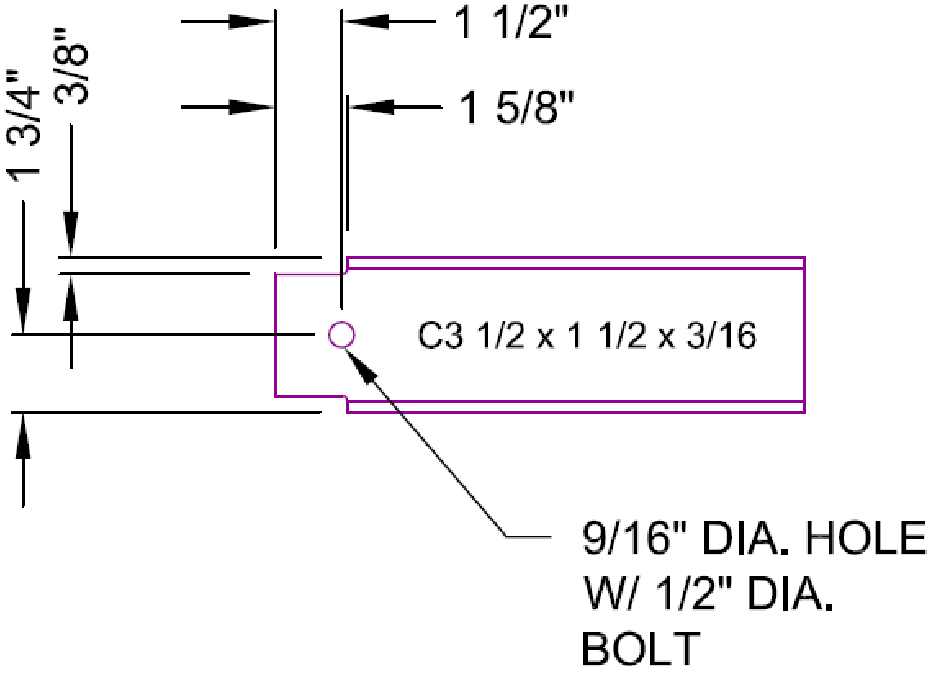

Figure 3.2. Condition #2

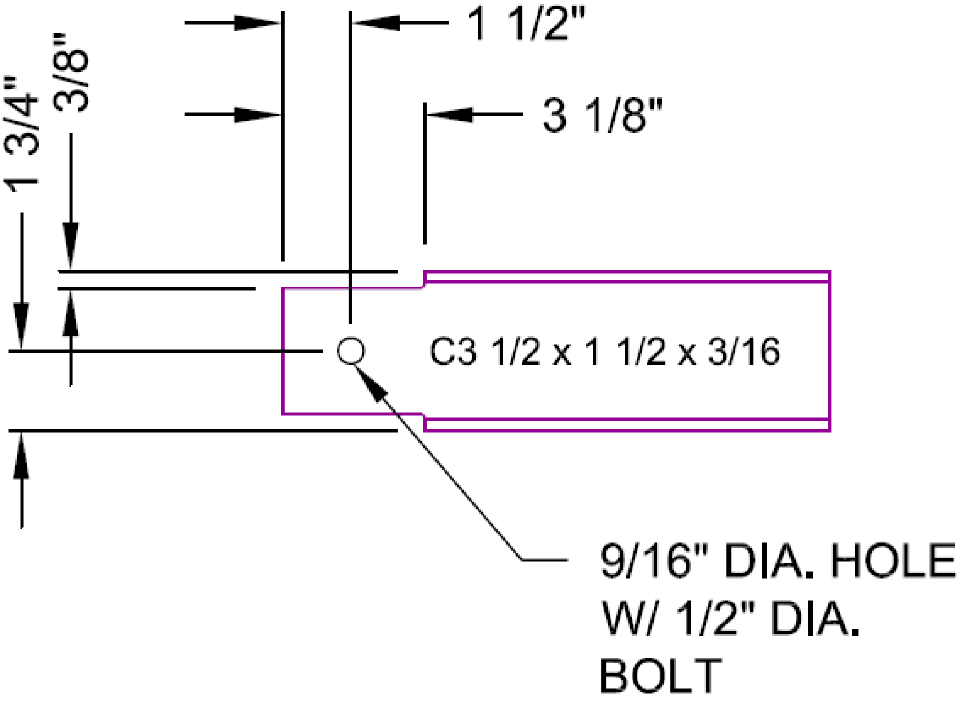

Figure 3.3. Condition #3

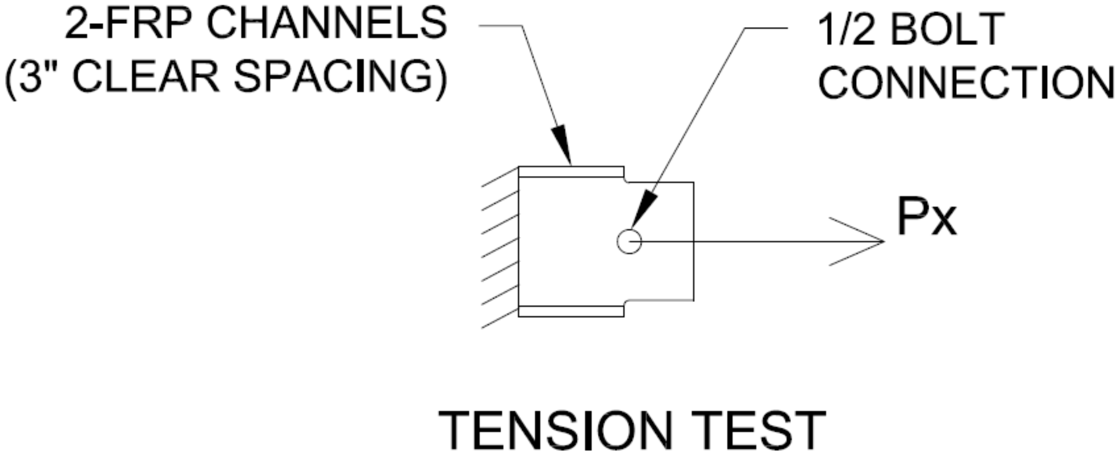

Figure 3.4. Tension Test

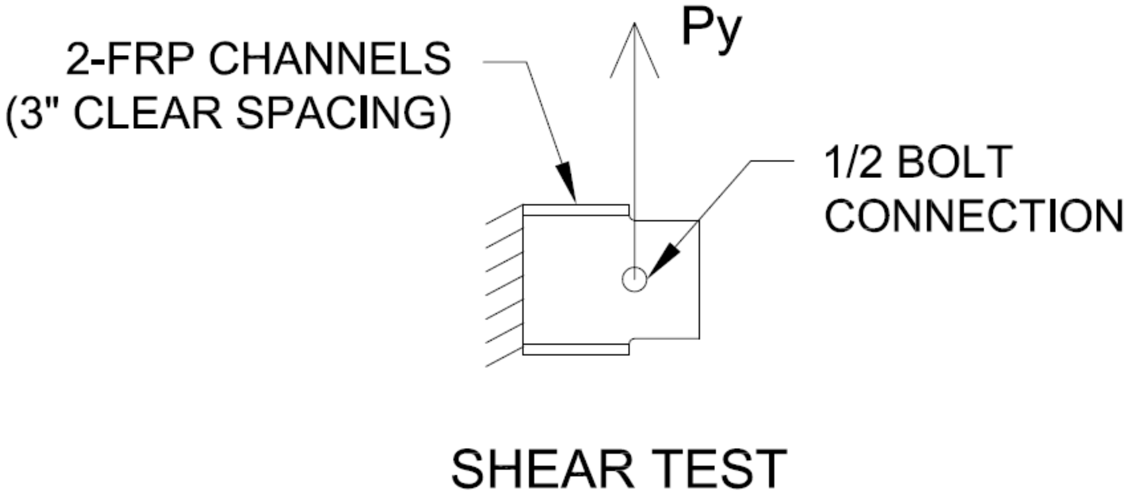

Figure 3.5. Shear Test

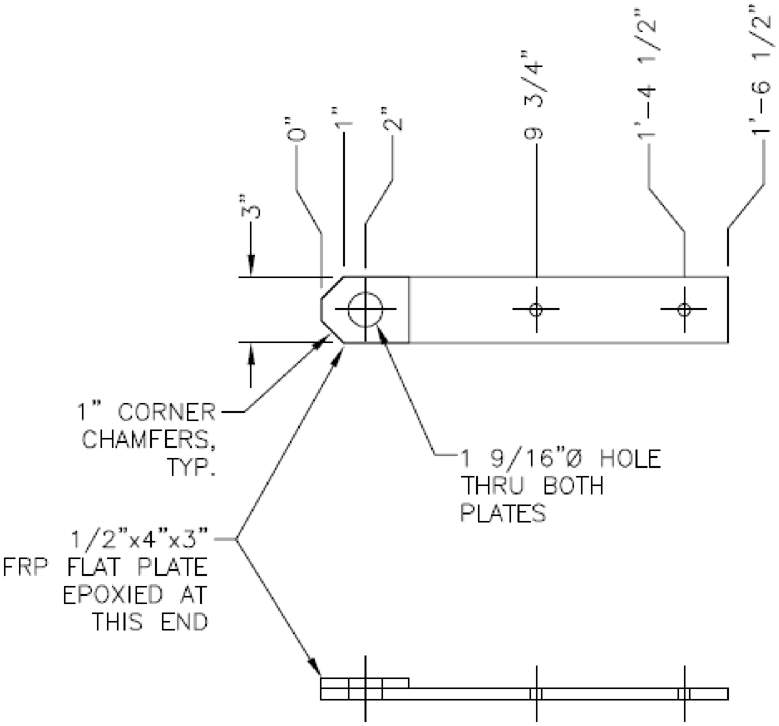

Figure 3.6. Geometry of Thickened Flat Plate

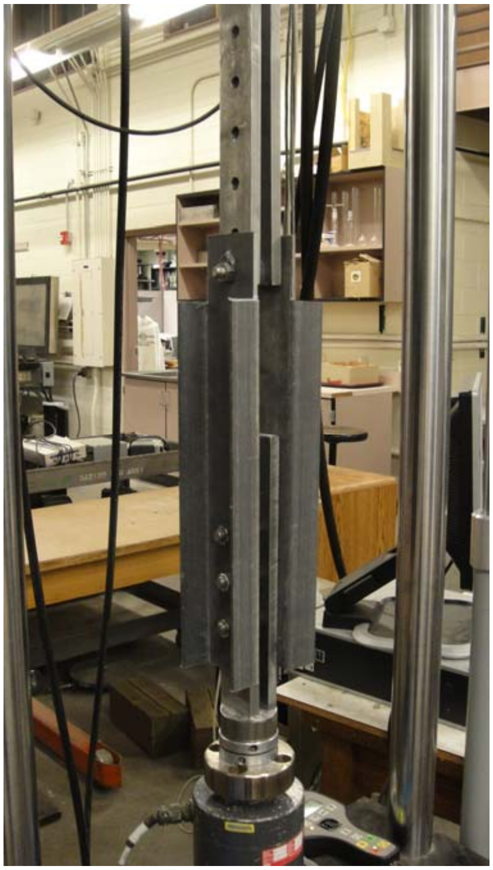

Figure 3.7. Axial Test Setup

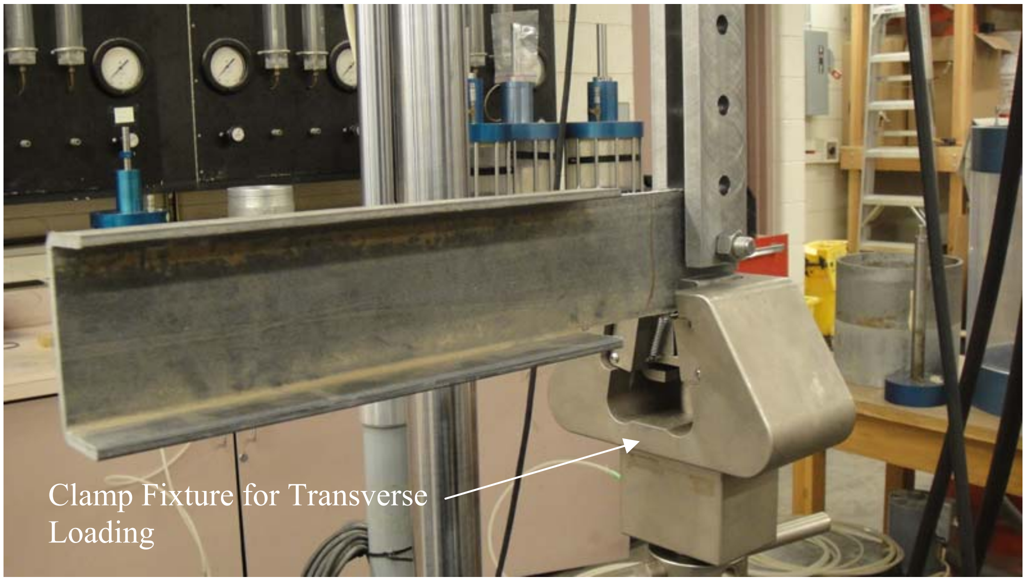

Figure 3.8. Transverse Test Setup

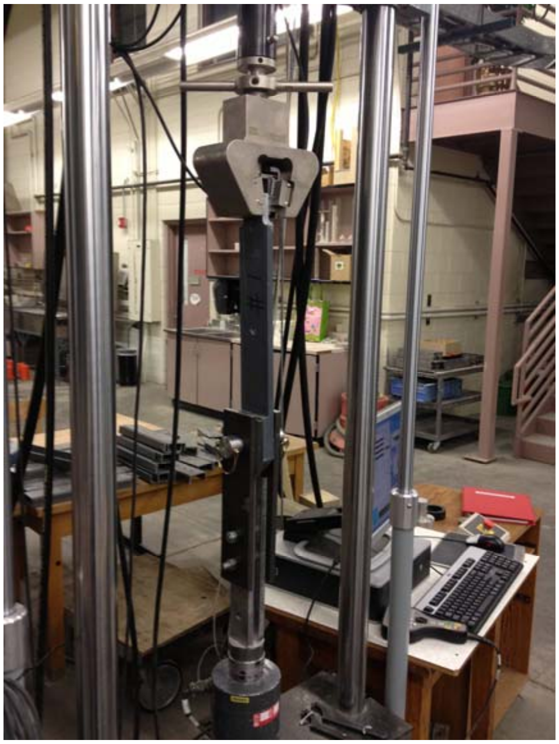

Figure 3.9. Thickened Flat Plate Test Setup

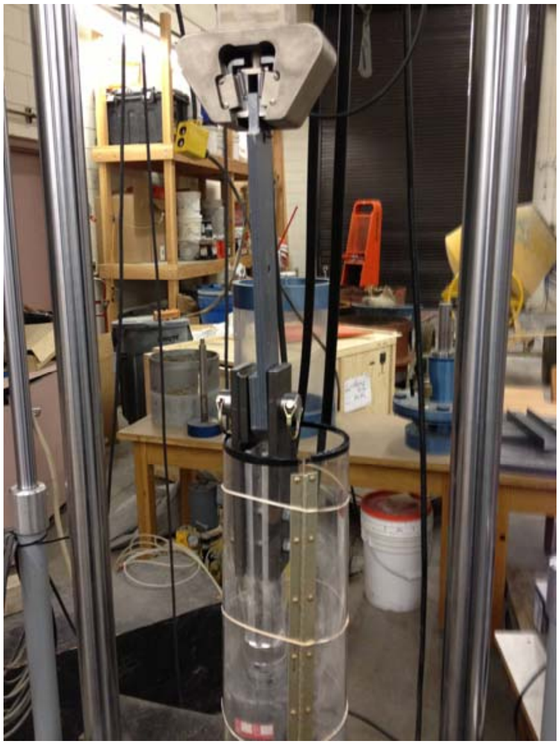

Figure 3.10. Thickened Flat Plate Test Setup

4. Finite Element Modeling

4.1 Introduction

A three-dimensional finite element model was developed to predict the behavior of the GFRP channel specimens using the structural analysis software ANSYS. The specimens were modeled using structural solid elements with orthotropic material properties. The model is a non-linear stress analysis incorporating an established failure criterion to determine stress, deflection, and predicted failure. ANSYS uses two general modes for modeling, interactive and batch. The interactive mode allows the user to use the GUI and other various tools to develop the model in the graphics window and allows for any modifications related to the analysis whereas, the batch mode uses command files that have been created or previously generated for the analysis. The model created utilizes the interactive mode. This chapter will discuss the development of the model along with the approach and methods used.

4.2 Modeling and Elements - Preprocessor

Building a model for the channel composite specimen consists of several steps. An eight-node brick solid elements (SOLID185) was selected to represent the GFRP channel member. This solid element has three translational degrees of freedom at each node. Orthotropic material properties are required and are defined using values from the manufacturer. The material properties include the modulus of elasticity *E*, in the x, y, and z directions, Poisson's ratio *υ*, in the xy, yz, xz directions, and the shear modulus *G*, in the xy, yz, xz directions, they are listed in Table 4.1. The channel geometry modeled has a depth of 3 ½ in. (89 mm) a flange width of 1 ½ in. (38 mm) and a thickness of 3/16 in

(5 mm), the dimensions are shown in Figure 3.1. A ½ in. (13 mm) diameter hole is added at a distance of 1 ½ in. (38 mm) from the end of the member.

Several types of constraints were applied to the model. The edge of the channel member was constrained in all six degrees of freedom. To prevent lateral movement and secondary bending effects of the member, a lateral support was added in the z-direction located at the bolt. The Mesh Tool was used for automatic mesh generation of the model which is beneficial for the ease of mesh refinement. Both the channel and bolt were meshed using tetrahedral solid elements. The load was applied in the longitudinal x-direction using 25% and 75% of the ultimate tensile failure load determined from the experimental testing. The corresponding load values are 584 lbs (2.6 kN) and 1,752 lbs (7.8 kN) respectively. Concentrated loads were applied over multiple nodes to replicate uniform pressure caused by loading of the bolt, see Figure 4.2.

4.3 Failure Criteria

The Tsai-Wu failure criterion used to predict the composite failure of the GFRP channel members. The Tsai-Wu failure criterion is a quadratic, interactive stress-based criterion that identifies failure, but does not distinguish between different failure modes (Tsai and Wu 1971). Failure occurs when the following condition is satisfied:

$$F_i \sigma_i + F_{ij} \sigma_i \sigma_j \leq 1.0 \tag{4-1}$$

Where F_i and F_{ij} are experimentally determined material strength parameters and σ_i and σ_j are the laminate stress in the fiber direction and the laminate stress transverse to the fiber direction, respectively. The failure criterion requires input values for material strengths which include the compressive, tensile, and shear strength of the composite in the x, y, and z directions. See Table 4.2 for the material strength used in the analysis.

4.4 Model Results

After the analysis was performed the results indicate a maximum deflection of 0.004 inches (0.1 mm) at the bolt hole. This value was based on an axial load of 584 lbs (2.6 kN) which was determined to be 25% of the ultimate load in the axial direction. When 75% of the ultimate axial load was applied of 1,752 lbs (7.8 kN) resulted in a maximum deflection of 0.012 inches (0.3 mm) at the same location adjacent to the bolt hole. These deflection values were significantly different from the displacements measured through testing. The finite element model yielded values considerably smaller. Based on load testing of the channel specimens the average deflection from an applied axial load of 584 lbs and 1,752 lbs were approximately 0.025 inches (0.6 mm) and 0.0725 inches (1.8 mm) respectively. The difference can be attributed by the restraint conditions of the two. The ANSYS model uses a fixed restraint at the end of the channel whereas; the testing of the channel specimens used three bolts for the support conditions. This resulted in high stress concentrations at the bolt locations leading to a larger total displacement from each bolt hole. In addition, there may have been a very small gap between the bolt and bolt hole surface in the three bolted connections used as a restraint which caused additional displacement. See Figure 4.2 and 4.4 for the deflection results from ANSYS.

Table 4.1. Material Properties for GFRP Channel Specimens (Extren 2013)

E_x (psi)	E_y (psi)	E_z (psi)	G_{xy} (psi)	G_{xz} (psi)	G_{yz} (psi)	v_{xy}	v_{xz}	v_{yz}
2,600,000	800,000	800,000	425,000	425,000	n/a	0.33	0.33	n/a

Table 4.2. Failure Criteria Strength Values

	x	**y**	**z**
Stress in Tension (psi)	30,000	7,000	7,000
Stress in Compression (psi)	30,000	15,000	15,000

	xy	**yz**	**xz**
Stress in Shear (psi)	4,500	4,500	4,500

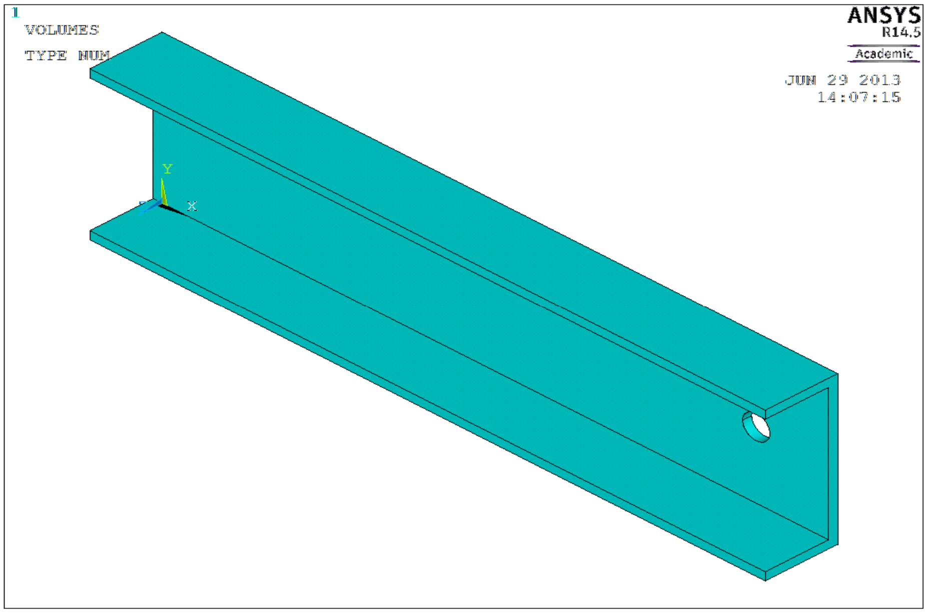

Figure 4.1. Channel Geometry of ANSYS Model

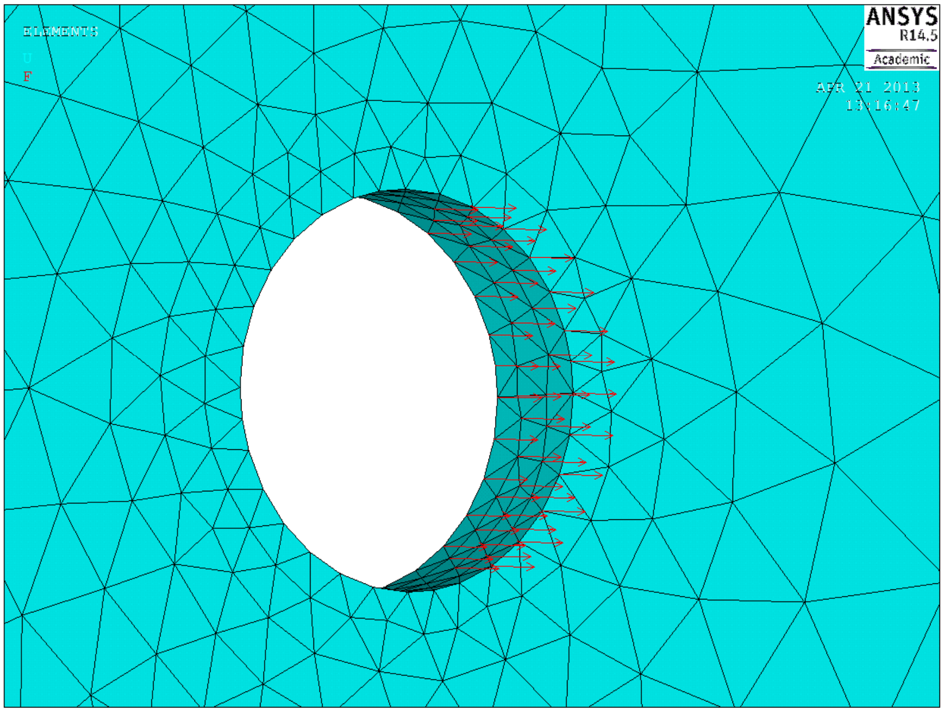

Figure 4.2. Applied Loading of Model

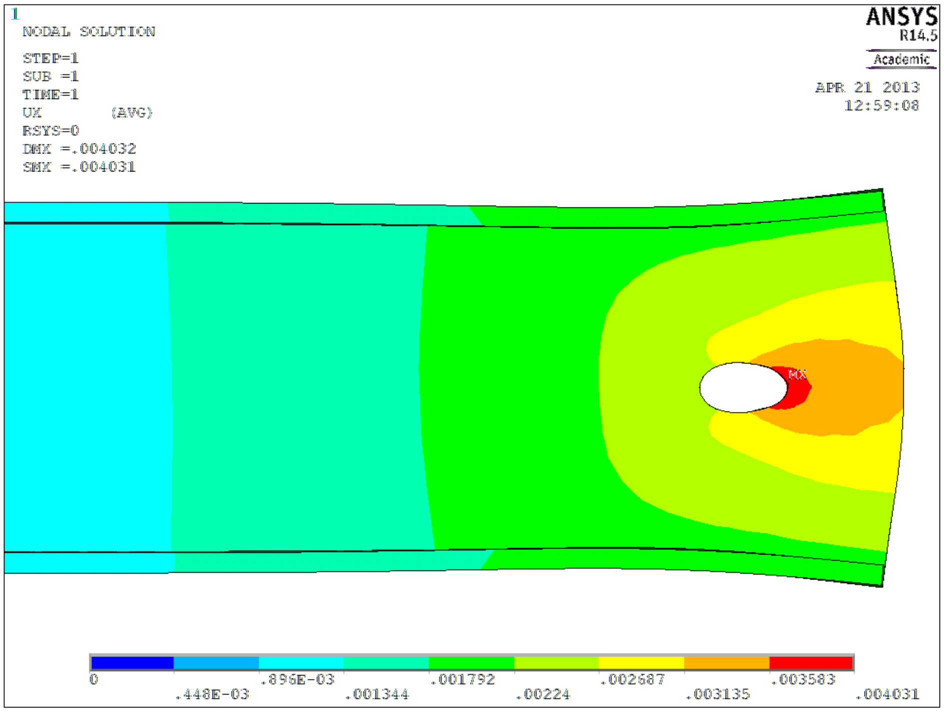

Figure 4.3. Displacement from 25% of Ultimate Load

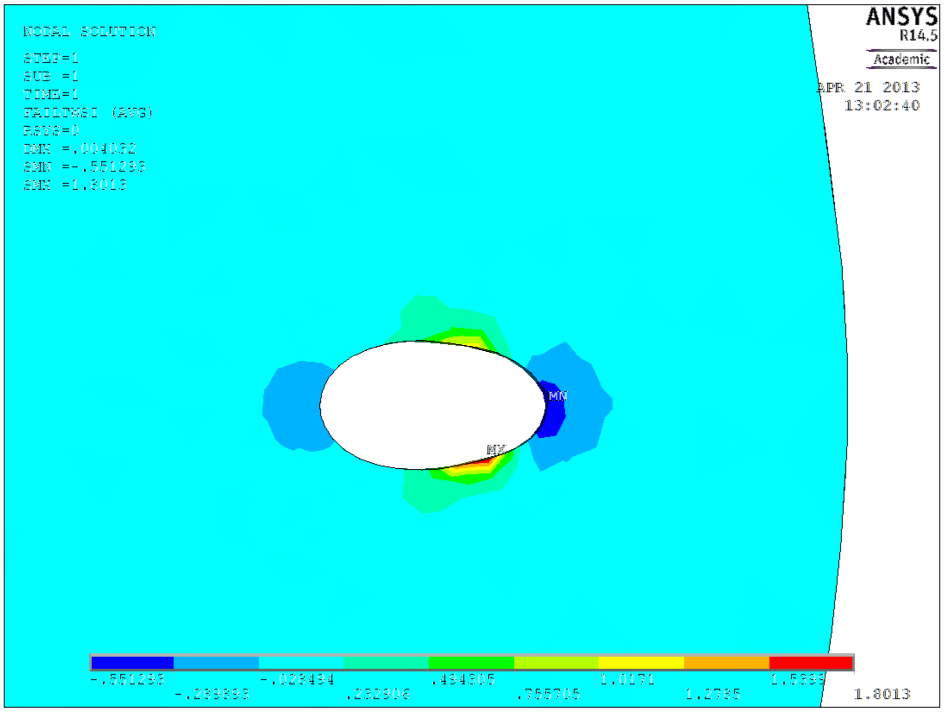

Figure 4.4. Tsai-Wu Strength Index – 25% of Ultimate Load

5. Test Results and Discussion

5.1 Introduction

This chapter presents the results obtained from material testing of the GFRP channel specimens. The testing consisted of loading the specimens in the axial and transverse direction. The behavior of the loaded specimens along with the various failure modes are discussed in detail. The mechanical properties of the GFRP specimens are established from the material testing and are evaluated in terms of the load-displacement response. The effect of different geometric configurations where the flange was cut near the applied load was studied. Stiffness degradation and ultimate strength from load cycles at different load levels are evaluated. The experimental program is divided into three phases. The primary objective of Phase I is to determine the ultimate strength of the GFRP specimens through monotonic loading in the axial and transverse directions. For Phase II the residual capacity of the connection is investigated with the specimens subjected to unidirectional cyclic loading at various load levels. Phase III involves investigating the residual capacity of the connection subjected to multidirectional cyclic loading at various load levels. The test results from all three phases will be discussed in the following sections.

5.2 Phase I Testing Results of GFRP Channels

A total of 30 GFRP specimens were used for axial testing to determine ultimate load capacity and to generate load-displacement curves. For transverse testing, a total of 30 specimens were used as well. The GFRP specimens have various flange geometry as discussed in Chapter 3. Table 5.1 displays the load capacity results for flange geometries

01, 02, and 03 which represent Condition #1, Condition #2, and Condition #3 respectively, in the axial and transverse directions. Ten specimens were tested for each flange geometry with monotonic loading to failure in both directions. The load-displacement curves for each test in Phase I is provided in Appendix A of this thesis. The load-displacement response indicates linear behavior until initial failure, followed by non-linear behavior until ultimate failure. Initial failure is represented by the first peak on the load-displacement curve and the ultimate failure is represented by the maximum load of the response. Figure 5.1 and Figure 5.2 displays a typical load-displacement curve for the GFRP specimens in the axial and transverse directions.

For AXIAL 01 the average of the 10 specimens tested had an initial failure load capacity and standard deviation of 2,214 lbs (9.8 kN) and 162 lbs (0.72 kN) respectively. TRANS 01 the average initial failure load capacity and standard deviation was 2,601 lbs (11.6 kN) and 345 lbs (1.5 kN), respectively. For the subsequent testing, the load levels of 25%, 50%, and 75% for Phase II and Phase III were obtained using the initial failure load from Phase I. AXIAL 01 and TRANS 01 was the full channel section with no flange cut modifications made. AXIAL 02, AXIAL 03, TRANS 02, and TRANS 03 had different flange geometries as noted in Chapter 3. Based on the final results there was no distinct trend and it can be concluded that removing a portion of the flange in the channel section does not impact the overall performance of the channel member, when loaded in the axial and transverse directions. The total average of all the specimens tested in the axial and transverse direction was 2,337 lbs (10.4 kN) and 2,588 lbs (11.5 kN) respectively. Therefore, the load levels used for Phase II and Phase III testing were 584 lbs, 1,168 lbs, and 1,752 lbs (2.6 kN, 5.2 kN, and 7.8 kN) for axial load levels of 25%, 50%, and 75% and 647 lbs, 1,294 lbs, and 1941 lbs (2.9 kN, 5.8 kN, and 8.6 kN) for transverse loading.

5.2.1 Phase I Failure Modes of GFRP Channels

Investigation of the failure mode for the axial and transverse monotonic load test showed different failure mechanisms for the axial and transverse tests. For the test with the applied load in the axial direction initial bearing failure occurred at the contact zone between the bolt and composite specimen followed by shear-out failure. As noted in Chapter 2 bearing failure occurs when excessive compressive stresses develop at the hole boundary surface. Shear-out failure is typically consequence of bearing failure with a short edge distance, *e* and can be characterized as a combination of in-plane and interlaminar shear failures. Initial bearing damage is followed by a series of peaks on the load-displacement curve that represents damage accumulation with the eventual sudden drop in load carrying capacity. The test is completed when the specimen reaches this point.

In the transverse direction the specimen experienced initial bearing failure similar to the axial test followed by net tension splitting failure. This was evident by the crack propagation in the transverse direction of the applied load. The behavior of the specimens loaded in the transverse direction differs from the axial tests; this is evident by the load-deflection curve which indicates less progressive damage before a sudden drop in load carrying capacity. The transverse load-displacement curves show less activity of damage accumulation with a smaller region of varying peaks after initial failure. Net tension failure is a function of both the joint geometry and the strength of the GFRP specimen. See Figure 5.4 through Figure 5.6 for the axial and transverse typical failure mode of the GFRP channel specimens.

5.2.2 Phase I Testing Results of GFRP Thickened Plates

A total of 10 GFRP plate thickened members were tested with monotonic loading to failure in the axial direction. The average failure load was 14,824 lbs (66 kN) with a standard deviation of 1,308 lbs (5.8 kN) As expected the failure load was significantly higher than the channel members due to the increased thickness of 1 inch (25 mm) which allows for more area at the contact zone between the bolt and the specimen. Table 5.2 displays the failure load for each thickened specimen with loading in the axial direction. The load-displacement curves indicate a linear response until ultimate failure. In comparison to the channel specimen load-displacement curves in the axial direction, the thickened plates do not experience progressive failure which is evident by one peak on the curve as opposed to numerous peaks for the channel specimens. Figure 5.3 shows a typical load-displacement curve of the thickened GFRP plates.

5.2.3 Phase I Failure Mode of GFRP Thickened Plates

Similar to the GFRP channel members the thickened plates experienced shear-out failure adjacent to the bolt hole. Unlike the channel members which experienced initial bearing failure around the bolt hole, the thickened specimens had no visible signs of bearing failure. This can be attributed to the fact the bearing strength capacity is larger than the shear-out capacity for the thickened specimens. On three of the thickened specimens tested debonding of the plates occurred followed immediately by shear-out failure due to the reduced cross section caused by the plates debonding. See Figure 5.7 for typical failure mode for the GFRP thickened members with monotonic loading in the axial direction and Figure 5.8 for debonding of the plates.

5.3 Phase II Testing Results of GFRP Channels

A total of eighteen specimens were tested for Phase II, nine specimens in the axial direction and nine specimens in the transverse direction. Each load level test (25%, 50%, and 75%) consisted of the same flange geometries used in Phase I, represented by 01, 02, and 03 in the axial and transverse direction. Each specimen underwent ten unidirectional load cycles in the axial and transverse direction of the appropriate load level before being loaded to failure in the respective direction to determine the residual capacity of the connection. For the cyclic tests, the specimens were loaded to a specific predefined load than unloaded when that load was reached. This procedure was performed consecutively ten times.

Figure 5.9 displays the load-displacement curves for the unidirectional cyclic load applied for Phase II. Based on the cyclic loading curves it appears that there is no significant stiffness degradation as the slope of the curves is relatively constant, any decrease in stiffness is minor. The load-displacement response was similar to Phase I with apparent progressive damage and linear behavior up until initial failure after the load cycles were completed and the specimens were loaded to failure. The load-displacement curves for the transverse loading to failure closely resembled Phase I testing as well. See

Figure 5.10 and Figure 5.11 for typical load-displacement curves with monotonic loading in the axial and transverse direction for Phase II.

The average residual load capacity of the three specimens that experienced axial cyclic loading of 25%, 50%, and 75% of ultimate load were 3,000 lbs, 2,836 lbs, and 2,537 lbs, (13.3 kN, 12.6 kN, and 11.3 kN) respectively. Based on these values we can see a distinct trend where the ultimate failure load is reduced as a higher load is applied for cyclic loading. This can be attributed to minor stiffness and strength degradation in the composite material due to repeated load effects. It is noted that the values above, the maximum load capacity was obtained from the load-displacement curves not the initial failure represented by the first peak on the curve.

Similarly, the average residual load capacity of the three specimens that experienced transverse cyclic loading of 25%, 50%, and 75% of the ultimate load were 3,120 lbs, 2,347 lbs, and 2,521 lbs, (13.9 kN, 10.4 kN, and 11.2 kN) respectively. The effect of cyclic loading in this case does not have a clear trend of decreasing strength with increasing load during the ten cycles. Although, it is clear that the failure load of the 75% specimens decreased in comparison to the 25% specimens. Table 5.3 summarizes the testing results for the channel specimens subject to cyclic loading.

5.3.1 Phase II Failure Modes of GFRP Channels

The failure modes for the GFRP channel specimens were similar to the failure modes experienced in Phase I. The only difference came from minor damage propagation and displacements caused by the load cycles which are shown in Figure 5.12. When the specimens were tested in the axial direction to determine the residual capacity of the connection, they experienced initial bearing damage at the contact zone followed by shear-out failure in the region adjacent to the bolt, similar to Phase I failure. Likewise, the transverse testing resulted in initial bearing damage around the bolt hole followed by tension splitting of the section.

5.4 Phase III Testing Results of GFRP Channels

Phase III consisted of multidirectional cyclic load testing of nine specimens. Three specimens were used for each load level of 25%, 50%, and 75% of the ultimate load determined in Phase I. All nine specimens had the same geometric configuration, see Figure 5.13. On one side of the flange no modifications were made, however, the opposite side required cutting the flange to fit the clamp fixture necessary for the transverse loading test. As described in Section 3.3.3 the multidirectional cyclic loading required alternating fixtures to load in both the axial and transverse direction as one load cycle. After ten cycles of multidirectional loading the specimens were loaded to failure. Two of the three sets (01-25, 01-50, 01-75, 02-25, 02-50, and 02-75) were loaded axially to failure to determine the residual capacity in the connection. The last set (03-25, 03-50, and 03-75) was loaded to failure in the transverse direction to determine the residual connection capacity.

The load-displacement curves for the multidirectional cyclic loading are displayed in Figure 5.14. Cyclic loading in the axial or transverse direction is not performed consecutively as the curves show; the axial cyclic loading and transverse cyclic loading are alternated. Thus, each specimen is subject to a total of twenty cycles of applied loading at the appropriate level rather than a total of ten cycles in Phase II. As a result there is more damage accumulation and stiffness degradation as seen in Figure 5.14; however, it is very minor. The load-displacement curves in the axial and transverse directions to failure after multidirectional load cycles resemble the curves generated in from Phase I and Phase II. Recall from Phase I and Phase II, linear behavior up until initial failure from the first peak followed by damage accumulation resulting in ultimate failure.

The average residual load capacity in the axial direction of the two specimens that experienced multidirectional cyclic loading of 25%, 50%, and 75% of the ultimate load were 2,826 lbs, 2,893 lbs, and 2,386 lbs (12.57 kN, 12.87 kN, and 10.61 kN) respectively. Based on these values it is apparent that there was a significant reduction in strength from the specimens which were subject to 75% multidirectional loading. The values above were determined using the maximum load from the load-displacement curves which is not necessarily the initial failure represented by the first peak. However, the average residual connection capacity of the two specimens based on initial damage that experienced multidirectional cyclic loading of 25%, 50%, and 75% of the ultimate load were 2,626 lbs, 2,321 lbs, and 1,894 lbs (11.68 kN, 10.32, and 8.42 kN) respectively. This shows significant strength degradation with each increase in load level.

For the residual connection capacity in the transverse direction after multidirectional cyclic loading only one set of specimens were tested. The connection capacity with cyclic loading of 25%, 50%, and 75% of the ultimate load was 2,168 lbs, 2,595 lbs, and 2,231 lbs (9.64 kN, 11.54 kN, and 9.92 kN) respectively. The effect of cyclic loading in this case does not have a clear trend of decreasing strength with increasing load during the multidirectional load cycles. The same is observed using the residual capacity based on initial failure. Table 5.4 summarizes the testing results for the channel specimens subject to multidirectional cyclic loading.

5.4.1 Phase III Failure Modes of GFRP Channels

For Phase III, the failure modes from monotonic axial and transverse testing after multidirectional load cycles were similar to Phase I and Phase II. The only difference came from displacements and damage caused from the repeated loads. For the 25% and 50% multidirectional load cycle tests the damage and displacements was minimal, however, for the 75% multidirectional load cycle tests the damage was more as shown in Figure 5.17. For failure in the axial direction the specimen experienced initial bearing failure followed by shear-out failure adjacent to the bolt hole. In the transverse direction, two of the three specimens experienced initial bearing failure followed by tension splitting at the bolt hole as expected based on the previous test, displayed in Figure 5.18 and Figure 5.19. However, for specimen 50-3 the tension splitting was located just above the clamp and below the hole seen in Figure 5.20 which was unusual based on the previous failure modes from testing in the transverse direction. Recall, once the test shows a sudden drop in load carrying capacity the test is completed.

5.5 Comparison of Phases

The following section will compare the behavior and results between each phase of the testing. Strength reduction, stiffness degradation, failure mechanisms, etc. will be discussed.

5.5.1 Comparison Among Different Flange Geometries in Phase I

Figure 5.21 show the comparison of load-displacement curves for specimens tested in Phase I. The comparison shows the effect different flange geometries have on the connection strength. Based on the load values and observation of the curve it can be concluded that variation in flange geometries has no significant effect on the behavior and ultimate strength of the connection in the axial and transverse directions. However, it is noted that for the axial specimens the initial failure load capacity increased with larger sections cut from the flange of the channel.

5.5.2 Comparison of Post-Cyclic Residual Behavior

The comparison of post-cyclic residual behavior is displayed in Figure 5.22. It is clear from the data and curves that multidirectional cyclic loading has a substantially higher impact on the residual behavior and strength of the connection compared to the residual behavior subject to unidirectional cyclic loading. In some instances the load capacity for specimens that underwent unidirectional cyclic loading was higher than the load capacity determined in Phase I which did not experience any cyclic loading. The curves show that the post-cyclic residual behavior from multidirectional cyclic loading generally had the smallest slope. In addition, the transverse specimens from Phase III had a longer region of damage accumulation with multiple peaks before failure compared to the transverse specimens from Phase I and Phase II.

5.5.3 Effect of Cyclic Loading on Residual Capacity

The effect of cyclic loading on the residual capacity for Phase II and Phase III is shown in Figure 5.23. The figure is divided into the capacity at the first peak and the capacity at the maximum peak. Generally, the residual capacities for Phase III experienced reduced connection capacity as the load level percent of cyclic loading increased. The same cannot be said for Phase II as there was no clear trend apparent that the cyclic loading had on the residual capacity. It is noted, that for the transverse specimens in Phase II the trend was similar when comparing the capacity at the first peak to the capacity at the maximum peak. In addition, there was very small variation in the capacity between the three specimens tested for each load level resulting in similar chart lines for each of the three specimens.

5.6 Design Recommendations

This section describes discusses design recommendations for pultruded GFRP structural channel members with bolted connections subject to axial and transverse loading.

5.6.1 Monte-Carlo Simulation

A Monte-Carlo simulation was performed to assist with developing design guidelines and recommendations for GFRP structural channel members. The simulation involves generating many random values to overcome limited experimental data. The algorithm used for the random sampling was the inverse transformation method (Devroye 1986). For the simulation 10,000 samples were used for the calibration of the resistance factor.

5.6.2 Calibration of Resistance Factor

The resistance factor for bolted GFRP channel members was determined using the following calibration method. The safety index β is used to adjust the level of safety performance in structural members and is calculated by the following equation:

$$\beta = \frac{R - E}{\sqrt{\sigma_R^2 + \sigma_E^2}} \tag{5-1}$$

Where R and E are the mean capacity and mean instantaneous load applied, respectively, and σ_R and σ_E are the corresponding standard deviations. The target safety index β was set to 2.5, 3.0, and 3.5. The denominator of Equation 5-1 can be approximated as the following equation:

$$\sqrt{\sigma_R^2 + \sigma_E^2} = \alpha(\sigma_R + \sigma_E) \tag{5-2}$$

Where α is the directional cosine or empirical constant to be determined. Combining equation 5-1 and 5-2 the following Load and Resistance Factor Design (LRFD) relationship is determined (Barker and Puckett 1997).

$$\varphi R_n = \gamma E_n \tag{5-3}$$

$$\varphi = \lambda_R(1 - \alpha\beta V_R) \tag{5-4}$$

$$\gamma = \lambda_E(1 - \alpha\beta V_E)$$

(5-5)

Where R_n and E_n are the nominal resistance and applied load, respectively, λ_R and λ_E are their bias factors, V_R and V_E are the coefficients of variations, and φ and γ are the resistance factor and load factor, respectively.

Table 5.5 summarizes the resistance factor calibration for specimens in monotonic unidirectional loading. As expected as the safety index β decreases the resistance factor φ increases. The resistance factor calibration indicates the transverse specimens yielded lower resistance factor value than the axial specimens, which is caused by higher coefficients of variation in the transverse specimens. The resistance factor calibration is divided into the first peak and maximum peak of the load-displacement curves. For design purposes resistance values determined from the first peak should be used as they are typically more conservative.

Table 5.1. Phase I Ultimate Failure Load of GFRP Channel Specimens with Monotonic Loading in the Axial and Transverse Directions.

Speciman	Capacity (lbs)	Max Capacity (lbs)	Speciman	Capacity (lbs)	Max Capacity (lbs)	Speciman	Capacity (lbs)	Max Capacity (lbs)
AXIAL-01-1	2090	2493	AXIAL-02-1	2118	2493	AXIAL-03-1	2103	2711
AXIAL-01-2	2206	2789	AXIAL-02-2	2167	2228	AXIAL-03-2	2357	2839
AXIAL-01-3	2080	2520	AXIAL-02-3	2473	3063	AXIAL-03-3	2296	2920
AXIAL-01-4	2175	2650	AXIAL-02-4	2458	2946	AXIAL-03-4	2419	2575
AXIAL-01-5	1996	2556	AXIAL-02-5	2302	3273	AXIAL-03-5	2057	2650
AXIAL-01-6	2465	2571	AXIAL-02-6	2286	2524	AXIAL-03-6	3136	3140
AXIAL-01-7	2357	2465	AXIAL-02-7	2048	2535	AXIAL-03-7	2680	2960
AXIAL-01-8	2109	2508	AXIAL-02-8	2501	2763	AXIAL-03-8	2200	2403
AXIAL-01-9	2214	2381	AXIAL-02-9	2476	2823	AXIAL-03-9	2669	2714
AXIAL-01-10	2455	2823	AXIAL-02-10	2637	3121	AXIAL-03-10	2569	2602
Average	2215	2576		2347	2777		2449	2751
Std Dev	162	140		192	330		326	216

Speciman	Capacity (lbs)	Max Capacity (lbs)	Speciman	Capacity (lbs)	Max Capacity (lbs)	Speciman	Capacity (lbs)	Max Capacity (lbs)
TRANS-01-1	2071	2161	TRANS-02-1	2091	2100	TRANS-03-1	2763	2772
TRANS-01-2	2394	2406	TRANS-02-2	1813	2315	TRANS-03-2	2754	2763
TRANS-01-3	2634	2667	TRANS-02-3	2529	2564	TRANS-03-3	2708	2738
TRANS-01-4	2852	2865	TRANS-02-4	2829	2879	TRANS-03-4	2586	2627
TRANS-01-5	2768	2776	TRANS-02-5	2585	2617	TRANS-03-5	2283	2305
TRANS-01-6	2476	2500	TRANS-02-6	2874	2905	TRANS-03-6	2546	2567
TRANS-01-7	2317	2338	TRANS-02-7	2498	2517	TRANS-03-7	2607	2645
TRANS-01-8	2538	2564	TRANS-02-8	2587	2622	TRANS-03-8	3152	3158
TRANS-01-9	3347	3362	TRANS-02-9	2840	2844	TRANS-03-9	2593	2616
TRANS-01-10	2617	2649	TRANS-02-10	2541	2562	TRANS-03-10	2441	2461
Average	2601	2629		2519	2593		2643	2665
Std Devation	345	332		336	252		230	225

Table 5.2. Phase I Ultimate Failure Load of GFRP Thickened Plate Members with Monotonic Loading in the Axial Direction.

Specimen	Capacity (lbs)
AXIAL-04-1	15655
AXIAL-04-2	14195
AXIAL-04-3	16229
AXIAL-04-4	16607
AXIAL-04-5	15021
AXIAL-04-6	13878
AXIAL-04-7	14711
AXIAL-04-8	13430
AXIAL-04-9	15931
AXIAL-04-10	12579
Average	14824
Std Dev	1308

Table 5.3. Phase II Residual Connection Capacity of Members Subject to Unidirectional Cyclic Loading

Specimen	Capacity (lbs)	Max Capacity (lbs)	Specimen	Capacity (lbs)	Max Capacity (lbs)
AXIAL-01-25	2835	2838	TRANS-01-25	2931	2934
AXIAL-02-25	2462	3022	TRANS-02-25	3185	3191
AXIAL-03-25	2161	3141	TRANS-03-25	3220	3236
AXIAL-01-50	2934	2934	TRANS-01-50	2057	2362
AXIAL-02-50	3016	3016	TRANS-02-50	2001	2285
AXIAL-03-50	2558	2558	TRANS-03-50	2083	2394
AXIAL-01-75	2295	2295	TRANS-01-75	2275	2523
AXIAL-02-75	2740	2740	TRANS-02-75	2573	2574
AXIAL-03-75	2575	2575	TRANS-03-75	2163	2465
Average-25	**2486**	**3000**	Average-25	**3112**	**3120**
Std Dev-25	338	153	Std Dev-25	158	163
Average-50	**2836**	**2836**	Average-50	**2047**	**2347**
Std Dev-50	225	244	Std Dev-50	42	56
Average-75	**2537**	**2537**	Average-75	**2337**	**2521**
Std Dev-75	225	225	Std Dev-75	212	55

Table 5.4. Phase III Residual Connection Capacity of Members Subject to Multidirectional Cyclic Loading

Specimen	Capacity (lbs)	Max Capacity (lbs)	Specimen	Capacity (lbs)	Max Capacity (lbs)
MULTI-AXIAL 01-25	2742	3103	MULTI-TRANS 03-25	1954	2168
MULTI-AXIAL 02-25	2549	2549	MULTI-TRANS 03-50	2184	2595
MULTI-AXIAL 01-50	2594	3129	MULTI-TRANS 03-75	2084	2231
MULTI-AXIAL 02-50	2047	2656			
MULTI-AXIAL 01-75	1942	2774			
MULTI-AXIAL 02-75	1846	1997			
Average-25	**2646**	**2826**			
Std Dev-25	136	392			
Average-50	**2321**	**2893**			
Std Dev-50	387	334			
Average-75	**1894**	**2386**			
Std Dev-75	68	549			

Table 5.5. Resistance Factor Calibration for Specimens in Monotonic Unidirectional Load (Phase I)
Where μ = mean (kN), σ = standard deviation, COV = coefficient of variance, Φ = resistance factor

	Specimem	Test								Monte-Carlo simulation							
		First peak				Maximum peak				First peak				Maximum peak			
		μ	σ	COV	Φ	μ	σ	COV	Φ	μ	σ	COV	Φ	μ	σ	COV	Φ
β =3.5	AXIAL01	9.85	0.72	0.07	0.89	11.46	0.62	0.05	0.94	9.86	1.15	0.12	0.92	11.44	1.10	0.1	0.96
	AXIAL02	10.44	0.86	0.08	0.86	12.35	1.47	0.12	0.74	10.33	1.18	0.11	0.89	11.71	1.25	0.11	0.83
	AXIAL03	10.89	1.45	0.13	0.69	12.24	0.96	0.08	0.87	10.72	1.27	0.12	0.80	12.39	1.15	0.09	0.93
	TRANS01	11.57	1.54	0.13	0.69	11.69	1.48	0.13	0.71	11.16	1.30	0.12	0.78	11.72	1.25	0.11	0.84
	TRANS02	11.20	1.50	0.13	0.69	11.53	1.12	0.10	0.82	10.67	1.28	0.12	0.79	11.38	1.16	0.10	0.92
	TRANS03	11.76	1.02	0.09	0.85	11.86	1.00	0.08	0.86	11.35	1.16	0.10	0.92	11.38	1.16	0.10	0.92
β =3.0	AXIAL01	9.85	0.72	0.07	0.90	11.46	0.62	0.05	0.94	9.88	1.15	0.12	0.93	11.44	1.10	0.10	0.97
	AXIAL02	10.44	0.86	0.08	0.88	12.35	1.47	0.12	0.78	10.35	1.18	0.11	0.91	11.74	1.25	0.11	0.86
	AXIAL03	10.89	1.45	0.13	0.73	12.24	0.96	0.08	0.89	10.73	1.27	0.12	0.83	12.34	1.15	0.09	0.94
	TRANS01	11.57	1.54	0.13	0.73	11.69	1.48	0.13	0.76	11.17	1.30	0.12	0.81	11.69	1.25	0.11	0.86
	TRANS02	11.20	1.50	0.13	0.73	11.53	1.12	0.10	0.84	10.63	1.28	0.12	0.82	11.37	1.16	0.10	0.93
	TRANS03	11.76	1.02	0.09	0.87	11.86	1.00	0.08	0.88	11.37	1.16	0.10	0.93	11.39	1.16	0.10	0.93
β =2.5	AXIAL01	9.85	0.72	0.07	0.92	11.46	0.62	0.05	0.95	9.89	1.15	0.12	0.94	11.44	1.10	0.10	0.97
	AXIAL02	10.44	0.86	0.08	0.90	12.35	1.47	0.12	0.82	10.35	1.18	0.11	0.92	11.72	1.25	0.11	0.88
	AXIAL03	10.89	1.45	0.13	0.78	12.24	0.96	0.08	0.91	10.71	1.27	0.12	0.85	12.40	1.15	0.09	0.95
	TRANS01	11.57	1.54	0.13	0.78	11.69	1.48	0.13	0.80	11.15	1.30	0.12	0.84	11.73	1.25	0.11	0.88
	TRANS02	11.20	1.50	0.13	0.78	11.53	1.12	0.10	0.87	10.69	1.27	0.12	0.86	11.39	1.16	0.10	0.94
	TRANS03	11.76	1.02	0.09	0.89	11.86	1.00	0.08	0.90	11.39	1.16	0.10	0.94	11.37	1.16	0.10	0.94

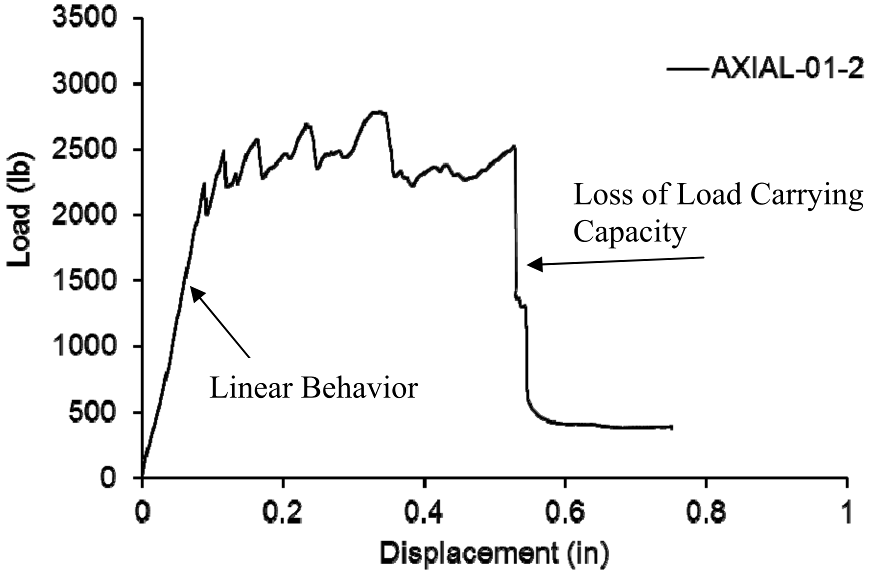

Figure 5.1. Load-Displacement Curve for Phase I Axial

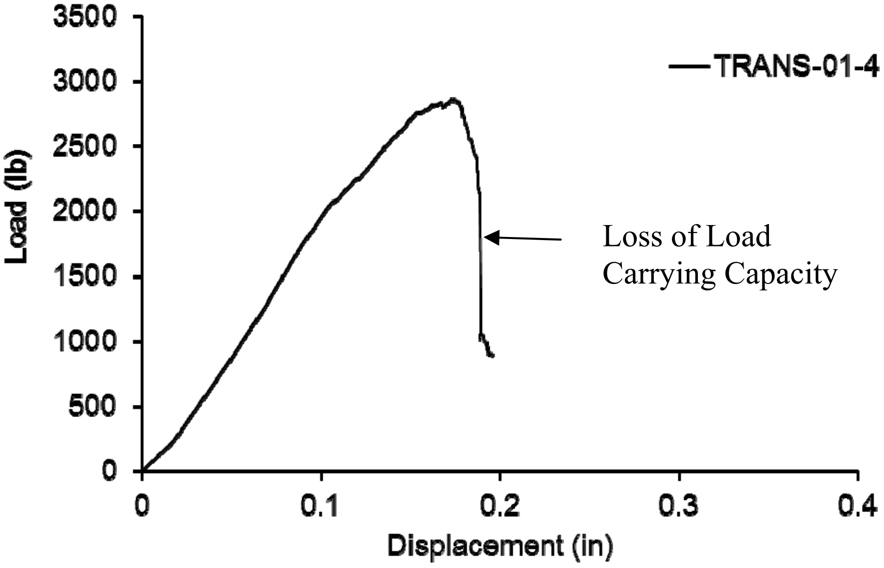

Figure 5.2. Load-Displacement Curve for Phase I Transverse

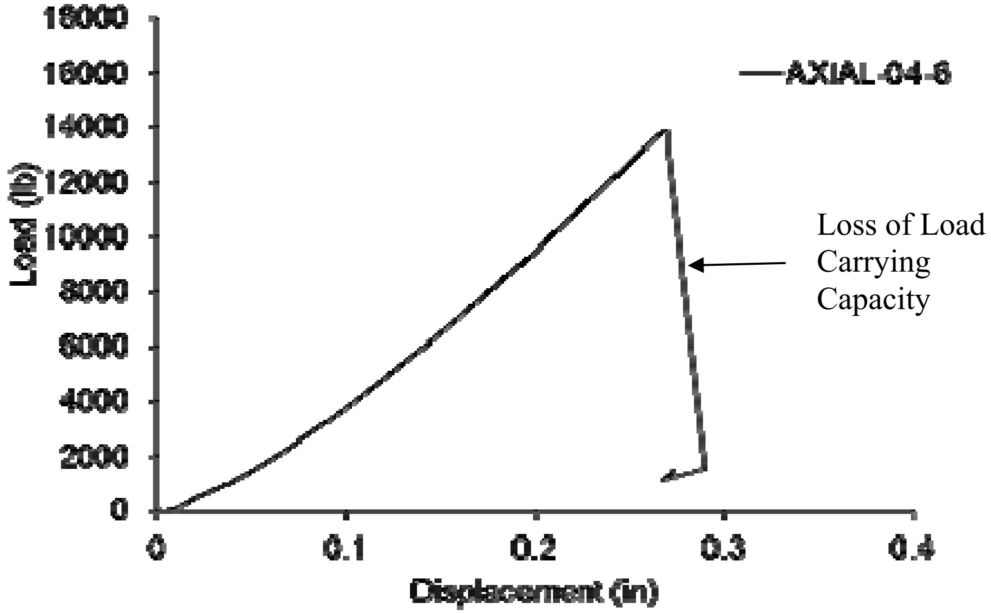

Figure 5.3. Load-Displacement Curve for Phase I Thickened Member Axial

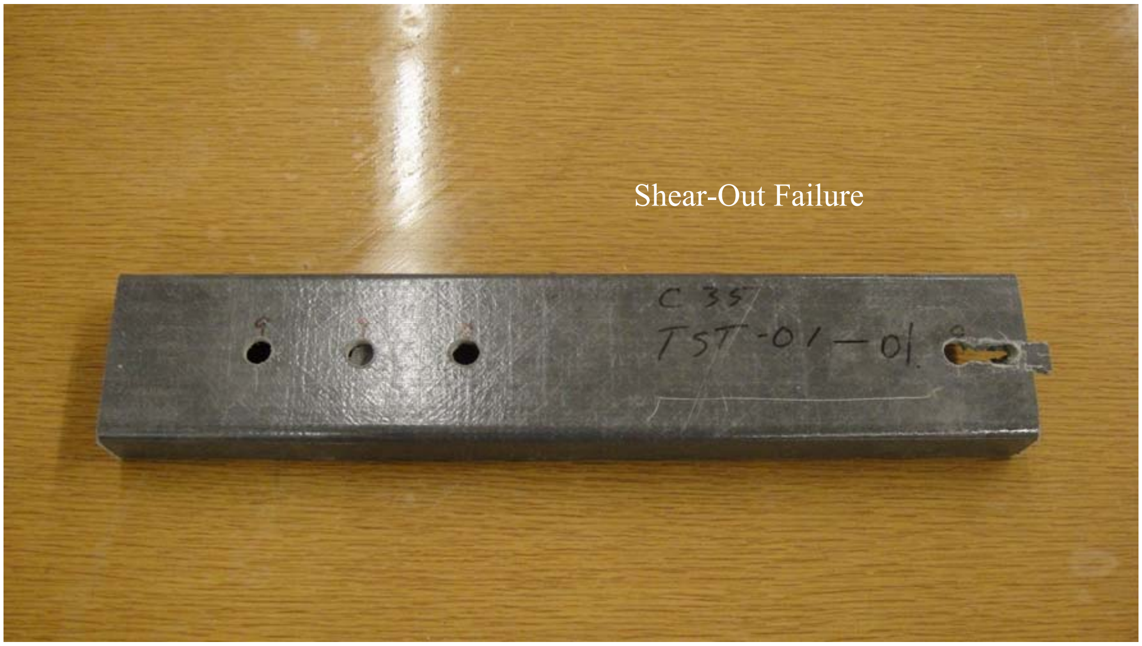

Figure 5.4. Typical Failure Mode: Monotonic Axial Load

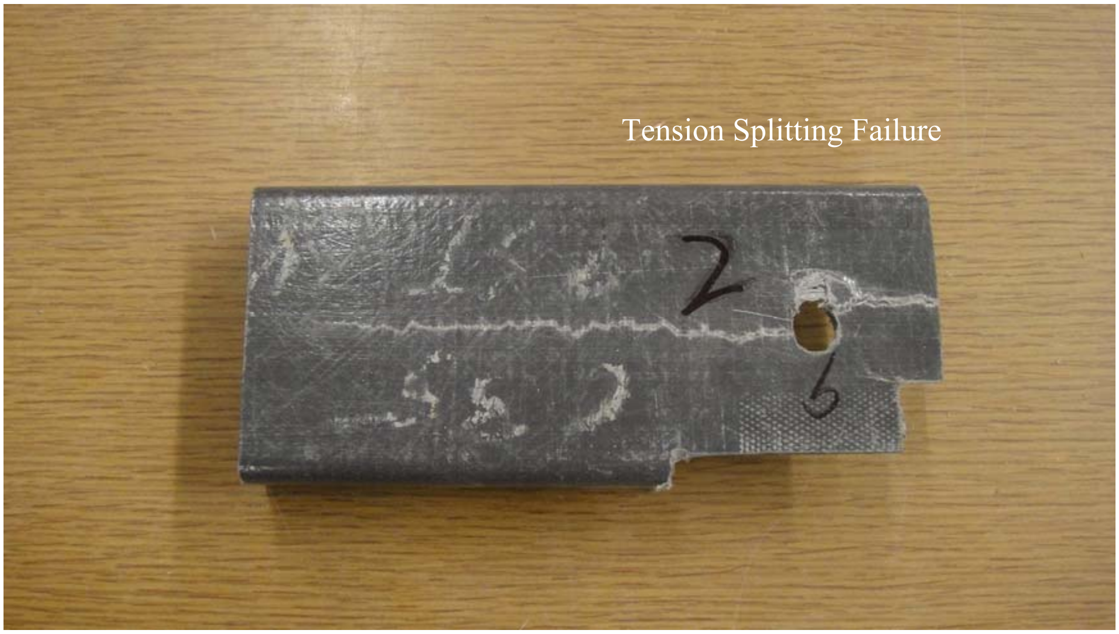

Figure 5.5. Typical Failure Mode: Monotonic Transverse Load

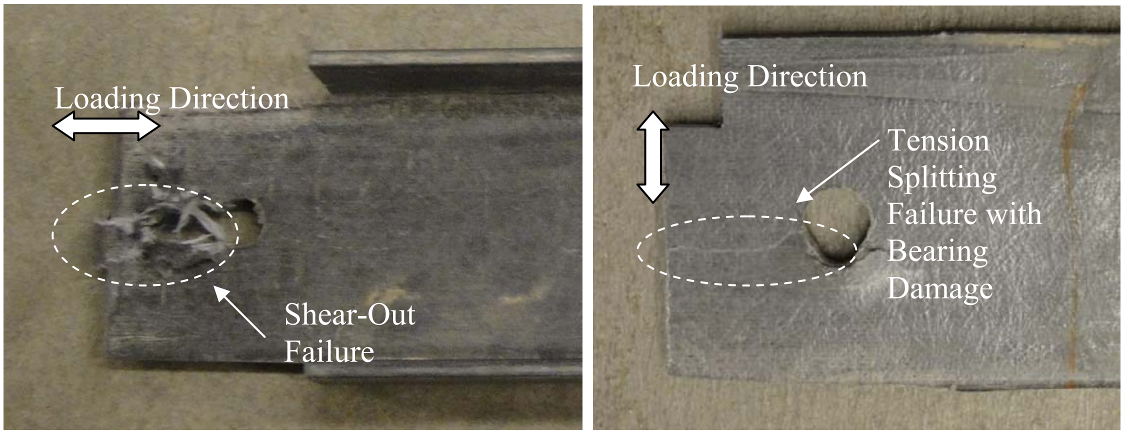

(a) (b)

Figure 5.6. Failure Mode: (a) Monotonic Axial Load; (b) Monotonic Transverse Load

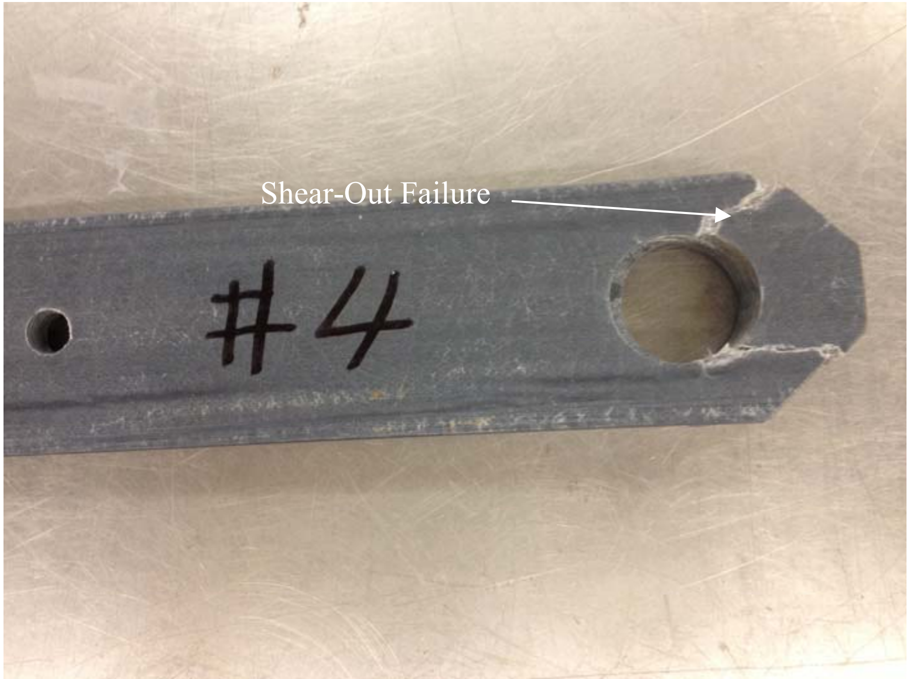

Figure 5.7. Typical Failure Mode of GFRP Thickened Plate from Axial Loading

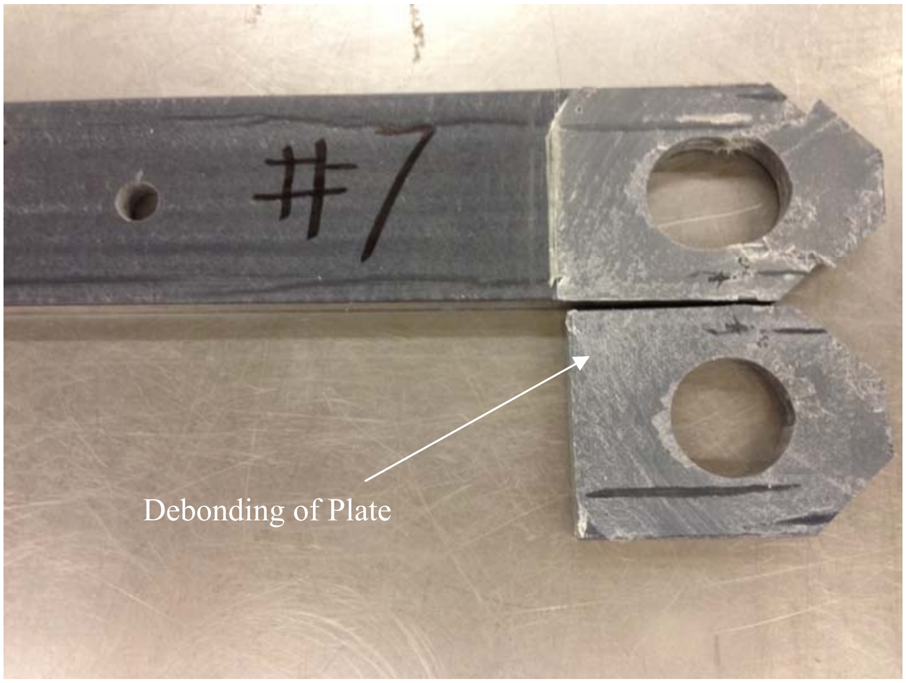

Figure 5.8. Debonding of GFRP Thickened Plate

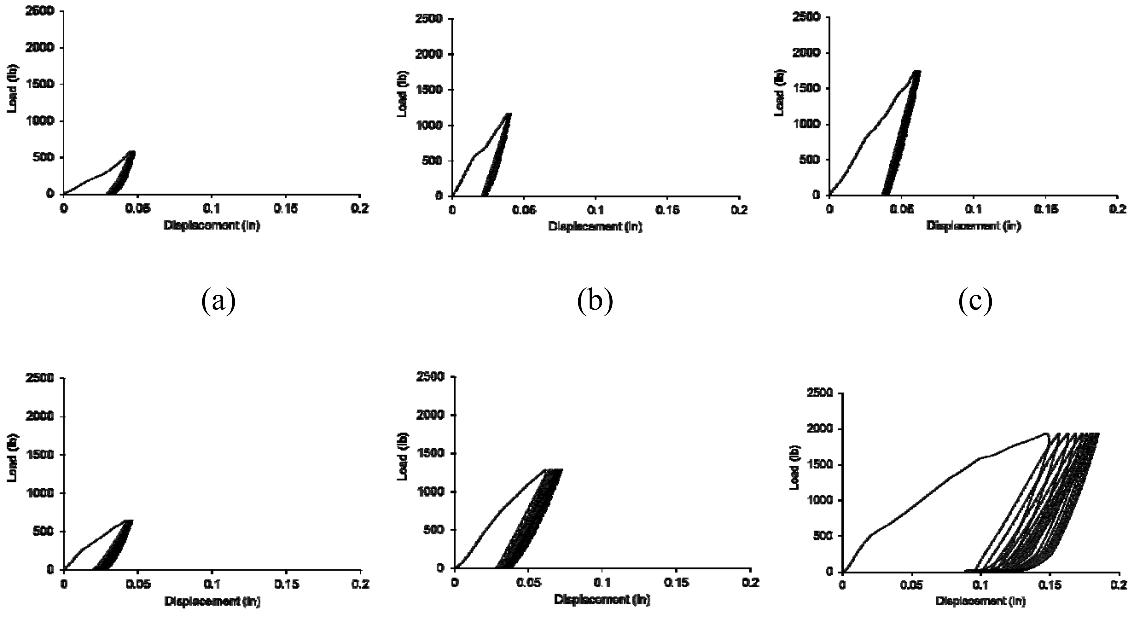

(a) (b) (c)

(d) (e) (f)

Figure. 5.9. Cyclic Unidirectional Load for Phase II Specimens: (a) axial load at 25%P_u; (b) axial load at 50%P_u; (c) axial load at 75%P_u; (d) transverse load at 25%P_u; (b) transverse load at 50%P_u; (c) transverse load at 75%P_u

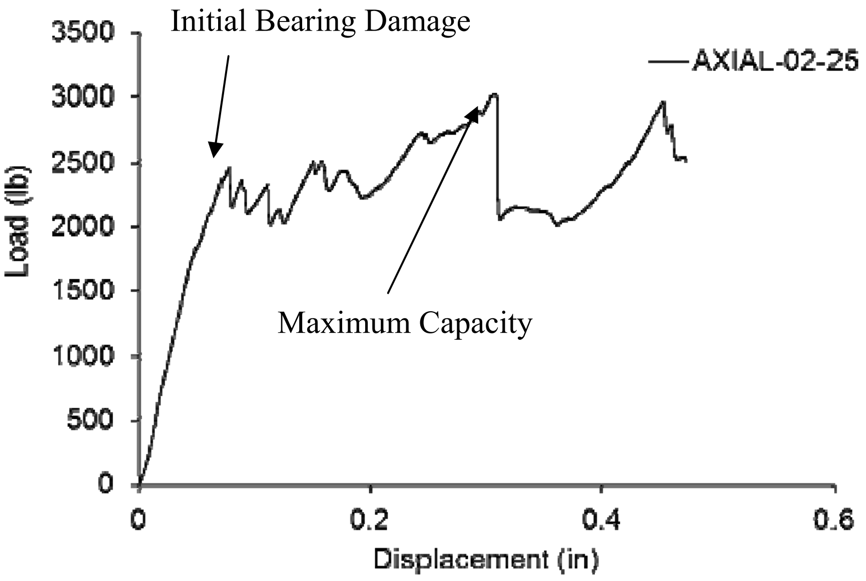

Figure 5.10. Load-Displacement Curve for Phase II Monotonic Axial Loading

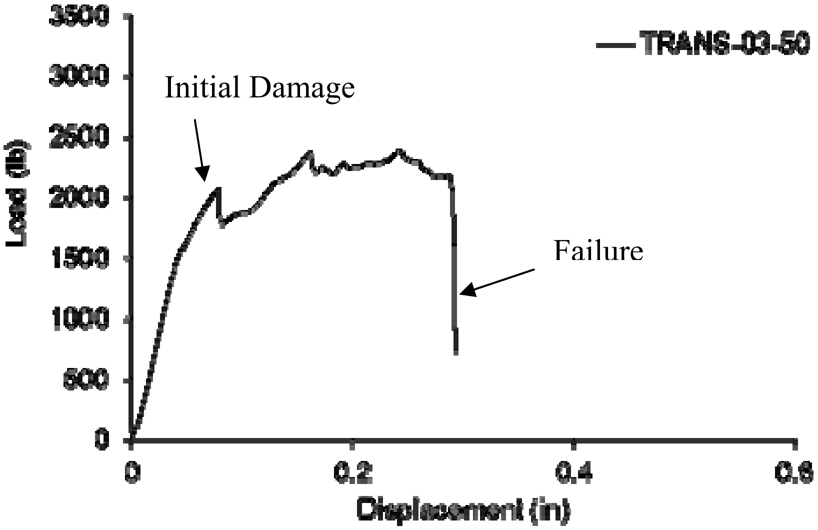

Figure 5.11. Load-Displacement Curve for Phase II Monotonic Transverse Loading

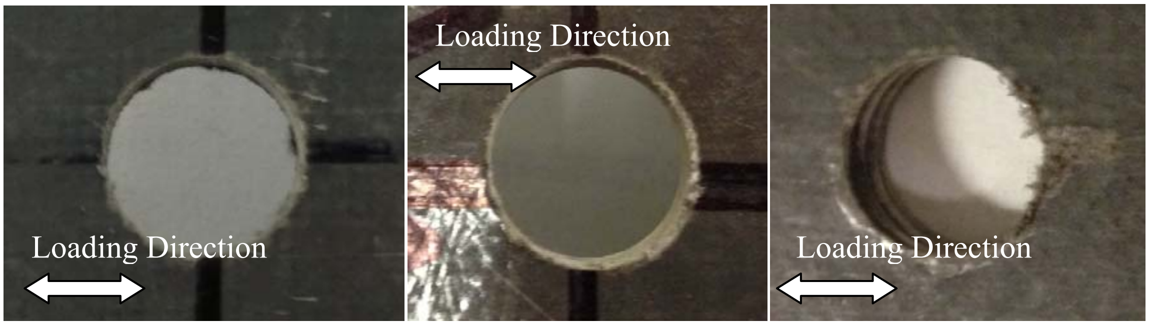

(a) (b) (c)

Figure 5.12. Damage Propagation with Load Cycles: (a) Axial Load at 25%P_u; (b) Axial Load at 50%P_u; (c) Axial Load at 75%P_u

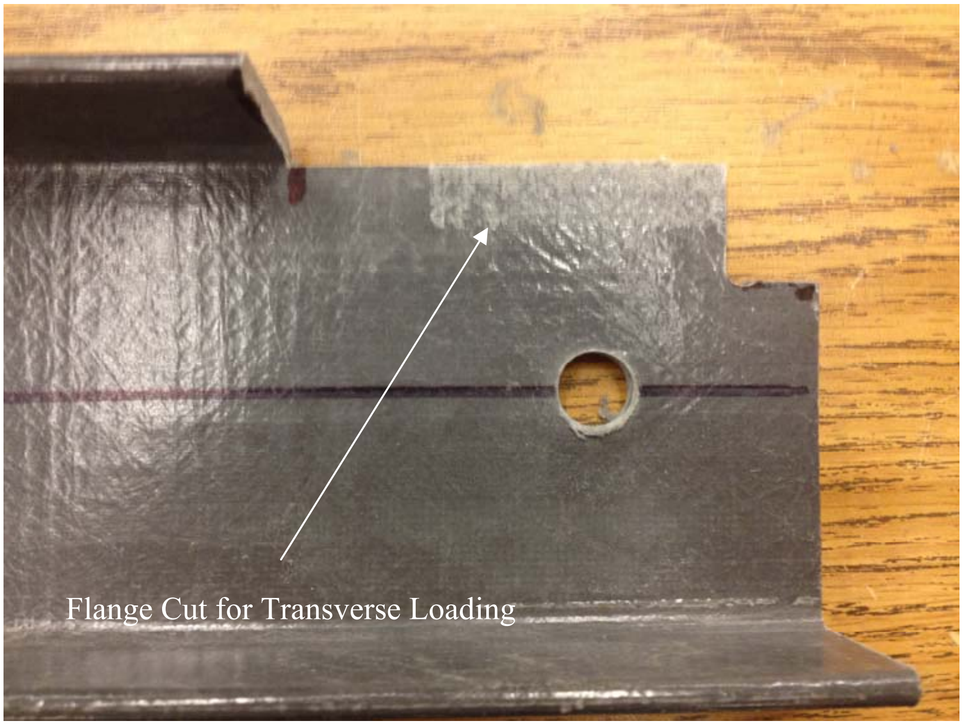

Figure 5.13. Geometry of GFRP Channel Specimens for Phase III

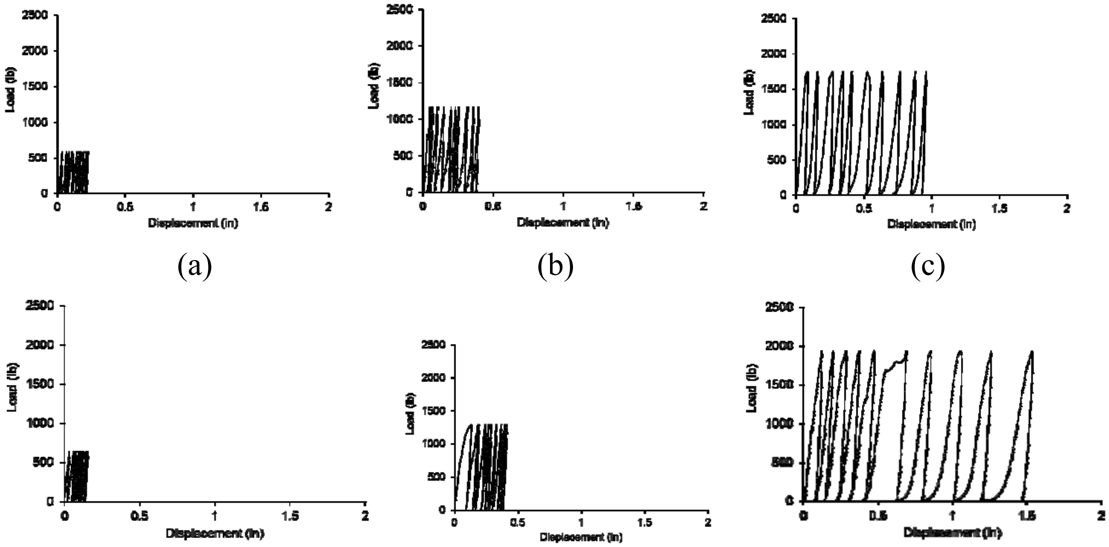

(a) (b) (c)

(d) (e) (f)

Figure. 5.14. Cyclic Multidirectional Load for Phase III Specimens: (a) axial load at 25%P_u; (b) axial load at 50%P_u; (c) axial load at 75%P_u; (d) transverse load at 25%P_u; (e) transverse load at 50%P_u; (f) transverse load at 75%P_u

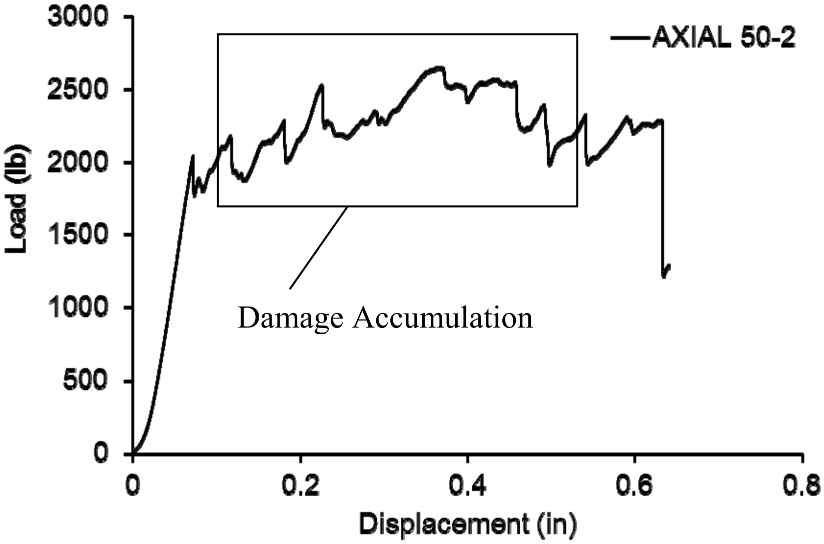

Figure 5.15. Load-Displacement Curve for Phase III Monotonic Axial Loading

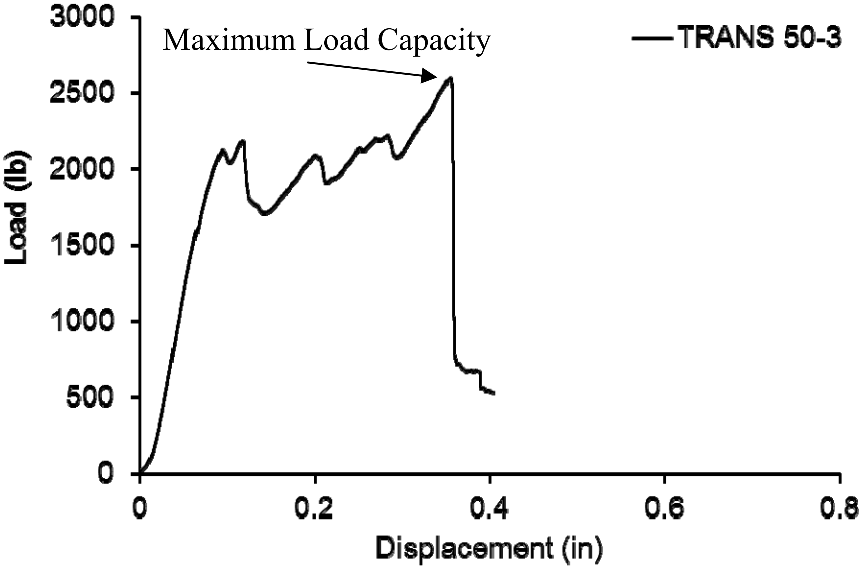

Figure 5.16. Load-Displacement Curve for Phase III Monotonic Transverse Loading

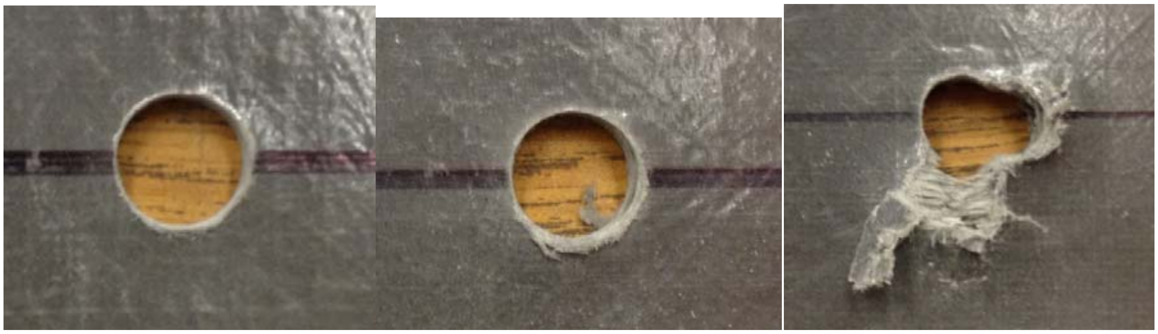

(a) (b) (c)

Figure 5.17. Damage Propagation with Load Cycles: (a) multidirectional load 25%P_u; (b) multidirectional load at 50%P_u; (c) multidirectional load at 75%P_u

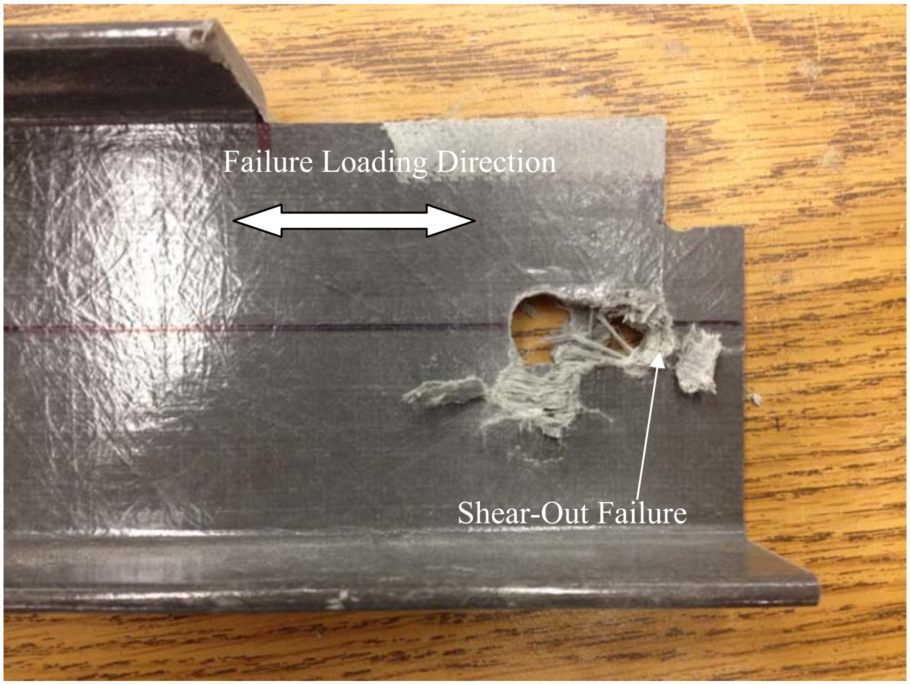

Figure 5.18. Typical Failure Mode: Monotonic Axial Load for Phase III after 75%P_u Multidirectional Cyclic Loading

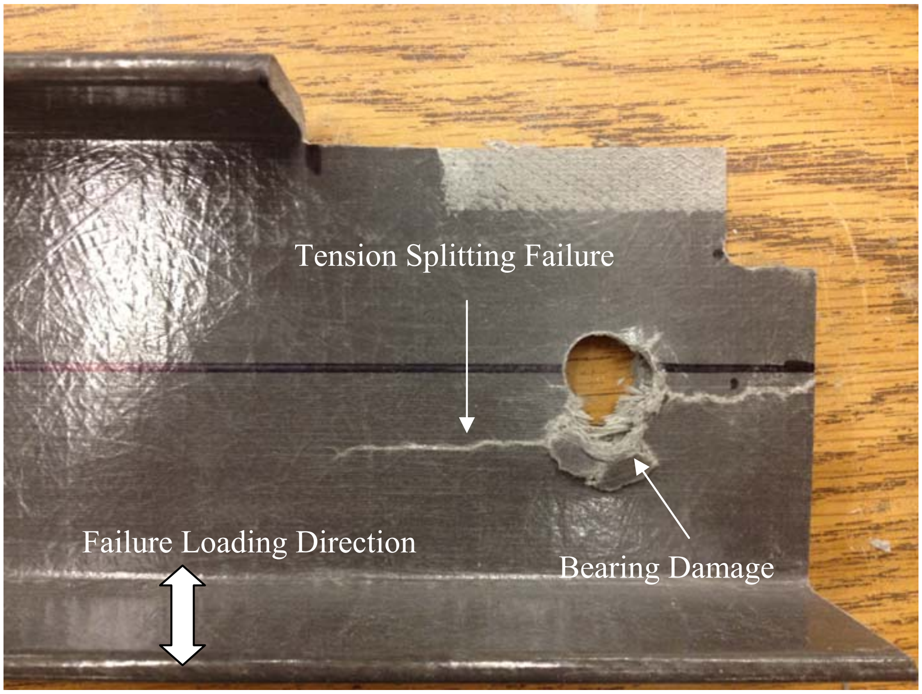

Figure 5.19. Typical Failure Mode: Monotonic Transverse Load for Phase III after 75%P_u Multidirectional Cyclic Loading

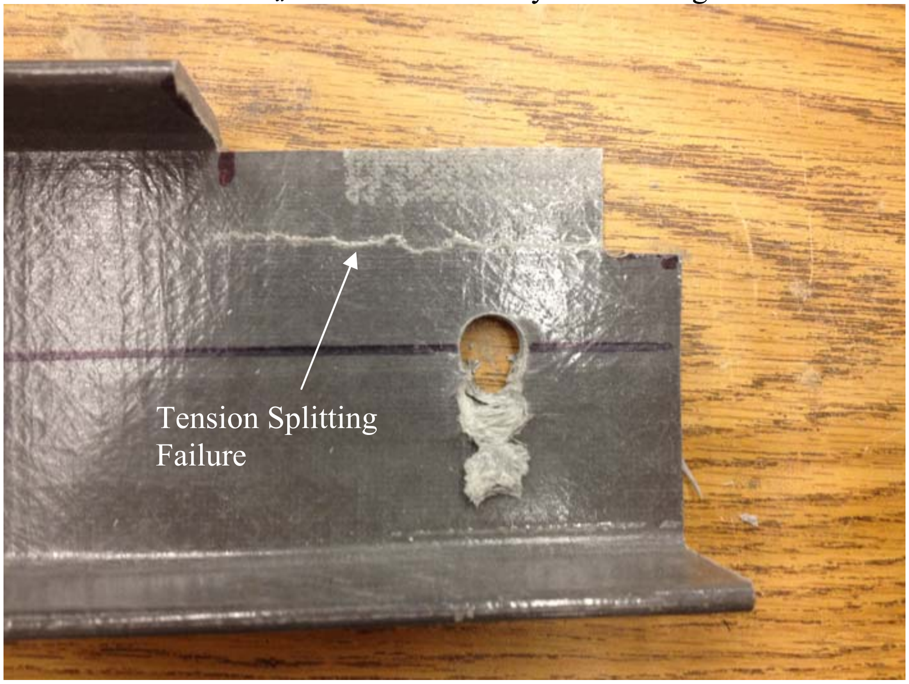

Figure 5.20. Failure Mode: Monotonic Transverse Load for Phase III after 75%P_u Multidirectional Cyclic Loading

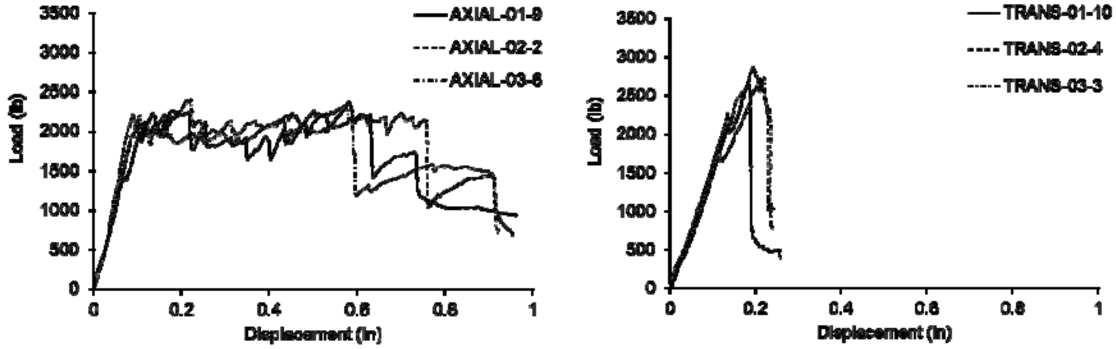

Figure 5.21. Load-displacement of Phase I-Comparison of Various Flange Geometry: (a) Axial load; (b) Transverse Load

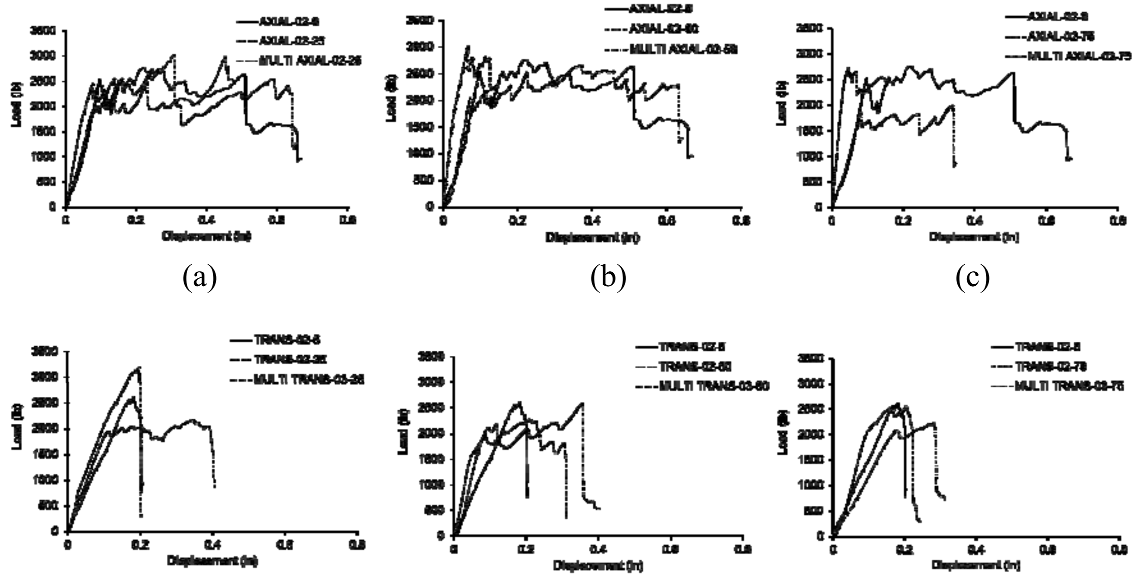

(a) (b) (c)

(d) (e) (g)

Figure 5.22. Comparison of Post-Cyclic Residual Behavior: (a) Axial Load at 25%P_u; (b) Axial Load at 50%P_u; (c) Axial Load at 75%P_u; (d) Transverse Load at 25%P_u; (e) Transverse Load at 50%P_u; (f) Transverse Load at 75%P_u

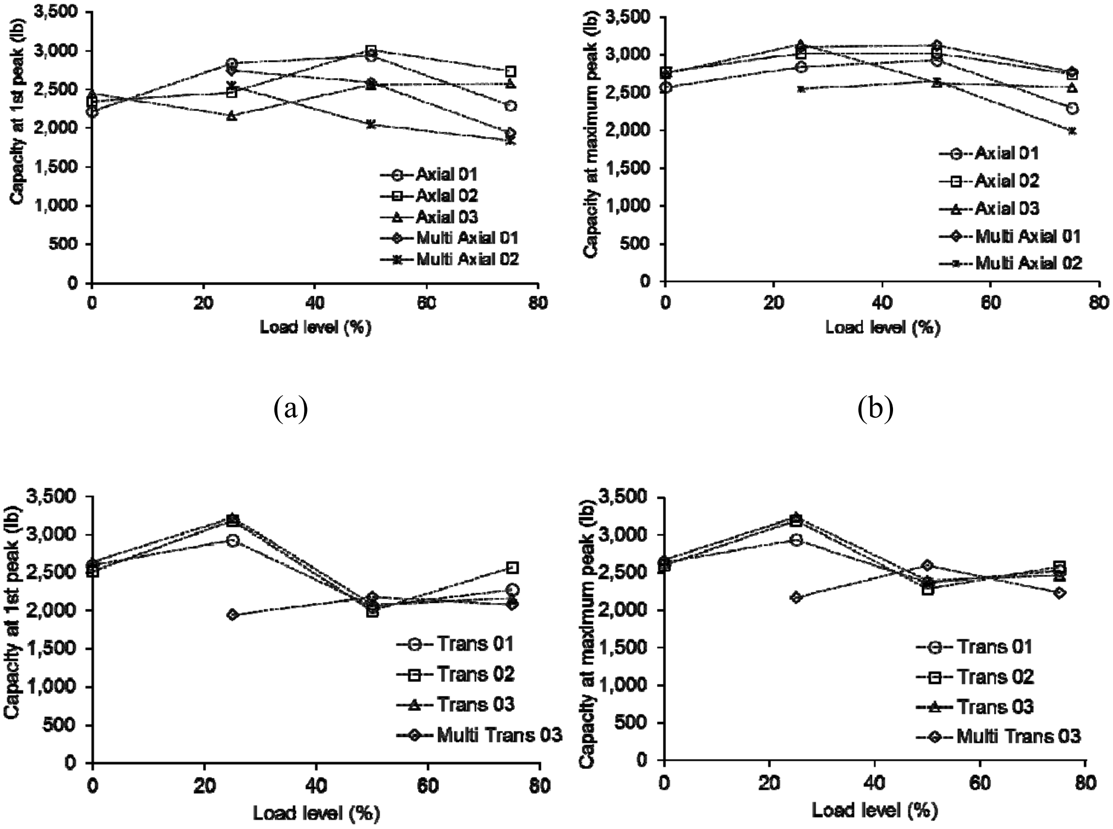

(a) (b)

(c) (d)

Figure 5.23. Effect of Cyclic Loading on Residual Capacity: (a) Axial Load at 1st Peak; (b) Axial Load at Maximum Peak; (c) Transverse Load at 1st Peak; (d) Transverse Load at Maximum Peak

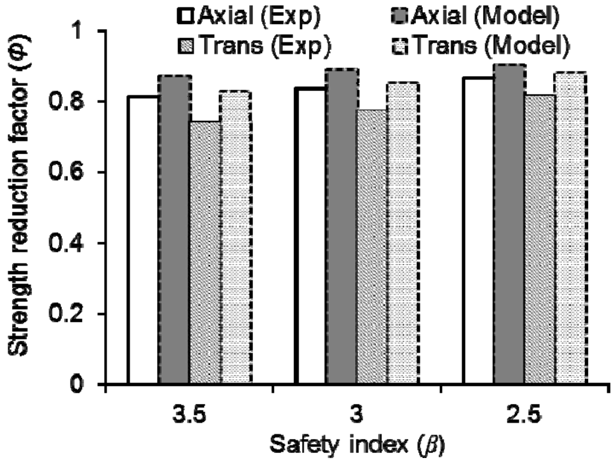

Figure 5.24. Comparison of Strength Reduction Factor (Φ) Based on Phase I

6. Summary and Conclusion

6.1 Summary

The connection capacity of Glass Fiber Reinforced Polymer (GFRP) structural channel members has been studied through experimental and analytical investigations. A total of 97 GFRP specimens were tested in the axial and transverse directions to determine strength capacity and was divided into three phases. Post-cyclic residual behavior was studied after unidirectional (Phase II) and multidirectional (Phase III) cyclic loading was performed on the test specimens. The effects of various parameters including various flange configurations, loading direction, and level of cyclic loading have been evaluated. The change in stiffness from the tests is also investigated due to unloading and reloading at various load levels.

A GFRP channel structural channel member with a single bolted connection near the edge is vulnerable to premature failure caused by high stress concentrations leading to initial bearing failure. Bearing failure is an undesirable failure mode because it fails to utilize the entire material strength of the member. The proposed solution to this problem is to increase the number of bolts used for the joint as well as adjusting the edge distance for optimal performance.

6.2 Conclusions

The following conclusions are drawn from the experimental study of GFRP structural channel members:

1. The load-displacement curves indicate linear behavior up to initial failure when testing the GFRP channel members in the axial and transverse directions.
2. The initial failure mechanism for the bolted connection results in initial bearing failure and is represented by the first peak on the load-displacement curve.
3. Progressive damage occurs and the specimens exhibit inelastic deformation around the bolt hole and does not yield similar to steel.
4. Testing show that using different flange configuration which consists of cutting the flange at various degrees, do not affect the overall connection capacity in the GFRP specimens in both the axial and transverse directions.
5. Monotonic axial loading results in a two phase failure mechanism. Initial bearing failure is observed followed by shear-out failure which results in significant loss of load carrying capacity.
6. Monotonic transverse loading also results in a two phase failure mechanism. Initial bearing failure first occurs followed by net tension failure. The net tension failure is characterized by splitting in the transverse direction of the load. The majority of the testing show the splitting occurring at the bolt hole with a couple of instance where the splitting occurred below the bolt hole and directly above the fixture clamp.
7. The thickened GFRP members with an additional bonded plate exhibit significantly increase in strength capacity which is expected due to the increased area. The failure mode observed is debonding of the bonded plate followed immediately by shear-out failure. This is expected due to a sudden reduction in

area. Initial bearing failure is not witnessed similar to all the other specimens tested.

8. Initial failure represented by the first peak on the load-displacement curve does not necessarily constitute the maximum capacity. After initial failure the specimen can still achieve a higher maximum capacity which is represented by the maximum peak on the load-displacement curve. This occurs in both the axial and transverse directions.
9. After initial failure the specimens experience a period of damage accumulation which is represented by a region of multiple peaks in the load-displacement curve until final failure when the specimens loses a significant amount of load-carrying capacity.
10. The load testing results do not indicate a reduction in strength capacity when comparing Phase II to Phase I. In some instances specimens from Phase II after unidirectional cyclic loading lead to higher connection capacities.
11. For Phase II axial loading the results indicate a reduction in residual strength capacity as the load level percent for cyclic unidirectional loading is increased.
12. For Phase III axial load to failure, the results indicate a reduction in residual strength capacity as the load level percent for multidirectional loading is increased.
13. The residual connection capacity of Phase III transverse specimens loaded to failure is significantly reduced after multidirectional cyclic loading when compared to Phase II and Phase I.

14. The residual connection capacity of Phase III axial specimens loaded to failure has a small reduction after multidirectional cyclic loading when compared to only unidirectional loading in Phase II.
15. The post-cyclic residual failure mode is the same as specimens from Phase I, which is shear-out and net tension failure. The only difference is deflections and damage accumulation that occur from the cyclic loading.
16. Minor stiffness degradation occurs from multidirectional cyclic loading.

6.3 Recommendations for Future Work

Additional research is required to fully understand the behavior of GFRP structural members with bolted connections. The following aspects should be addressed:

1. Developing a finite element model to predict damage accumulation around the bolt hole.
2. Investigating GFRP connections with multiple bolts to fully optimize the material strength in the member.
3. Investigation of edge distance on GFRP connections to fully optimize the material strength capacity.
4. Evaluation of the stress concentrations experimentally and numerically around the bolt hole.
5. Investigation of simultaneous multidirectional monotonic and cyclic loading on the connection capacity.
6. Generate and establish a complete design standard used for practicing structural engineers for bolted GFRP connection

Appendix A. Load Displacement Curves for Phase I – Axial and Transverse

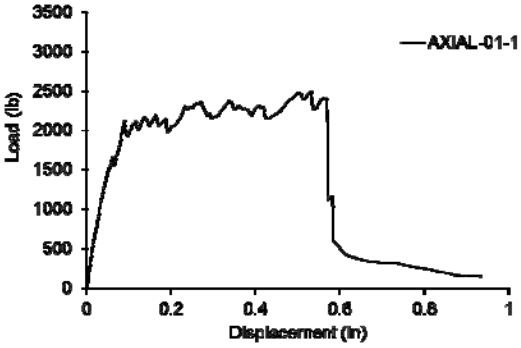

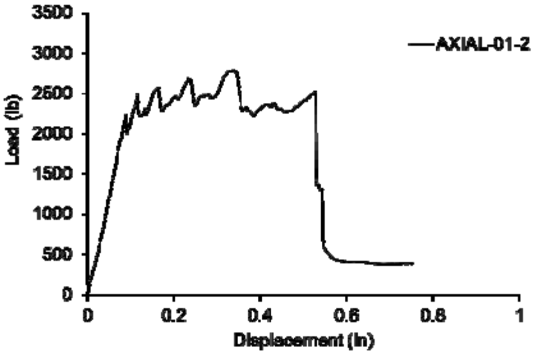

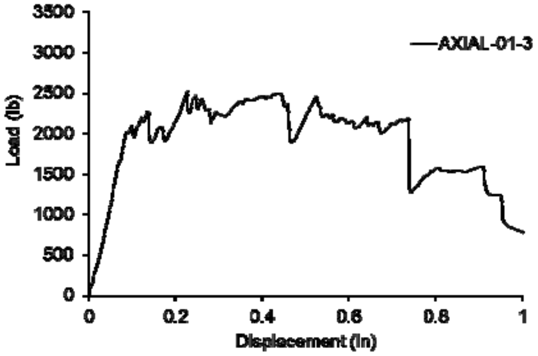

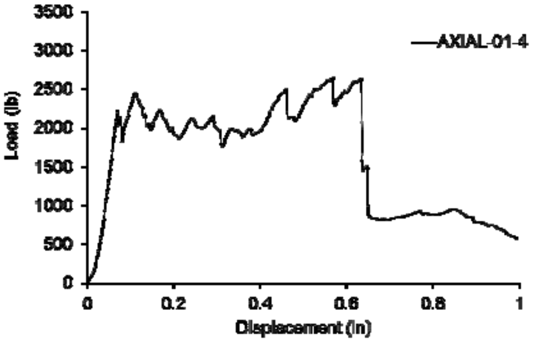

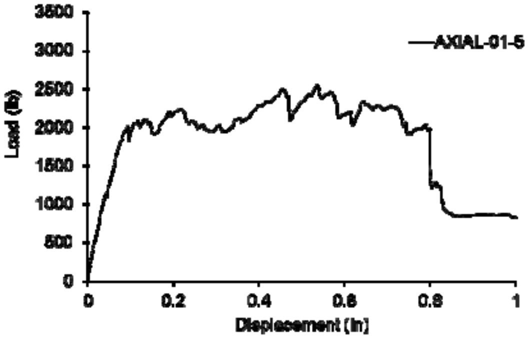

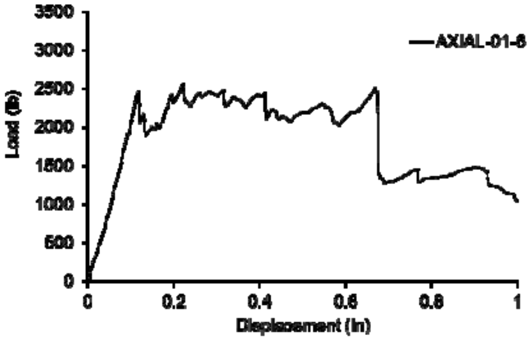

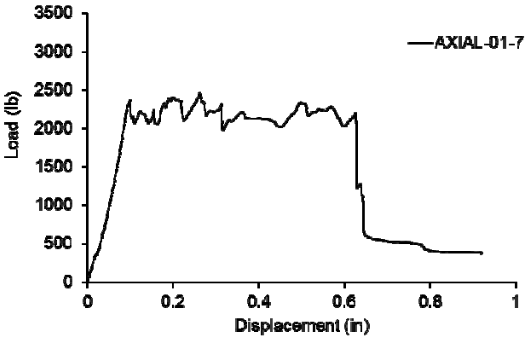
AXIAL-01-7
Load (lb)
0
500
1000
1500
2000
2500
3000
3500
Displacement (in)
0
0.2
0.4
0.6
0.8
1

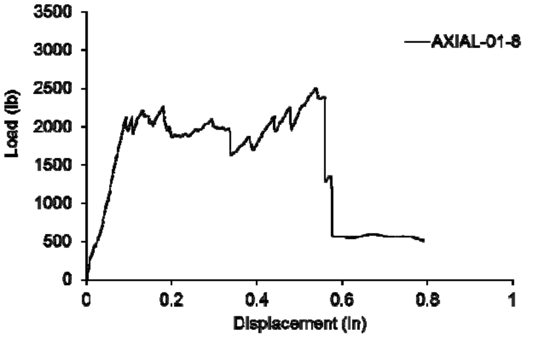
AXIAL-01-8
Load (lb)
0
500
1000
1500
2000
2500
3000
3500
Displacement (in)
0
0.2
0.4
0.6
0.8
1

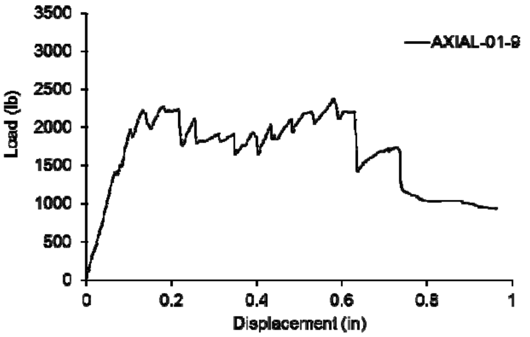
AXIAL-01-9
Load (lb)
0
500
1000
1500
2000
2500
3000
3500
Displacement (in)
0
0.2
0.4
0.6
0.8
1

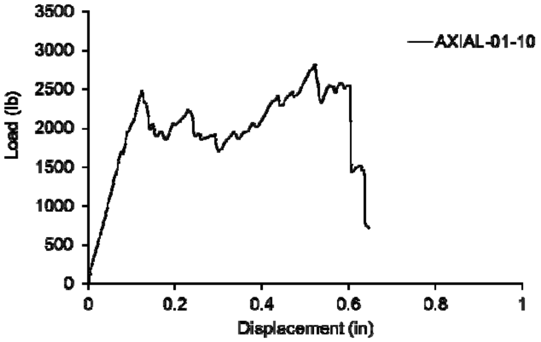
AXIAL-01-10
Load (lb)
0
500
1000
1500
2000
2500
3000
3500
Displacement (in)
0
0.2
0.4
0.6
0.8
1

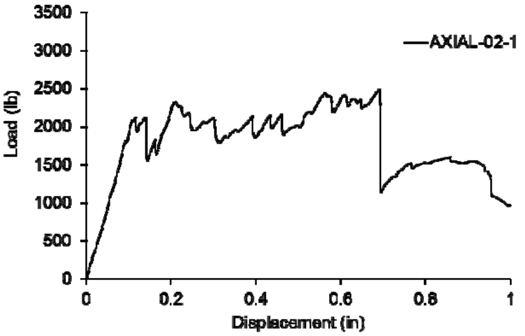
AXIAL-02-1
Load (lb)
0
500
1000
1500
2000
2500
3000
3500
Displacement (in)
0
0.2
0.4
0.6
0.8
1

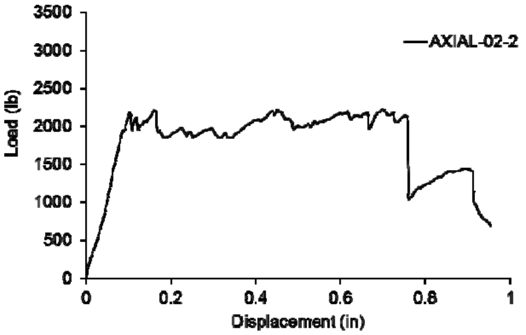
AXIAL-02-2
Load (lb)
0
500
1000
1500
2000
2500
3000
3500
Displacement (in)
0
0.2
0.4
0.6
0.8
1

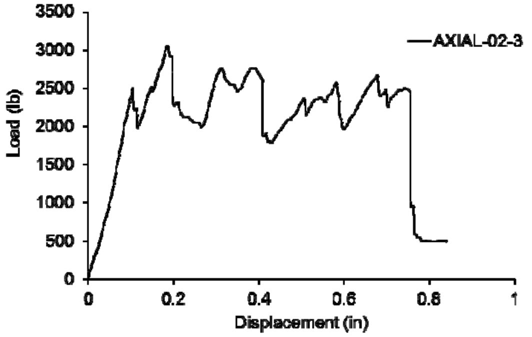
AXIAL-02-3
Load (lb)
3500
3000
2500
2000
1500
1000
500
0
0
0.2
0.4
0.6
0.8
1
Displacement (in)

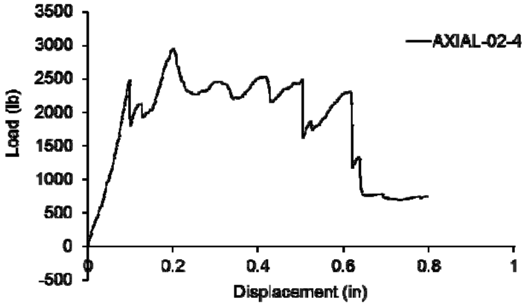
AXIAL-02-4
Load (lb)
3500
3000
2500
2000
1500
1000
500
0
-500
0
0.2
0.4
0.6
0.8
1
Displacement (in)

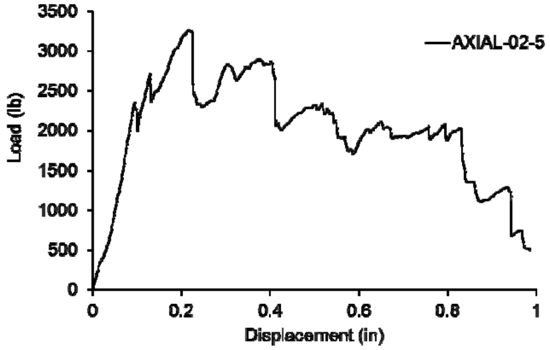
AXIAL-02-5
Load (lb)
3500
3000
2500
2000
1500
1000
500
0
0
0.2
0.4
0.6
0.8
1
Displacement (in)

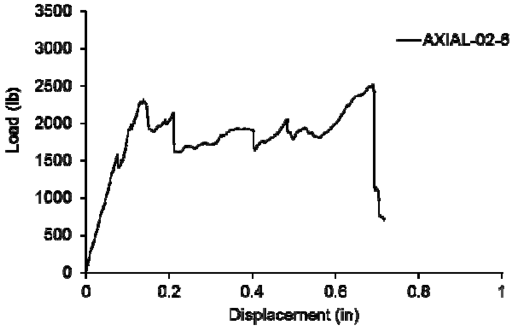
AXIAL-02-6
Load (lb)
3500
3000
2500
2000
1500
1000
500
0
0
0.2
0.4
0.6
0.8
1
Displacement (in)

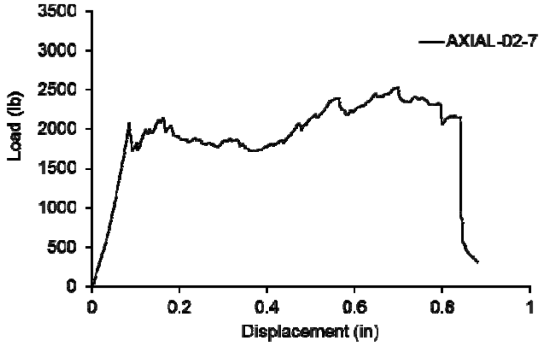
AXIAL-02-7
Load (lb)
3500
3000
2500
2000
1500
1000
500
0
0
0.2
0.4
0.6
0.8
1
Displacement (in)

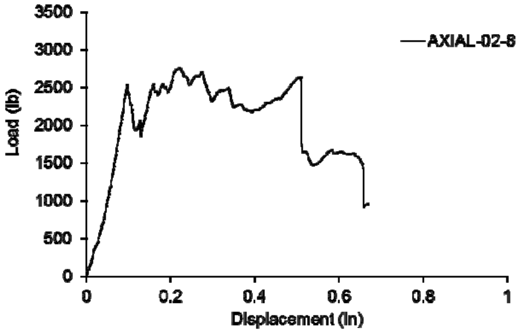
AXIAL-02-8
Load (lb)
3500
3000
2500
2000
1500
1000
500
0
0
0.2
0.4
0.6
0.8
1
Displacement (in)

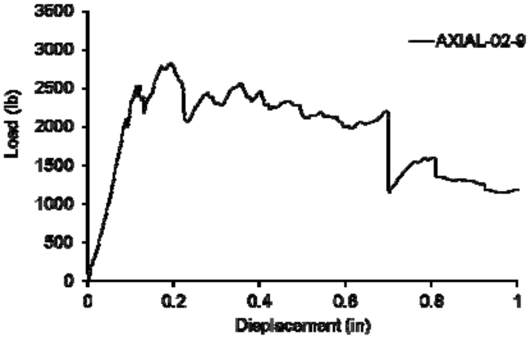
3500
3000
2500
2000
1500
1000
500
0
Load (lb)
0
0.2
0.4
0.6
0.8
1
Displacement (in)
AXIAL-02-9

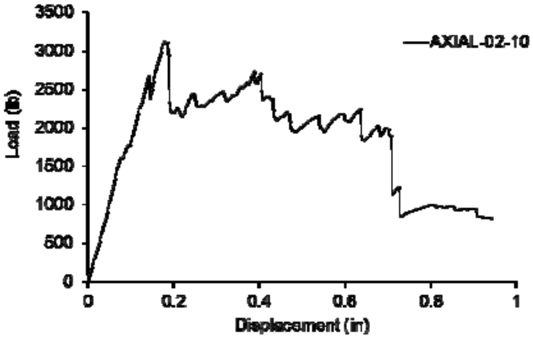
3500
3000
2500
2000
1500
1000
500
0
Load (lb)
0
0.2
0.4
0.6
0.8
1
Displacement (in)
AXIAL-02-10

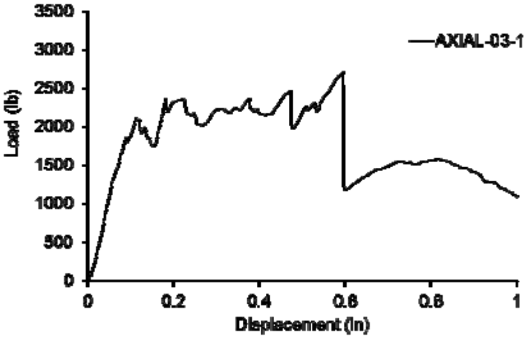
3500
3000
2500
2000
1500
1000
500
0
Load (lb)
0
0.2
0.4
0.6
0.8
1
Displacement (in)
AXIAL-03-1

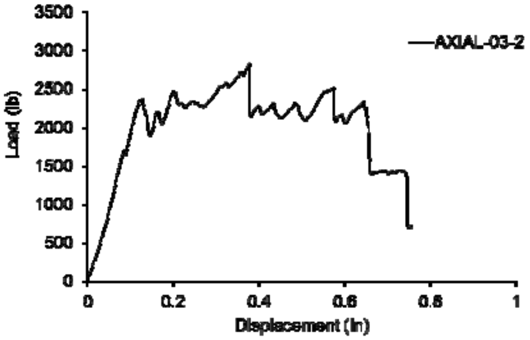
3500
3000
2500
2000
1500
1000
500
0
Load (lb)
0
0.2
0.4
0.6
0.8
1
Displacement (in)
AXIAL-03-2

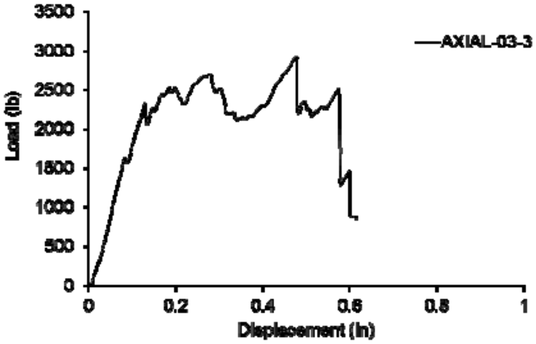
3500
3000
2500
2000
1500
1000
500
0
Load (lb)
0
0.2
0.4
0.6
0.8
1
Displacement (in)
AXIAL-03-3

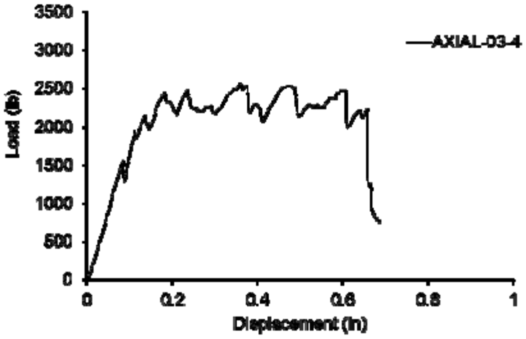
3500
3000
2500
2000
1500
1000
500
0
Load (lb)
0
0.2
0.4
0.6
0.8
1
Displacement (in)
AXIAL-03-4

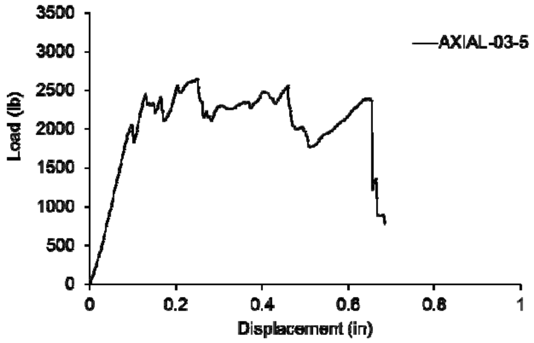
AXIAL-03-5
Load (lb)
3500
3000
2500
2000
1500
1000
500
0
Displacement (in)
0
0.2
0.4
0.6
0.8
1

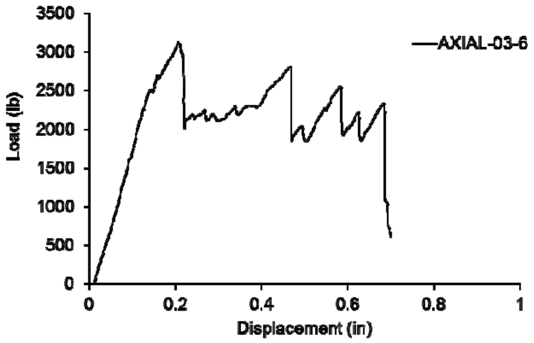
AXIAL-03-6
Load (lb)
3500
3000
2500
2000
1500
1000
500
0
Displacement (in)
0
0.2
0.4
0.6
0.8
1

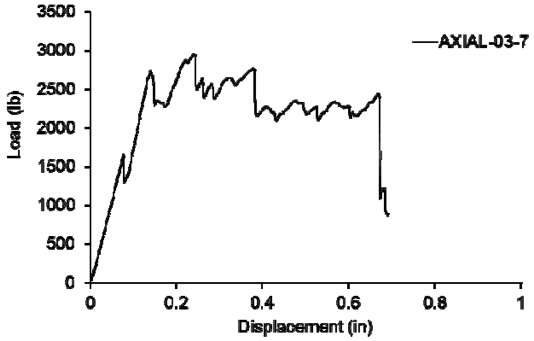
AXIAL-03-7
Load (lb)
3500
3000
2500
2000
1500
1000
500
0
Displacement (in)
0
0.2
0.4
0.6
0.8
1

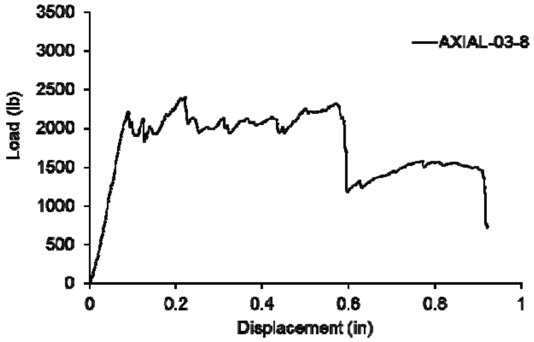
AXIAL-03-8
Load (lb)
3500
3000
2500
2000
1500
1000
500
0
Displacement (in)
0
0.2
0.4
0.6
0.8
1

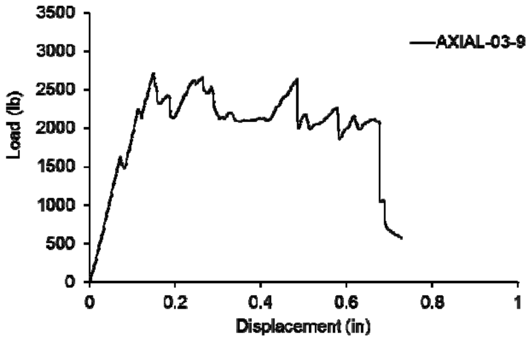
AXIAL-03-9
Load (lb)
3500
3000
2500
2000
1500
1000
500
0
Displacement (in)
0
0.2
0.4
0.6
0.8
1

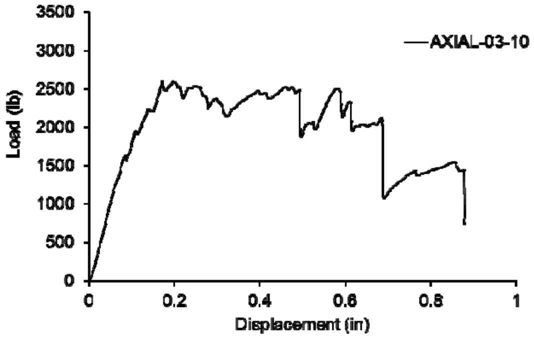
AXIAL-03-10
Load (lb)
3500
3000
2500
2000
1500
1000
500
0
Displacement (in)
0
0.2
0.4
0.6
0.8
1

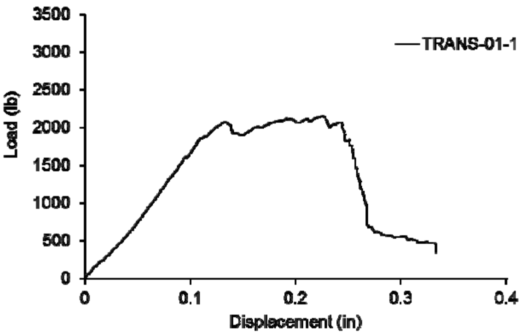
TRANS-01-1
Load (lb)
3500
3000
2500
2000
1500
1000
500
0
0
0.1
0.2
0.3
0.4
Displacement (in)

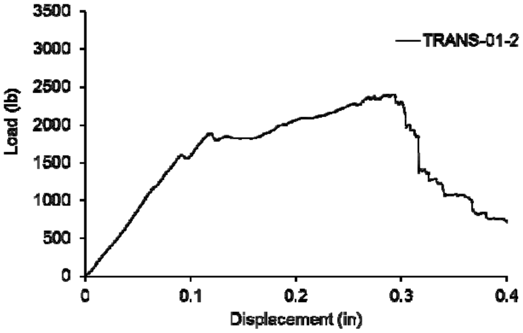
TRANS-01-2
Load (lb)
3500
3000
2500
2000
1500
1000
500
0
0
0.1
0.2
0.3
0.4
Displacement (in)

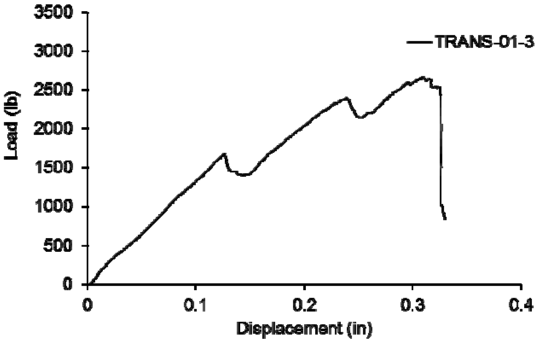
TRANS-01-3
Load (lb)
3500
3000
2500
2000
1500
1000
500
0
0
0.1
0.2
0.3
0.4
Displacement (in)

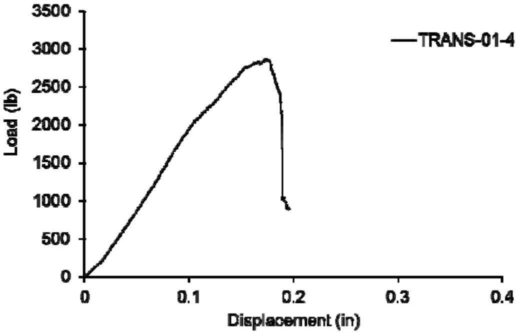
TRANS-01-4
Load (lb)
3500
3000
2500
2000
1500
1000
500
0
0
0.1
0.2
0.3
0.4
Displacement (in)

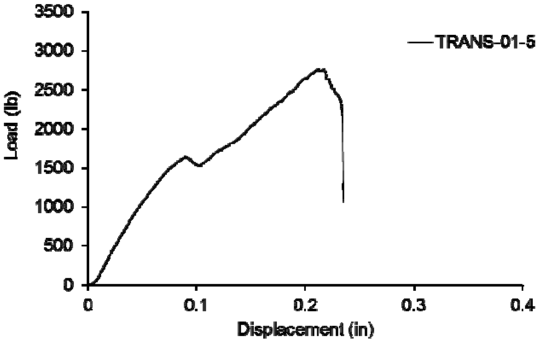
TRANS-01-5
Load (lb)
3500
3000
2500
2000
1500
1000
500
0
0
0.1
0.2
0.3
0.4
Displacement (in)

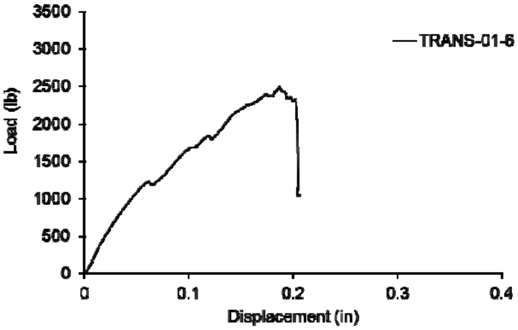
TRANS-01-6
Load (lb)
3500
3000
2500
2000
1500
1000
500
0
0
0.1
0.2
0.3
0.4
Displacement (in)

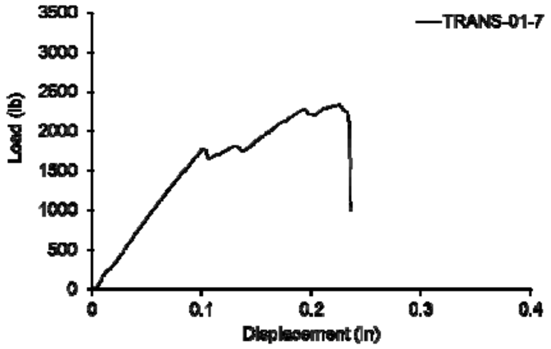
3500
3000
2500
2000
1500
1000
500
0
Load (lb)
0
0.1
0.2
0.3
0.4
Displacement (in)
TRANS-01-7

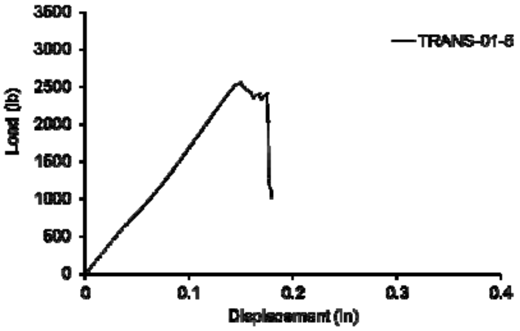
3500
3000
2500
2000
1500
1000
500
0
Load (lb)
0
0.1
0.2
0.3
0.4
Displacement (in)
TRANS-01-8

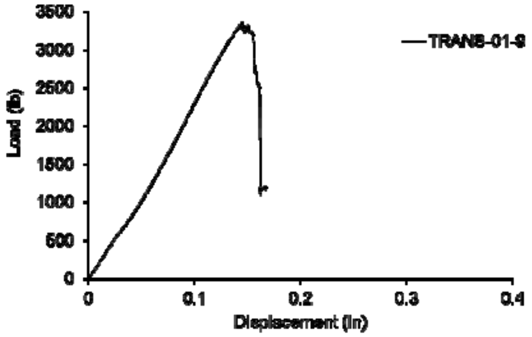
3500
3000
2500
2000
1500
1000
500
0
Load (lb)
0
0.1
0.2
0.3
0.4
Displacement (in)
TRANS-01-9

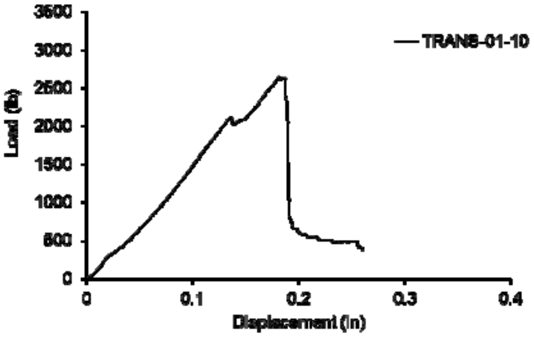
3500
3000
2500
2000
1500
1000
500
0
Load (lb)
0
0.1
0.2
0.3
0.4
Displacement (in)
TRANS-01-10

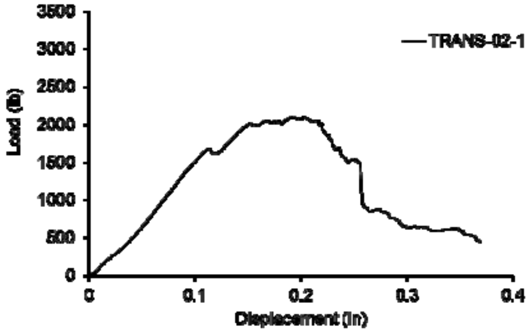
3500
3000
2500
2000
1500
1000
500
0
Load (lb)
0
0.1
0.2
0.3
0.4
Displacement (in)
TRANS-02-1

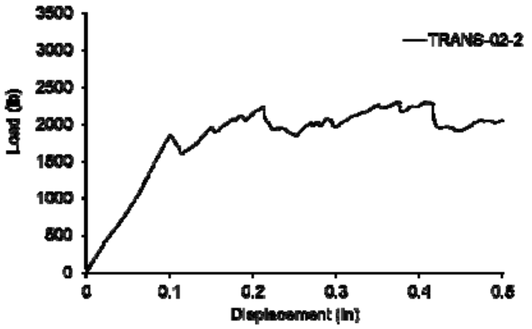
3500
3000
2500
2000
1500
1000
500
0
Load (lb)
0
0.1
0.2
0.3
0.4
0.5
Displacement (in)
TRANS-02-2

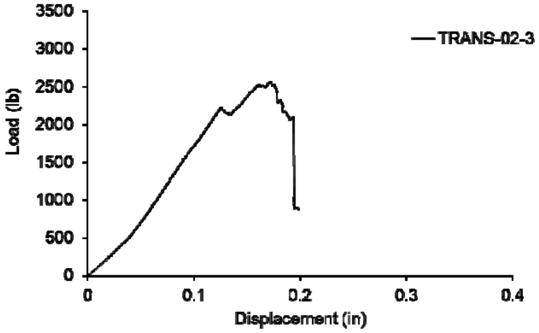
TRANS-02-3
Load (lb)
3500
3000
2500
2000
1500
1000
500
0
0
0.1
0.2
0.3
0.4
Displacement (in)

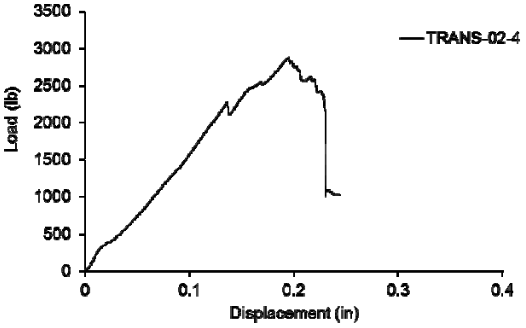
TRANS-02-4
Load (lb)
3500
3000
2500
2000
1500
1000
500
0
0
0.1
0.2
0.3
0.4
Displacement (in)

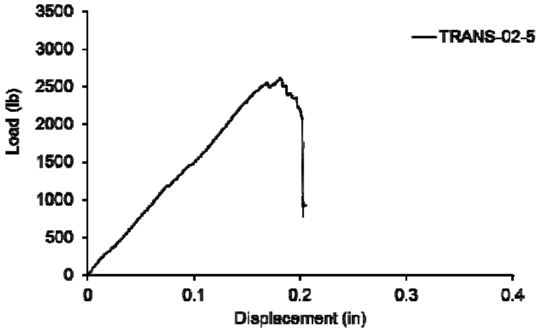
TRANS-02-5
Load (lb)
3500
3000
2500
2000
1500
1000
500
0
0
0.1
0.2
0.3
0.4
Displacement (in)

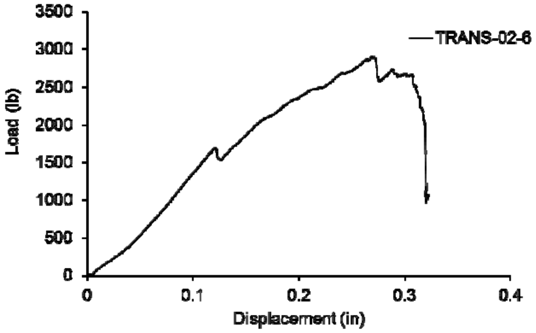
TRANS-02-6
Load (lb)
3500
3000
2500
2000
1500
1000
500
0
0
0.1
0.2
0.3
0.4
Displacement (in)

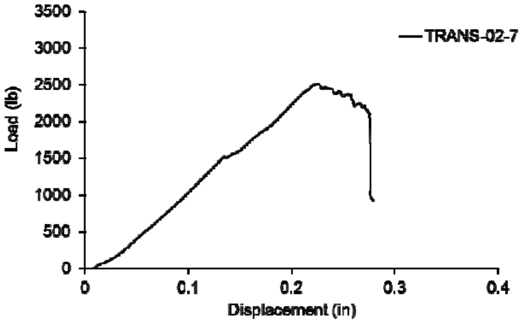
TRANS-02-7
Load (lb)
3500
3000
2500
2000
1500
1000
500
0
0
0.1
0.2
0.3
0.4
Displacement (in)

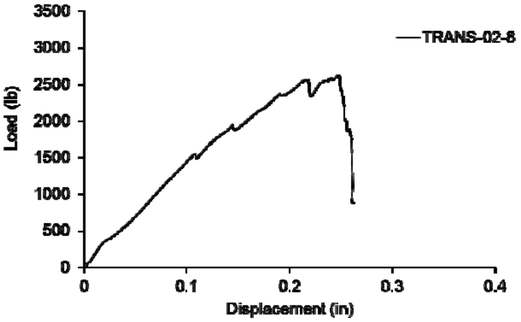
TRANS-02-8
Load (lb)
3500
3000
2500
2000
1500
1000
500
0
0
0.1
0.2
0.3
0.4
Displacement (in)

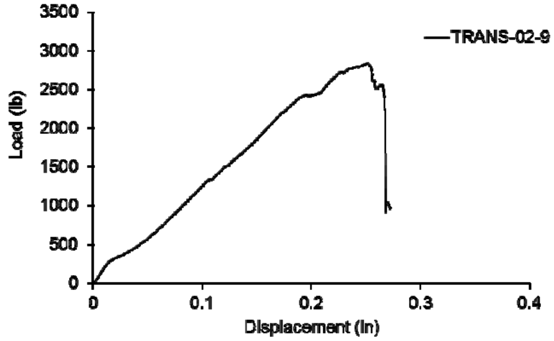
TRANS-02-9
Load (lb)
3500
3000
2500
2000
1500
1000
500
0
0
0.1
0.2
0.3
0.4
Displacement (in)

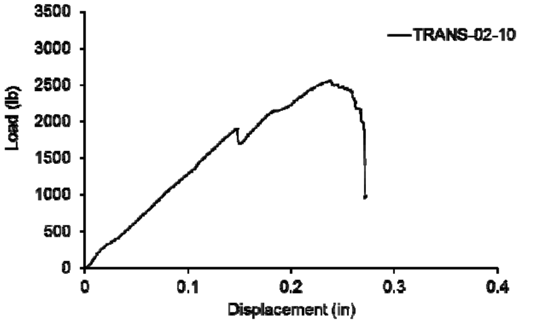
TRANS-02-10
Load (lb)
3500
3000
2500
2000
1500
1000
500
0
0
0.1
0.2
0.3
0.4
Displacement (in)

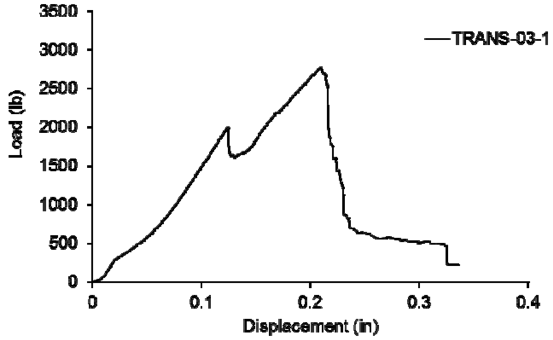
TRANS-03-1
Load (lb)
3500
3000
2500
2000
1500
1000
500
0
0
0.1
0.2
0.3
0.4
Displacement (in)

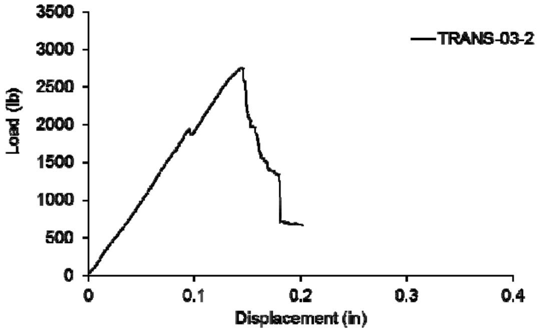
TRANS-03-2
Load (lb)
3500
3000
2500
2000
1500
1000
500
0
0
0.1
0.2
0.3
0.4
Displacement (in)

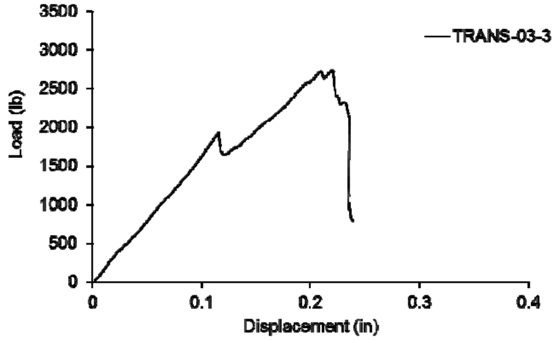
TRANS-03-3
Load (lb)
3500
3000
2500
2000
1500
1000
500
0
0
0.1
0.2
0.3
0.4
Displacement (in)

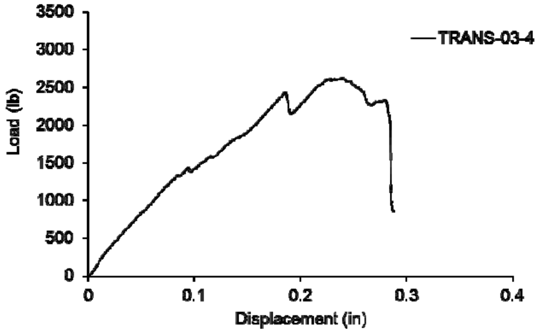
TRANS-03-4
Load (lb)
3500
3000
2500
2000
1500
1000
500
0
0
0.1
0.2
0.3
0.4
Displacement (in)

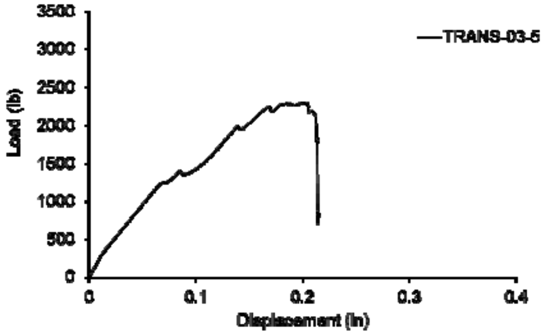

TRANS-03-5
Load (lb)
0
500
1000
1500
2000
2500
3000
3500
0
0.1
0.2
0.3
0.4
Displacement (in)

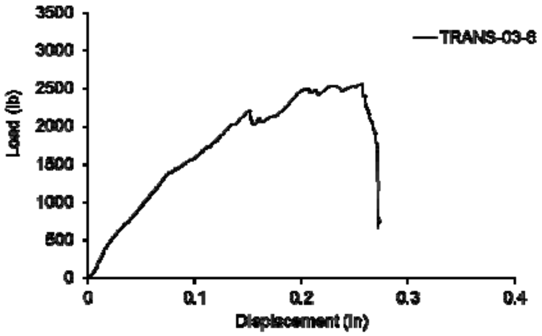

TRANS-03-6
Load (lb)
0
500
1000
1500
2000
2500
3000
3500
0
0.1
0.2
0.3
0.4
Displacement (in)

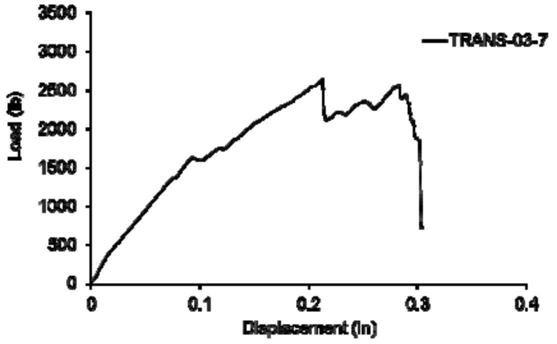

TRANS-03-7
Load (lb)
0
500
1000
1500
2000
2500
3000
3500
0
0.1
0.2
0.3
0.4
Displacement (in)

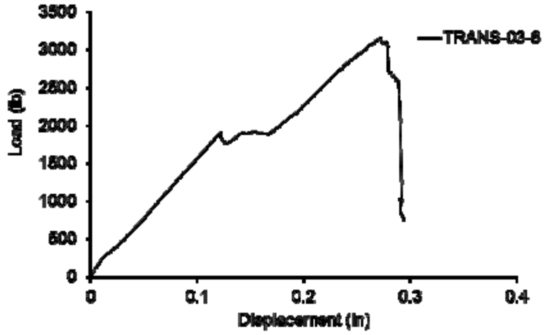

TRANS-03-8
Load (lb)
0
500
1000
1500
2000
2500
3000
3500
0
0.1
0.2
0.3
0.4
Displacement (in)

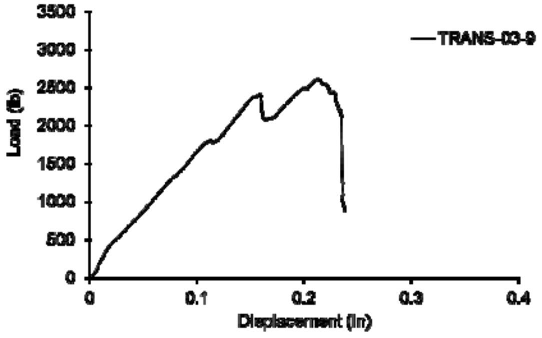

TRANS-03-9
Load (lb)
0
500
1000
1500
2000
2500
3000
3500
0
0.1
0.2
0.3
0.4
Displacement (in)

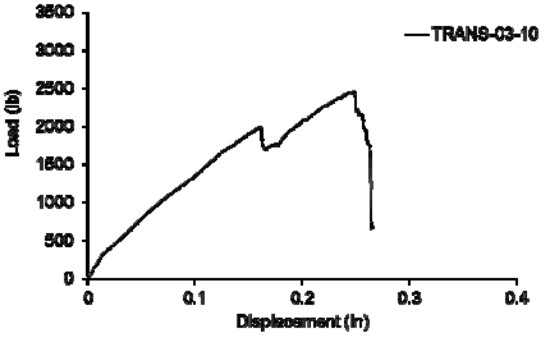

TRANS-03-10
Load (lb)
0
500
1000
1500
2000
2500
3000
3500
0
0.1
0.2
0.3
0.4
Displacement (in)

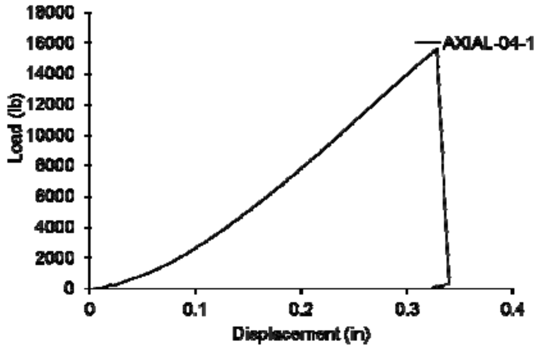

AXIAL-04-1
Load (lb)
0
2000
4000
6000
8000
10000
12000
14000
16000
18000
Displacement (in)
0
0.1
0.2
0.3
0.4

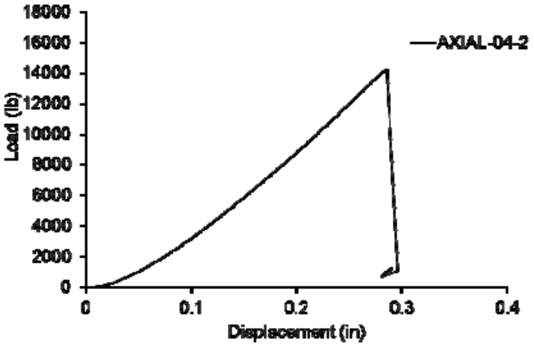

AXIAL-04-2
Load (lb)
0
2000
4000
6000
8000
10000
12000
14000
16000
18000
Displacement (in)
0
0.1
0.2
0.3
0.4

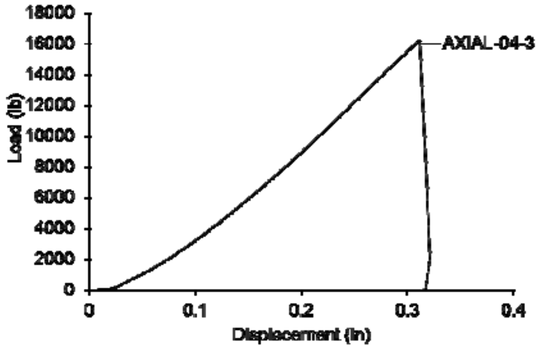

AXIAL-04-3
Load (lb)
0
2000
4000
6000
8000
10000
12000
14000
16000
18000
Displacement (in)
0
0.1
0.2
0.3
0.4

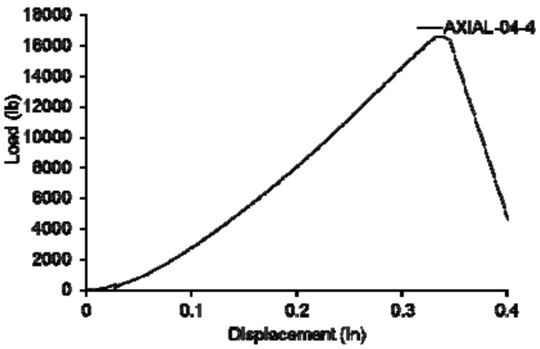

AXIAL-04-4
Load (lb)
0
2000
4000
6000
8000
10000
12000
14000
16000
18000
Displacement (in)
0
0.1
0.2
0.3
0.4

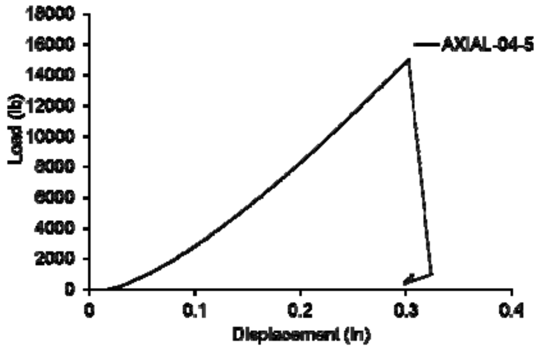

AXIAL-04-5
Load (lb)
0
2000
4000
6000
8000
10000
12000
14000
16000
18000
Displacement (in)
0
0.1
0.2
0.3
0.4

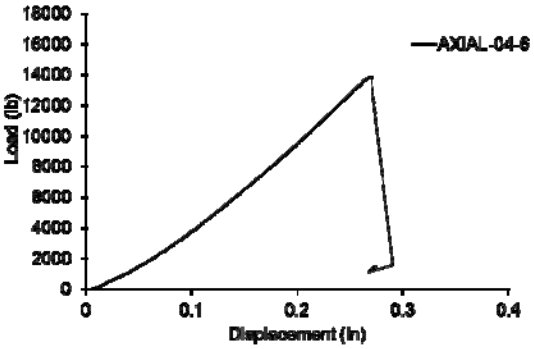

AXIAL-04-6
Load (lb)
0
2000
4000
6000
8000
10000
12000
14000
16000
18000
Displacement (in)
0
0.1
0.2
0.3
0.4

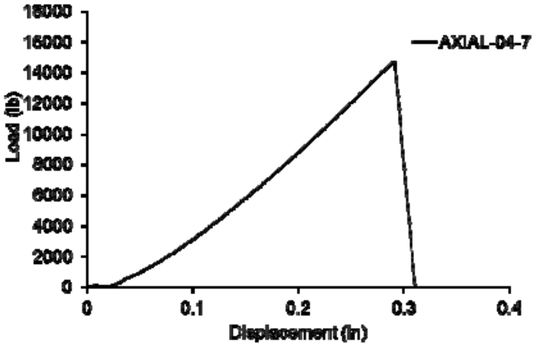

AXIAL-04-7
Load (lb)
18000
16000
14000
12000
10000
8000
6000
4000
2000
0
0
0.1
0.2
0.3
0.4
Displacement (in)

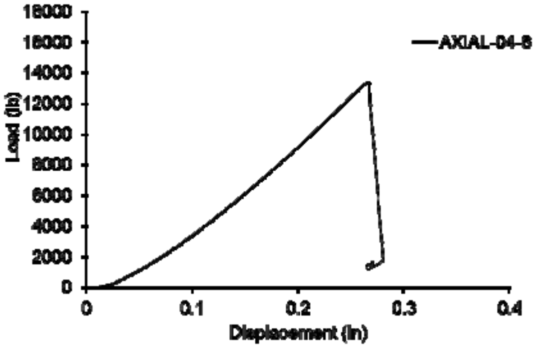

AXIAL-04-8
Load (lb)
18000
16000
14000
12000
10000
8000
6000
4000
2000
0
0
0.1
0.2
0.3
0.4
Displacement (in)

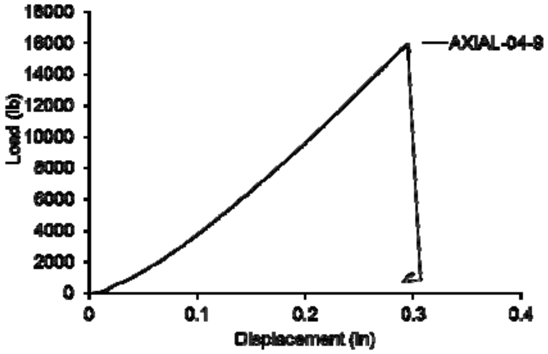

AXIAL-04-9
Load (lb)
18000
16000
14000
12000
10000
8000
6000
4000
2000
0
0
0.1
0.2
0.3
0.4
Displacement (in)

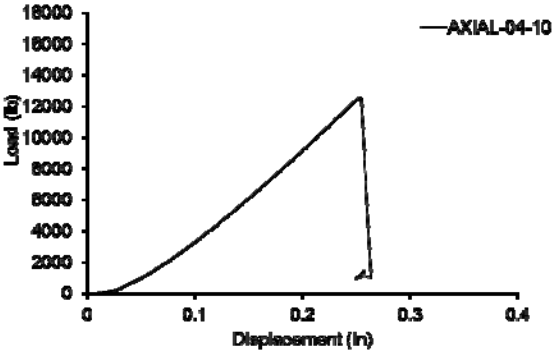

AXIAL-04-10
Load (lb)
18000
16000
14000
12000
10000
8000
6000
4000
2000
0
0
0.1
0.2
0.3
0.4
Displacement (in)

Appendix B. Load Displacement Curves for Phase II – Residual Capacity

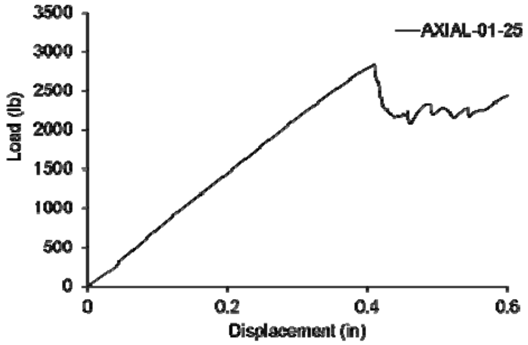

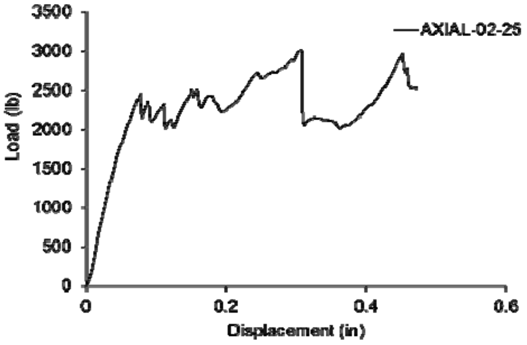

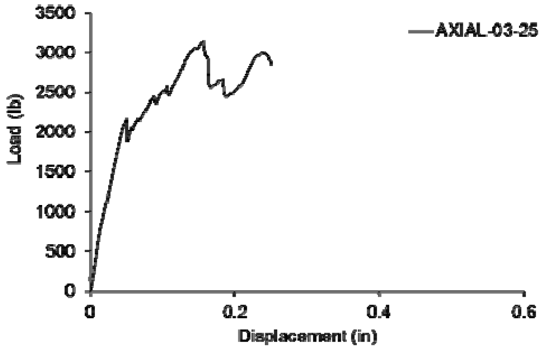

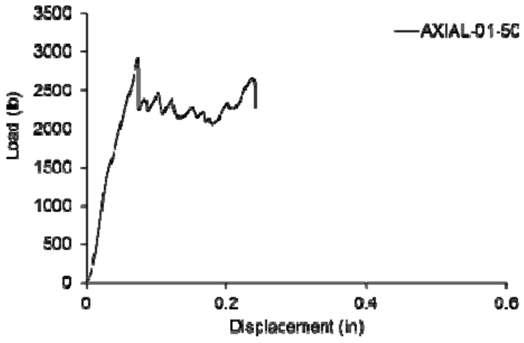

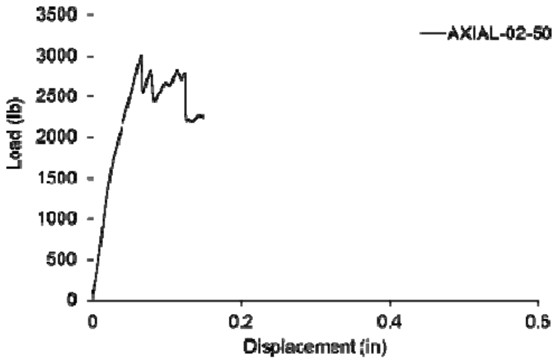

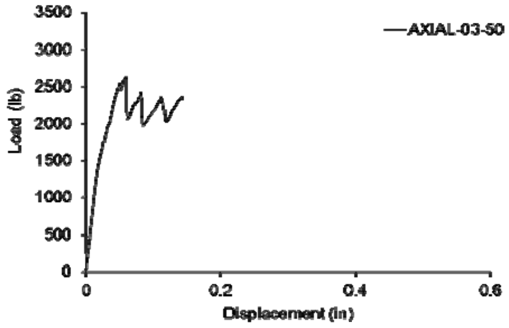

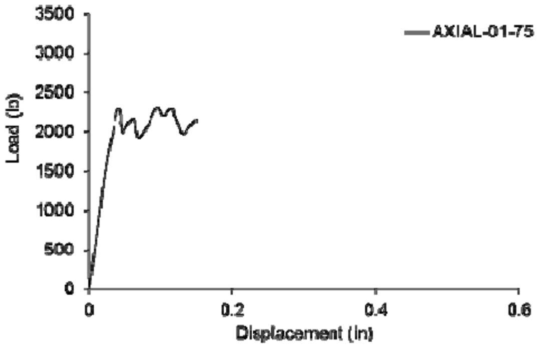
AXIAL-01-75
Load (lb)
3500
3000
2500
2000
1500
1000
500
0
0
0.2
0.4
0.6
Displacement (in)

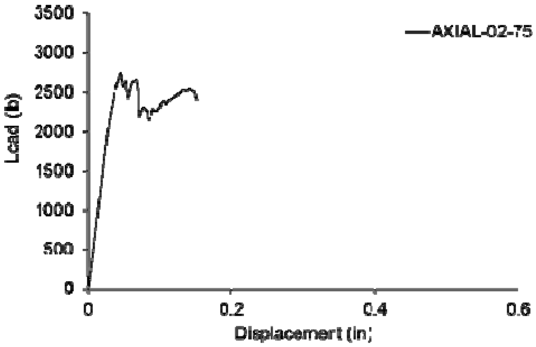
AXIAL-02-75
Load (lb)
3500
3000
2500
2000
1500
1000
500
0
0
0.2
0.4
0.6
Displacement (in)

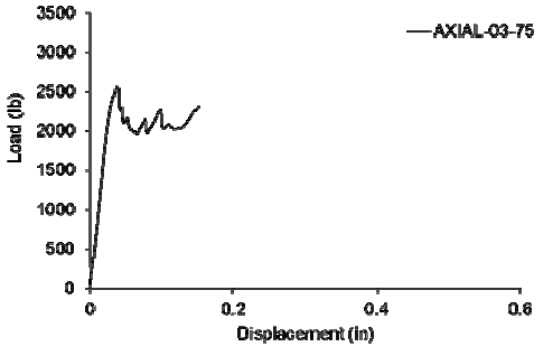
AXIAL-03-75
Load (lb)
3500
3000
2500
2000
1500
1000
500
0
0
0.2
0.4
0.6
Displacement (in)

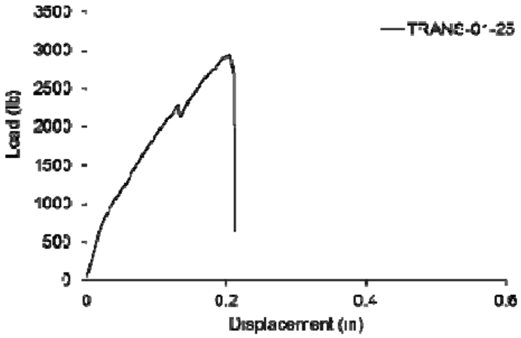
TRANS-01-25
Load (lb)
3500
3000
2500
2000
1500
1000
500
0
0
0.2
0.4
0.6
Displacement (in)

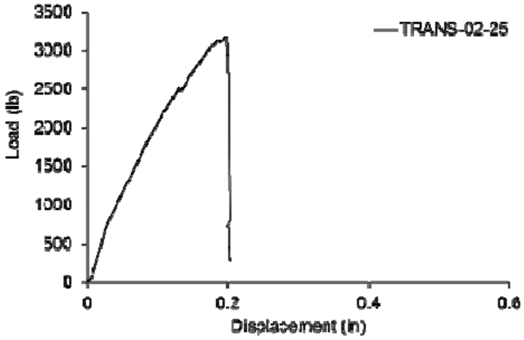
TRANS-02-25
Load (lb)
3500
3000
2500
2000
1500
1000
500
0
0
0.2
0.4
0.6
Displacement (in)

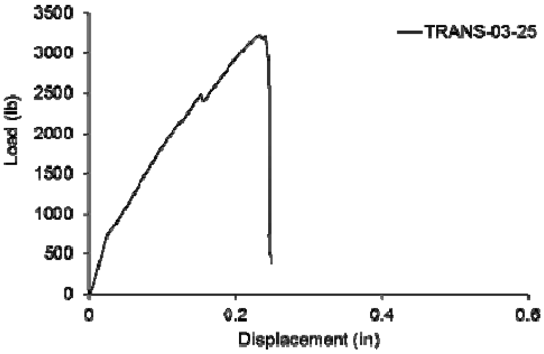
TRANS-03-25
Load (lb)
3500
3000
2500
2000
1500
1000
500
0
0
0.2
0.4
0.6
Displacement (in)

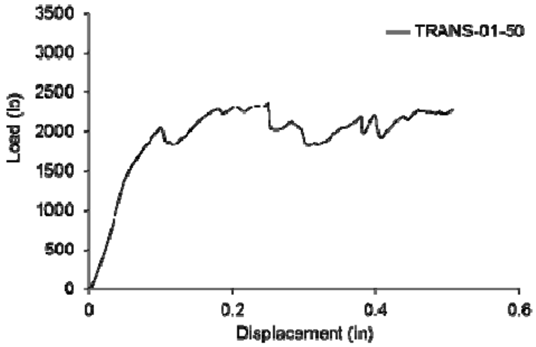
TRANS-01-50
Load (lb)
Displacement (in)
0
500
1000
1500
2000
2500
3000
3500
0
0.2
0.4
0.6

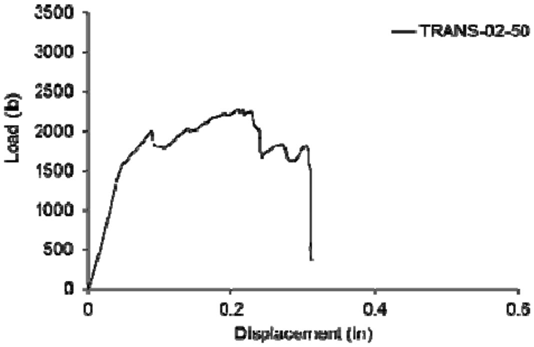
TRANS-02-50
Load (lb)
Displacement (in)
0
500
1000
1500
2000
2500
3000
3500
0
0.2
0.4
0.6

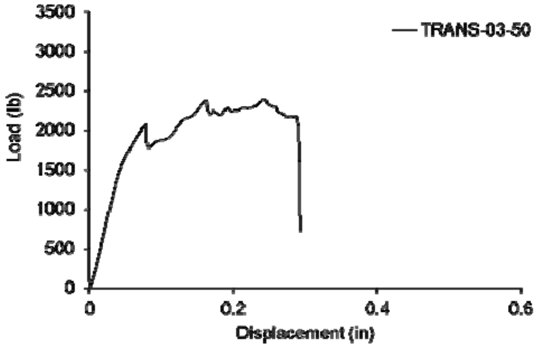
TRANS-03-50
Load (lb)
Displacement (in)
0
500
1000
1500
2000
2500
3000
3500
0
0.2
0.4
0.6

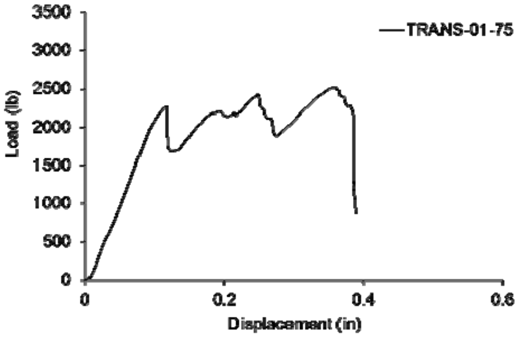
TRANS-01-75
Load (lb)
Displacement (in)
0
500
1000
1500
2000
2500
3000
3500
0
0.2
0.4
0.6

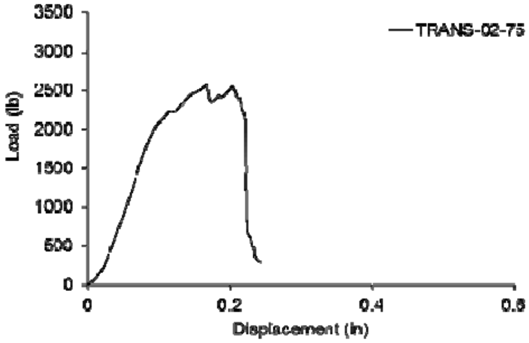
TRANS-02-75
Load (lb)
Displacement (in)
0
500
1000
1500
2000
2500
3000
3500
0
0.2
0.4
0.6

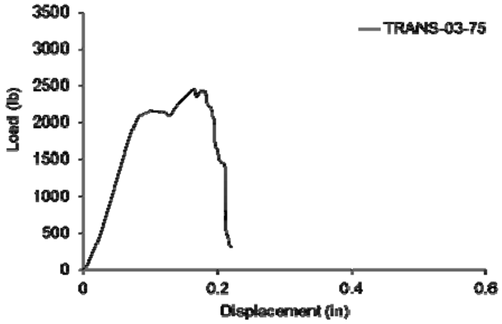
TRANS-03-75
Load (lb)
Displacement (in)
0
500
1000
1500
2000
2500
3000
3500
0
0.2
0.4
0.6

Appendix C. Load Displacement Curves for Phase III – Residual Capacity

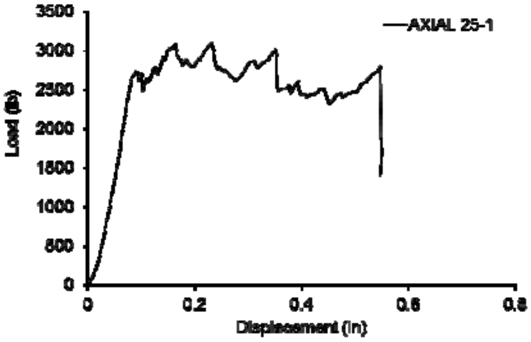

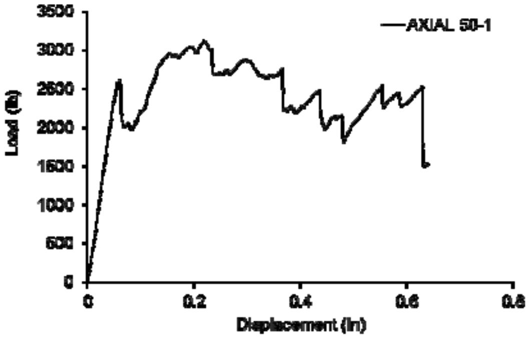

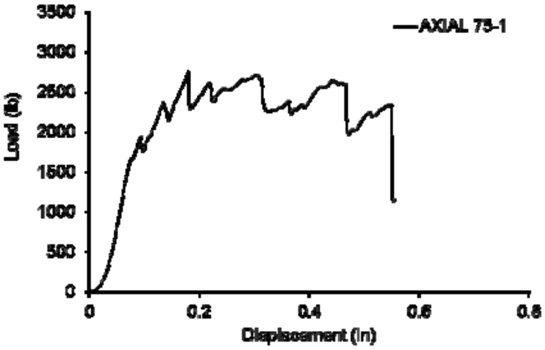

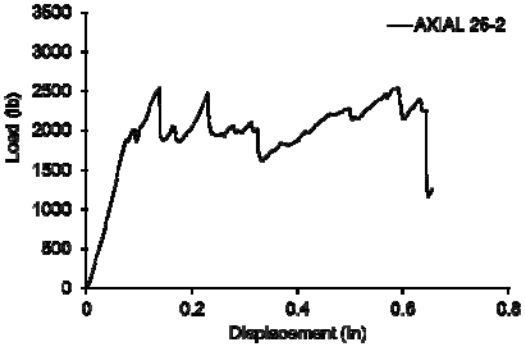

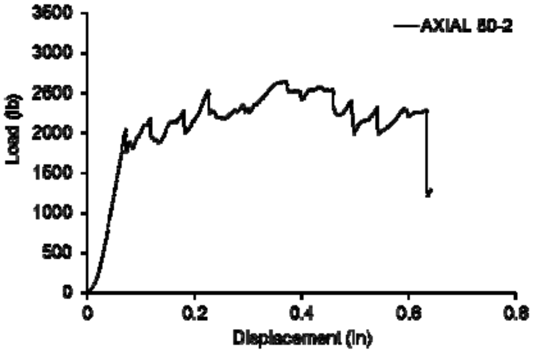

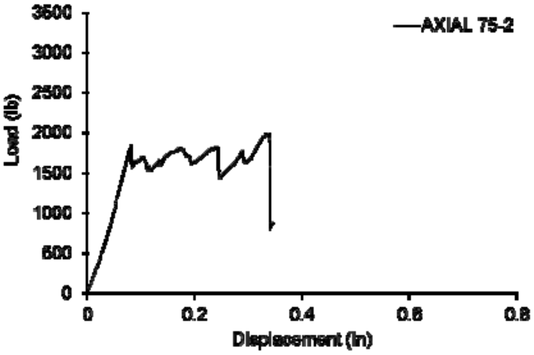

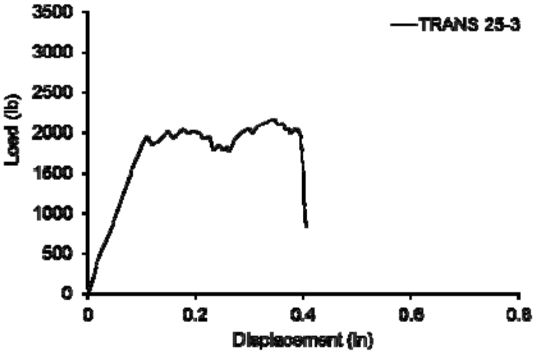
TRANS 25-3
Load (lb)
3500
3000
2500
2000
1500
1000
500
0
0
0.2
0.4
0.6
0.8
Displacement (in)

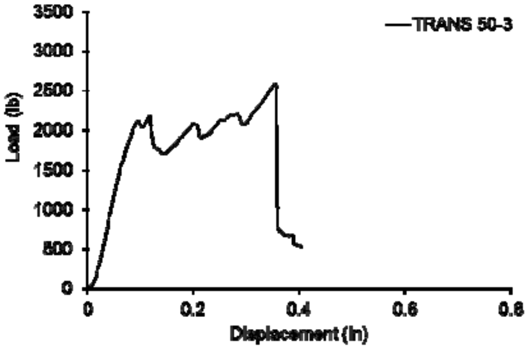
TRANS 50-3
Load (lb)
3500
3000
2500
2000
1500
1000
500
0
0
0.2
0.4
0.6
0.8
Displacement (in)

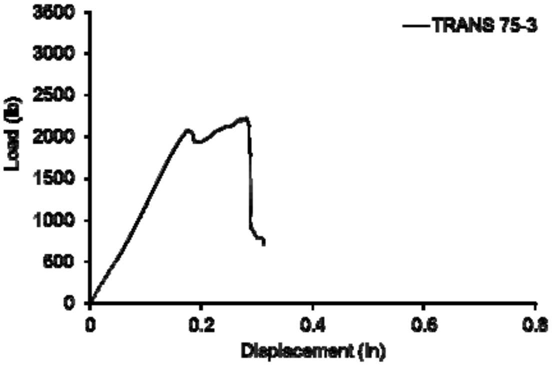
TRANS 75-3
Load (lb)
3500
3000
2500
2000
1500
1000
500
0
0
0.2
0.4
0.6
0.8
Displacement (in)

Appendix D. Phase I Testing Failure Photos – Axial and Transverse

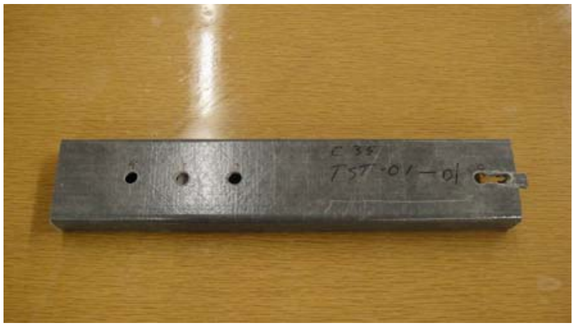

Axial 01-01

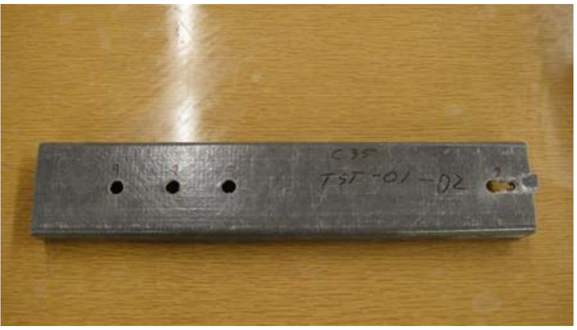

Axial 01-02

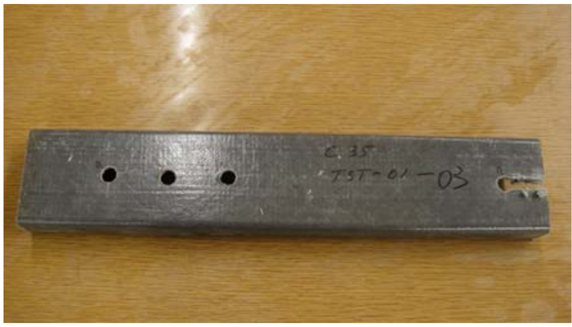

Axial 01-03

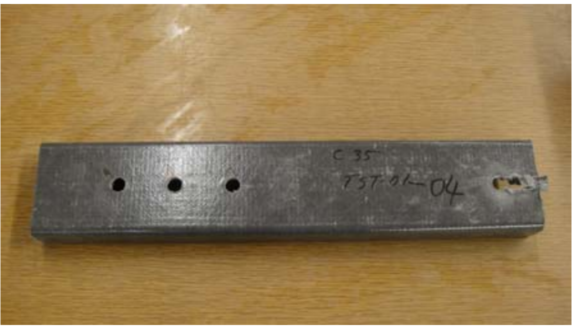

Axial 01-04

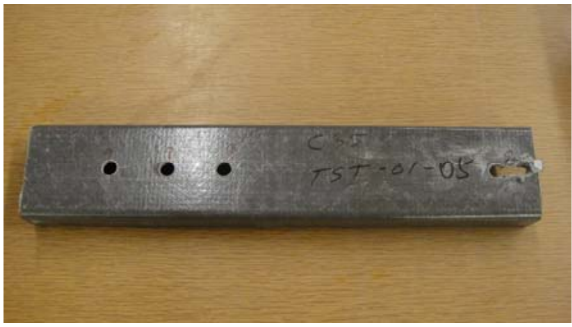

Axial 01-05

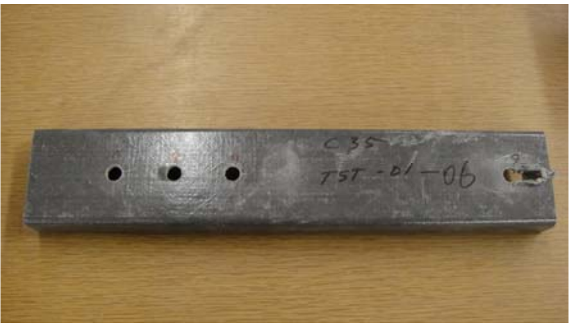

Axial 01-06

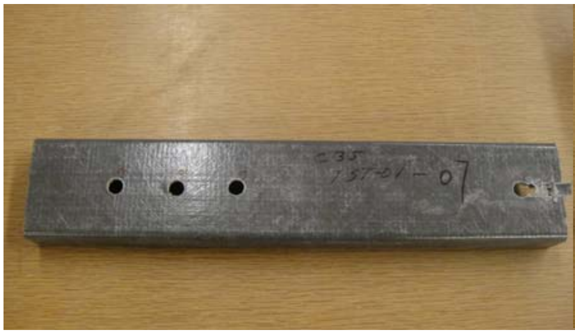

Axial 01-07

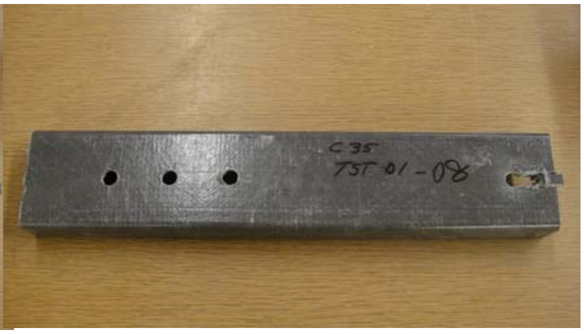

Axial 01-08

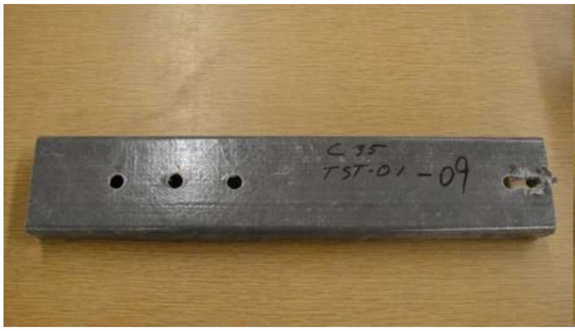

Axial 01-09

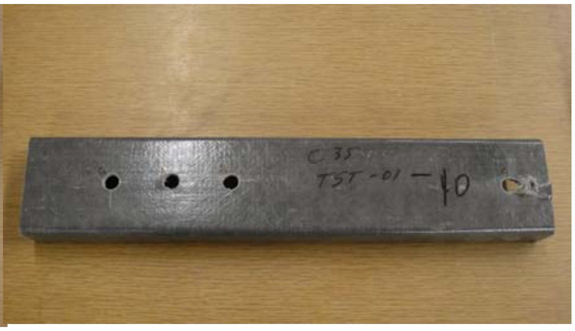

Axial 01-10

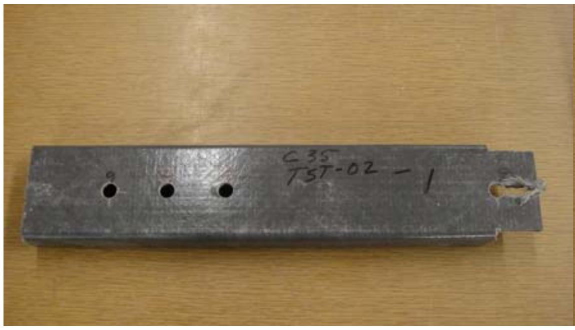

Axial 02-01

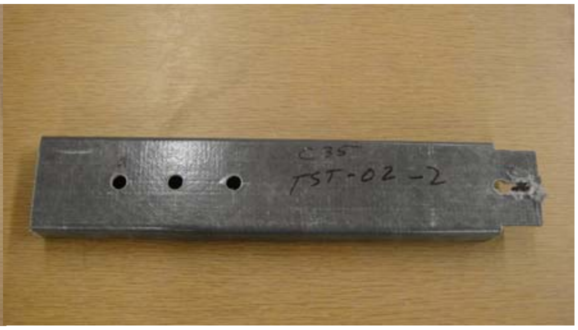

Axial 02-02

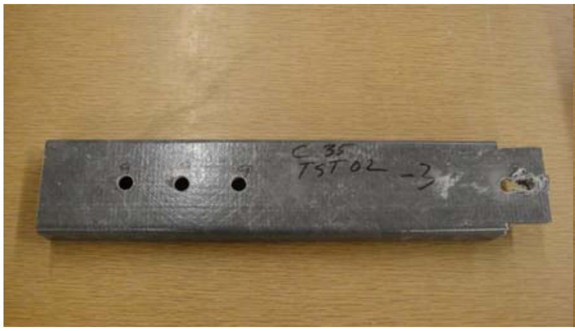

Axial 02-03

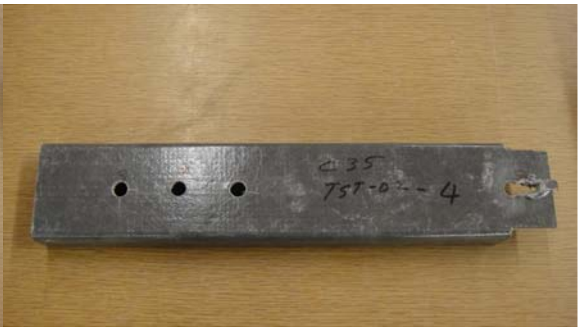

Axial 02-04

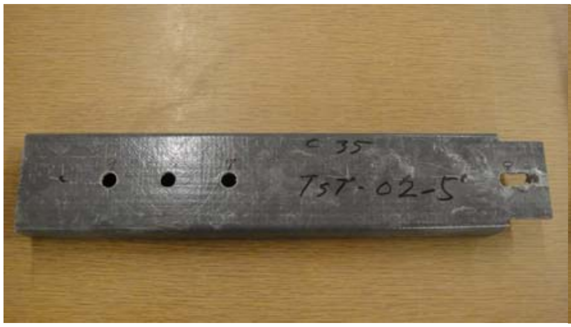

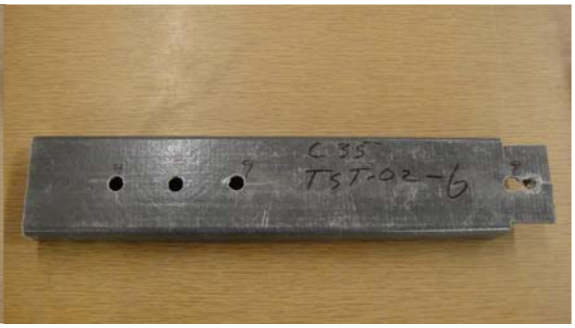

Axial 02-05

Axial 02-06

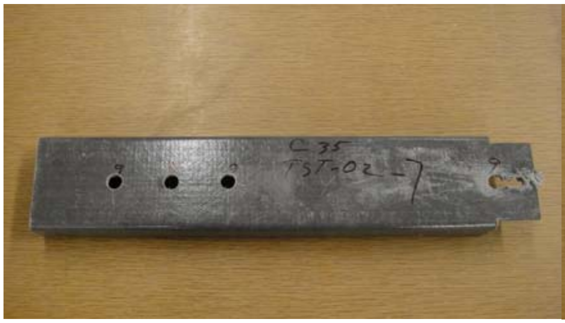

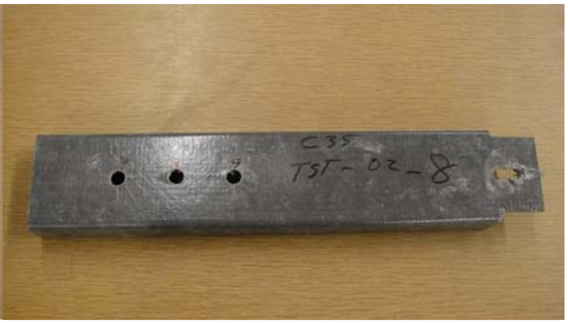

Axial 02-07

Axial 02-08

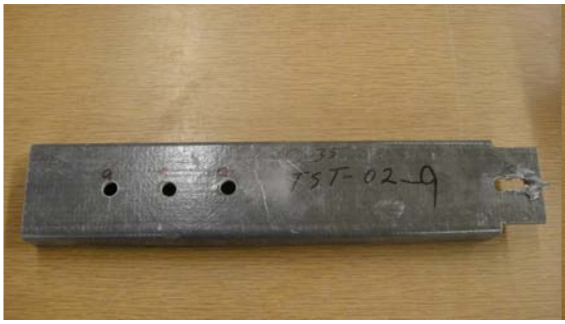

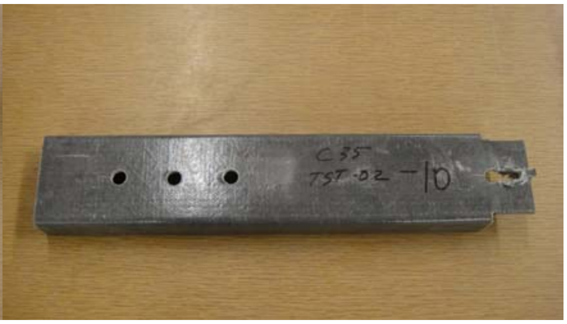

Axial 02-09

Axial 02-10

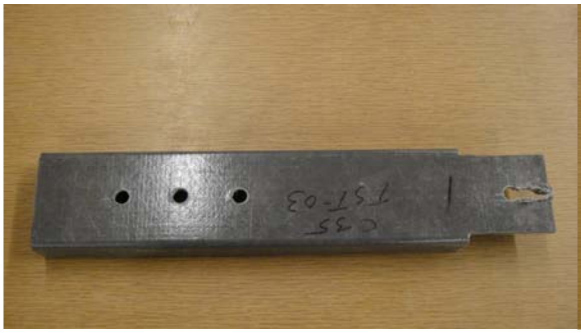

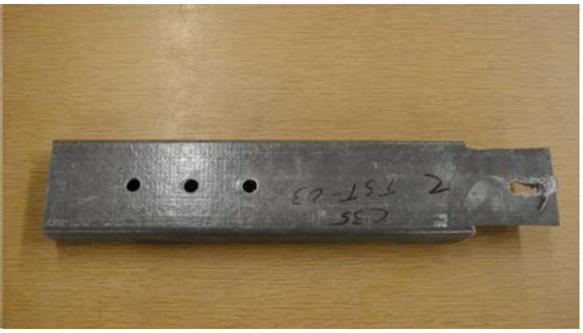

Axial 03-01

Axial 03-02

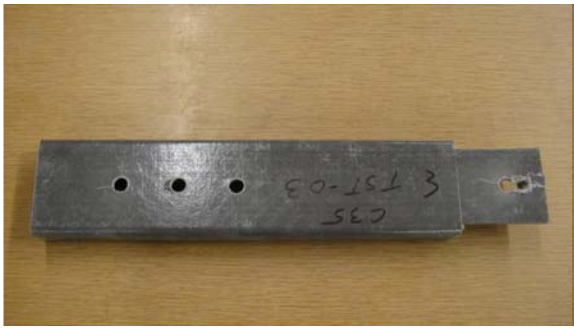

Axial 03-03

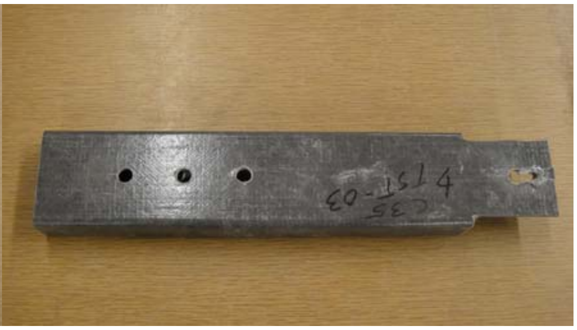

Axial 03-04

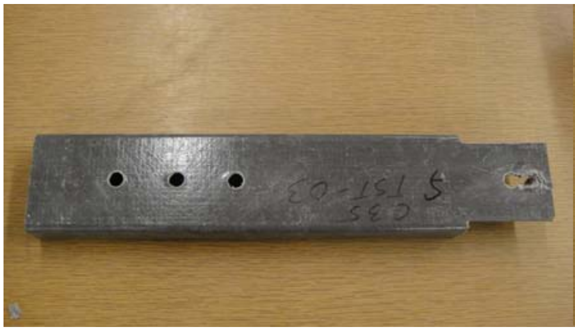

Axial 03-05

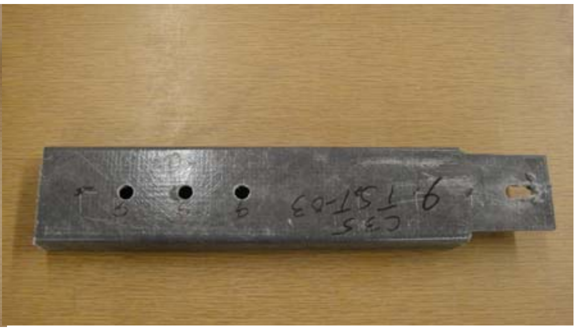

Axial 03-06

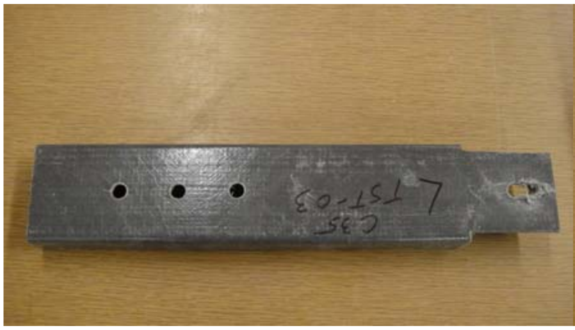

Axial 03-07

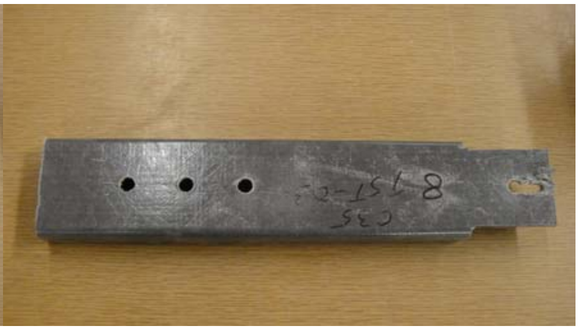

Axial 03-08

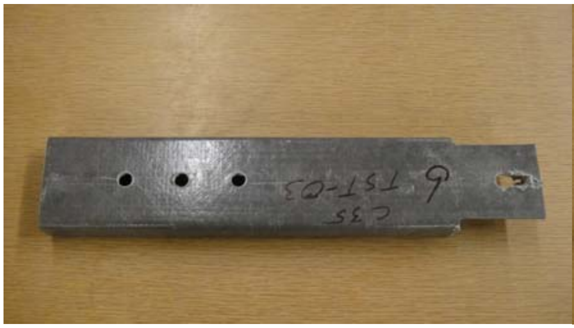

Axial 03-09

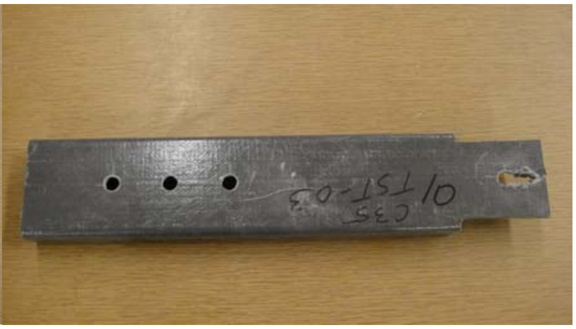

Axial 03-10

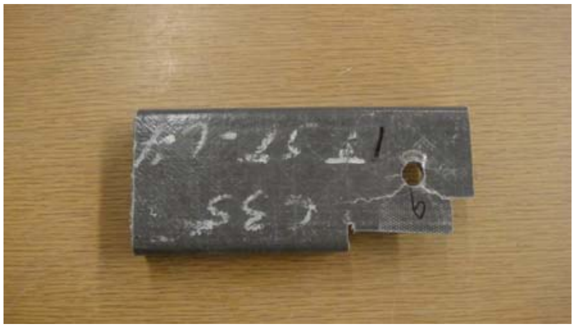

Transverse 01-01

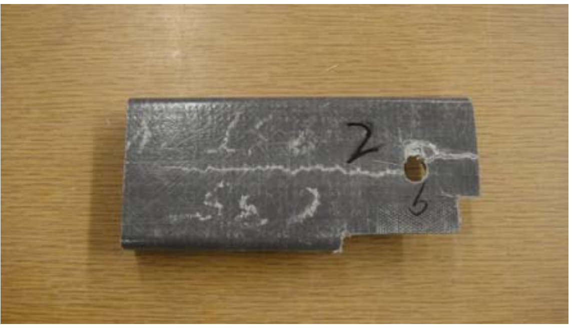

Transverse 01-02

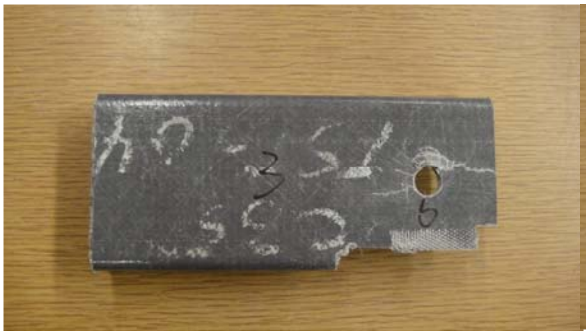

Transverse 01-03

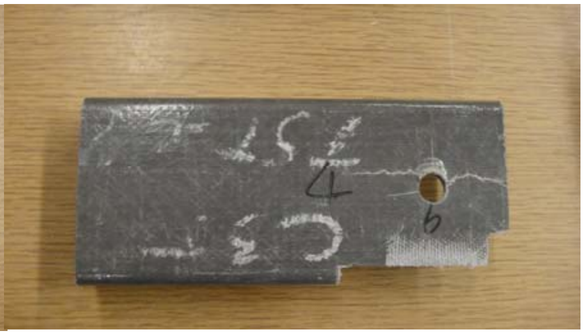

Transverse 01-04

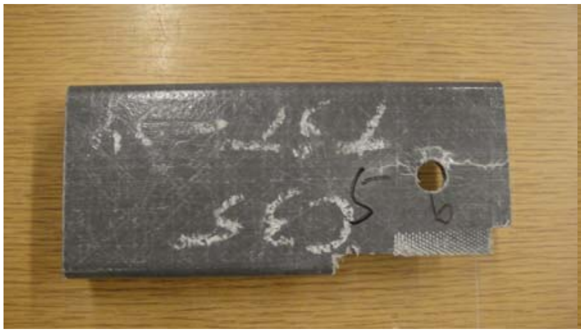

Transverse 01-05

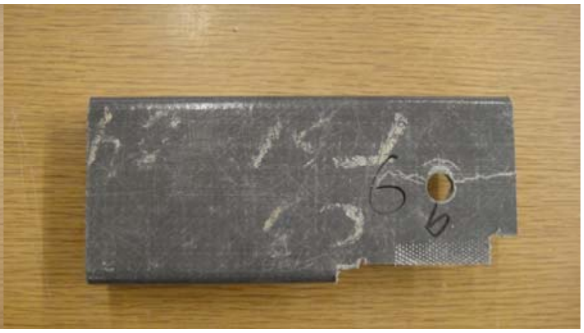

Transverse 01-06

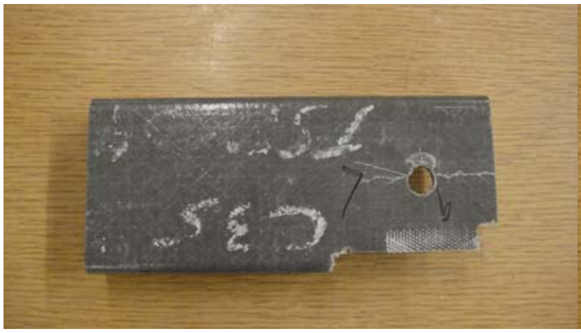

Transverse 01-07

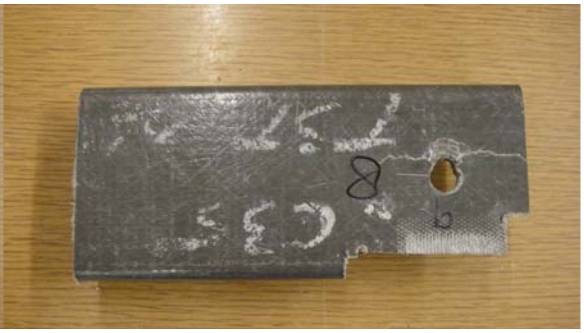

Transverse 01-08

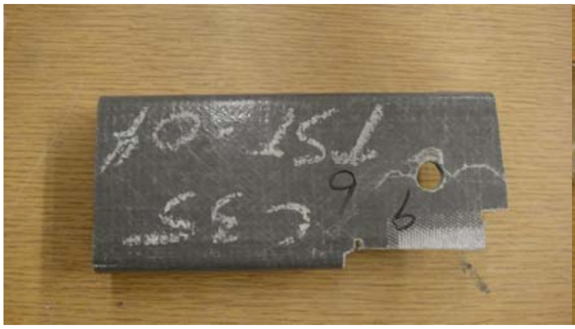
Transverse 01-09

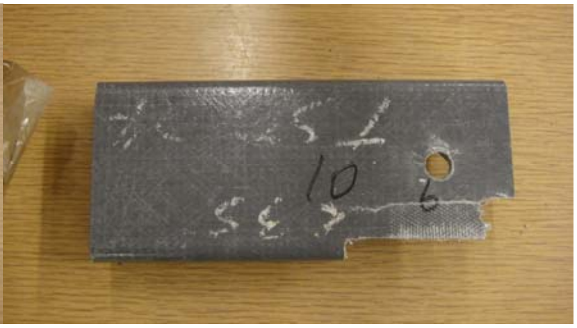
Transverse 01-10

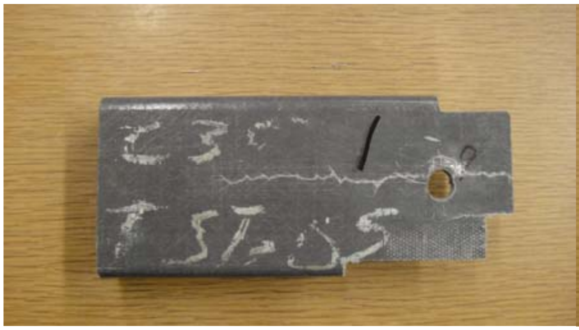
Transverse 02-01

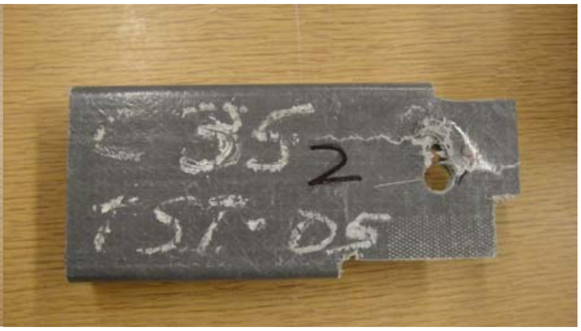
Transverse 02-02

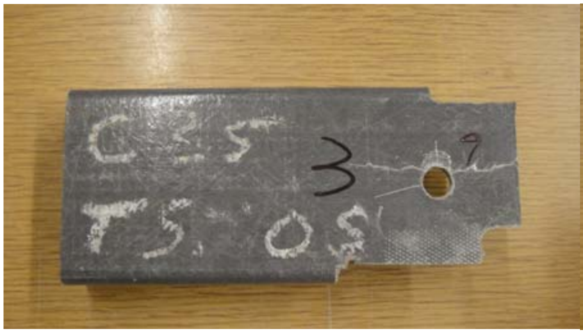
Transverse 02-03

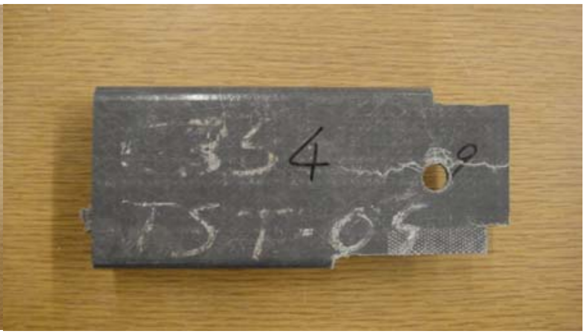
Transverse 02-04

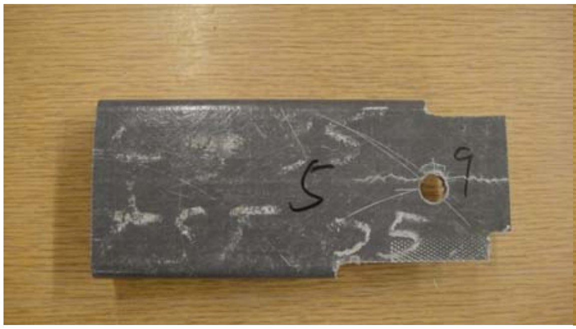
Transverse 02-05

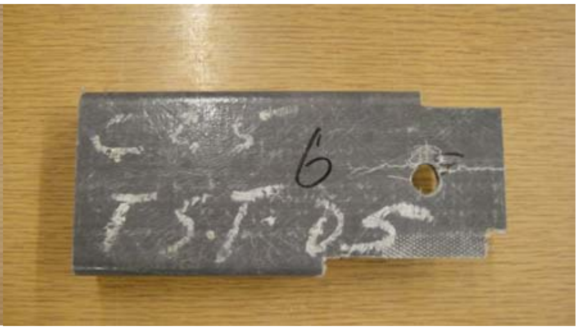
Transverse 02-06

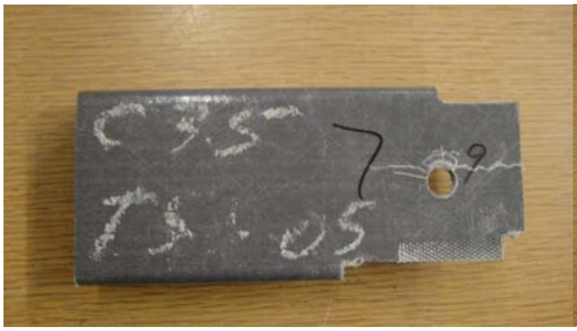

Transverse 02-07

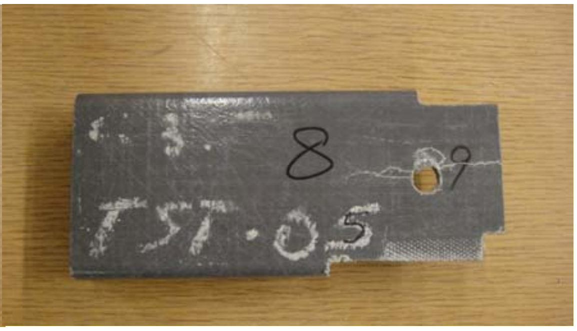

Transverse 02-08

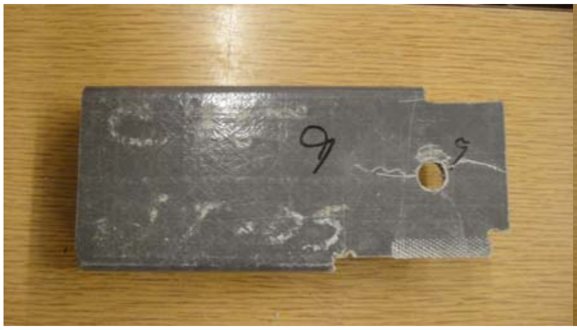

Transverse 02-09

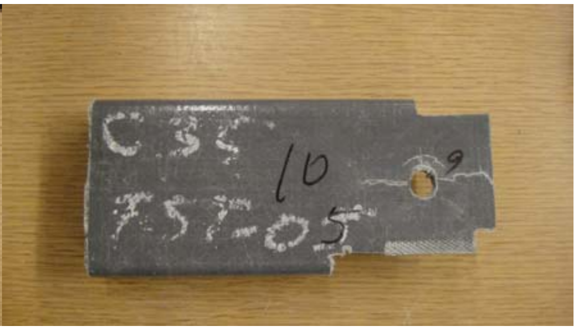

Transverse 02-10

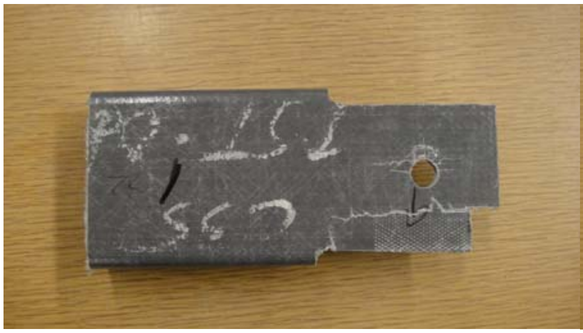

Transverse 03-01

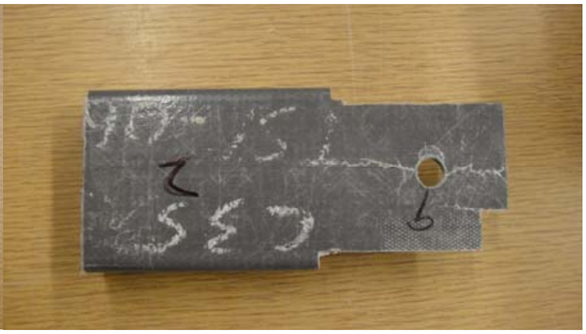

Transverse 03-02

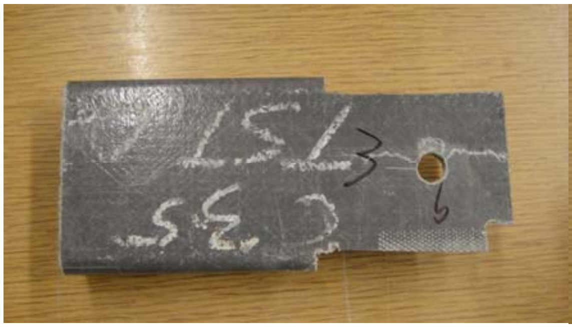

Transverse 03-03

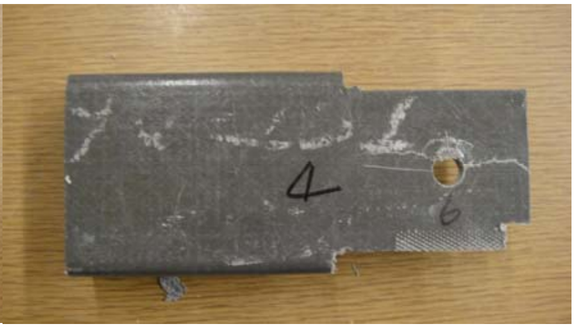

Transverse 03-04

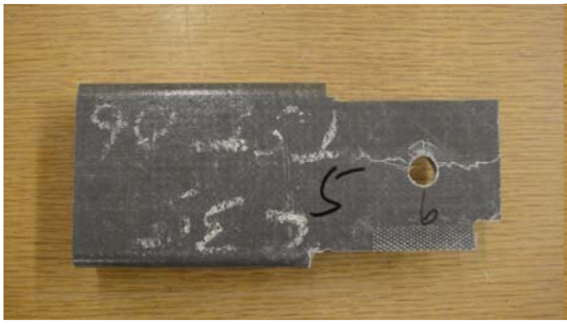

Transverse 03-05

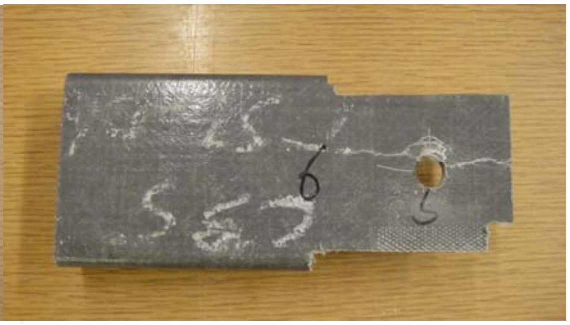

Transverse 03-06

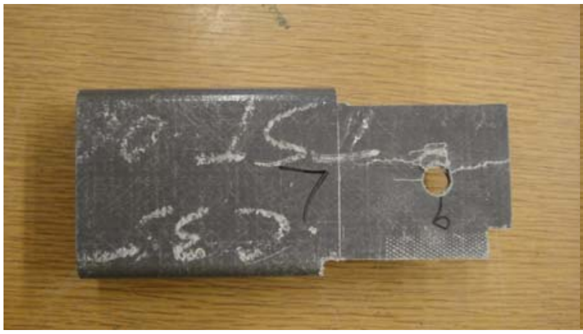

Transverse 03-07

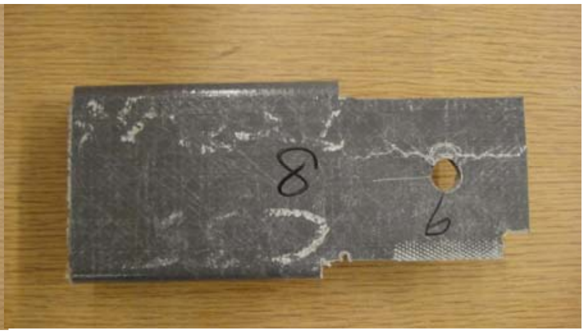

Transverse 03-08

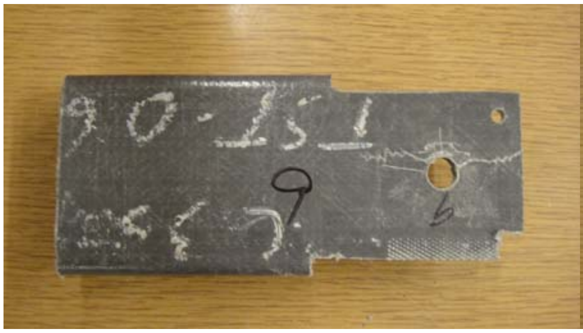

Transverse 03-09

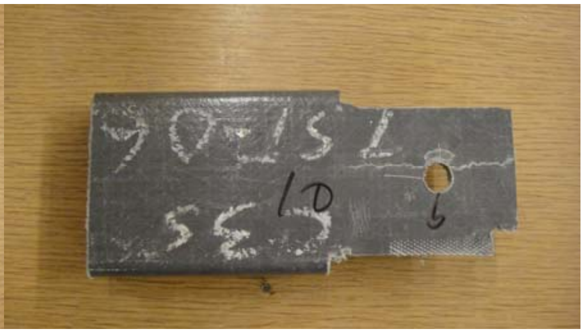

Transverse 03-10

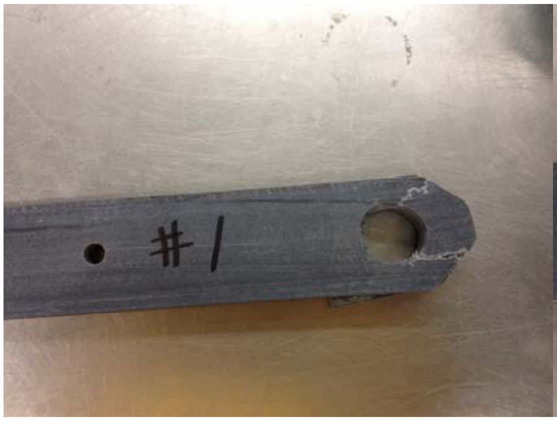

Axial 04-01

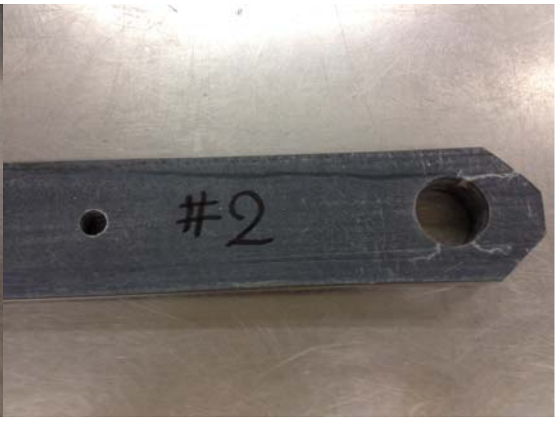

Axial 04-02

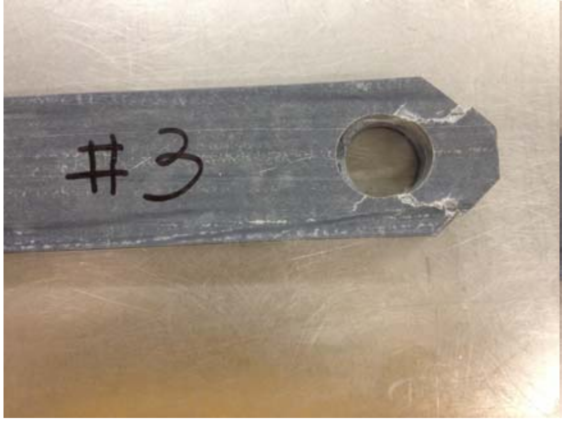

Axial 04-03

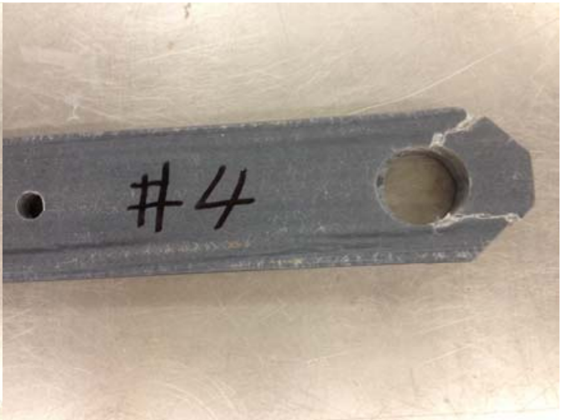

Axial 04-04

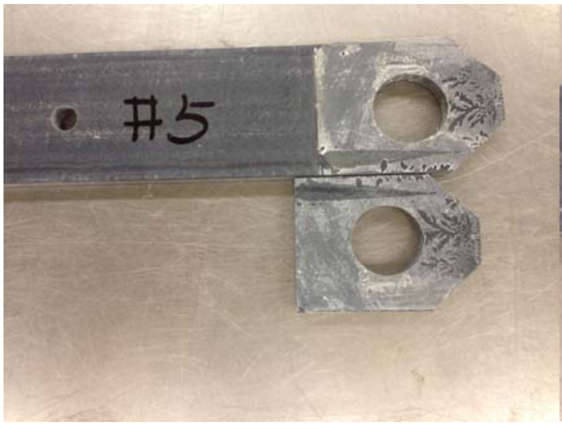

Axial 04-05

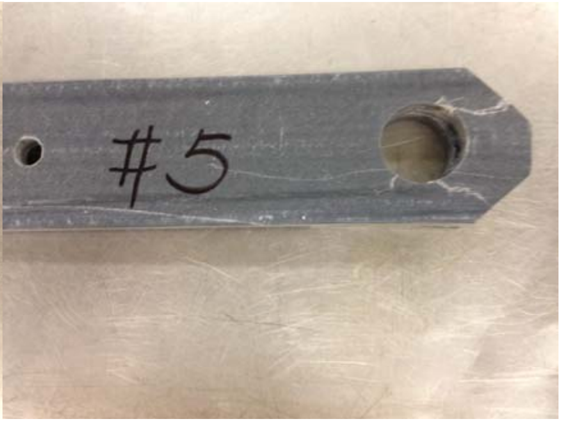

Axial 04-05

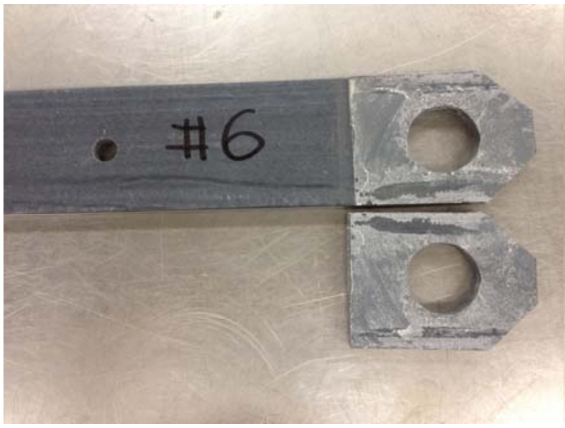

Axial 04-06

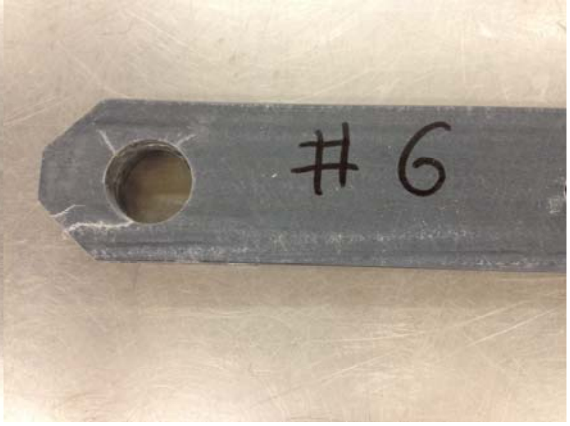

Axial 04-06

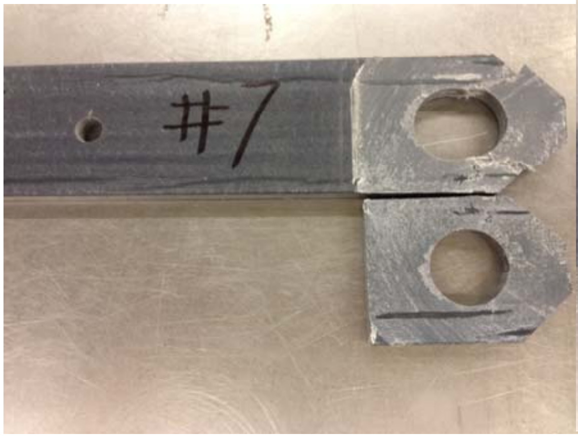

Axial 04-07

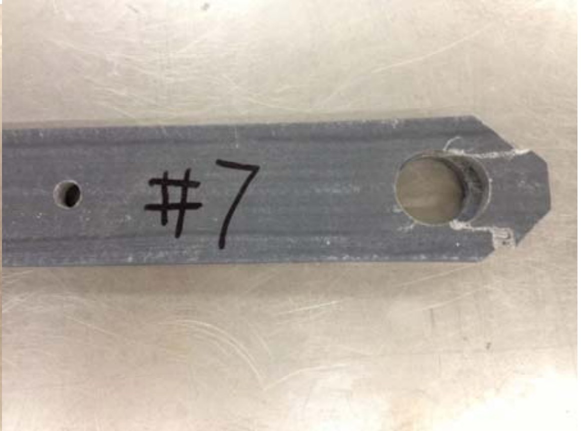

Axial 04-07

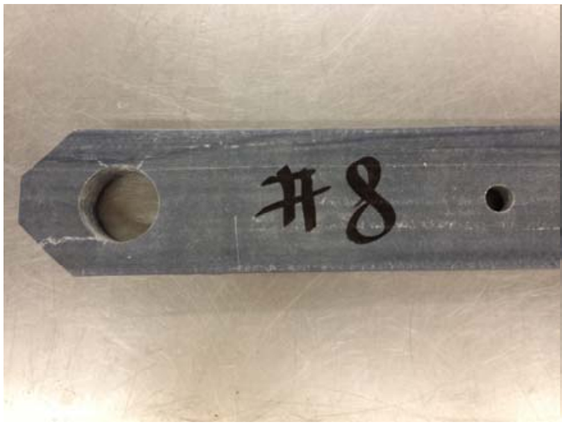

Axial 04-08

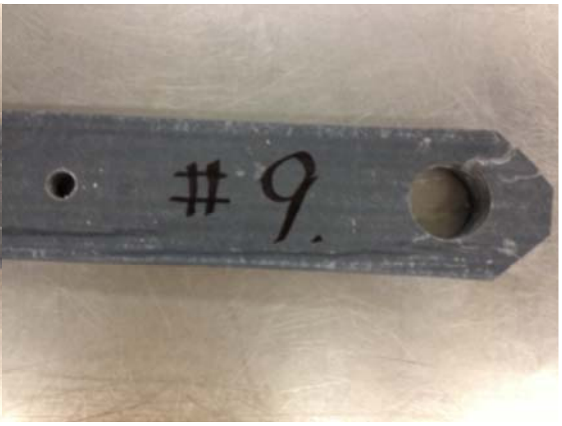

Axial 04-09

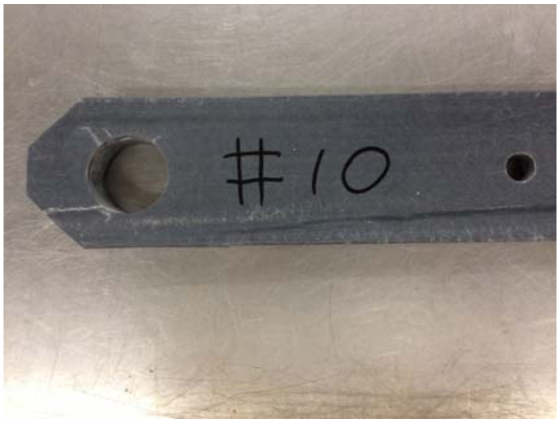

Axial 04-10

Appendix E. Phase II Testing Photos – Damage From Cyclic Loading

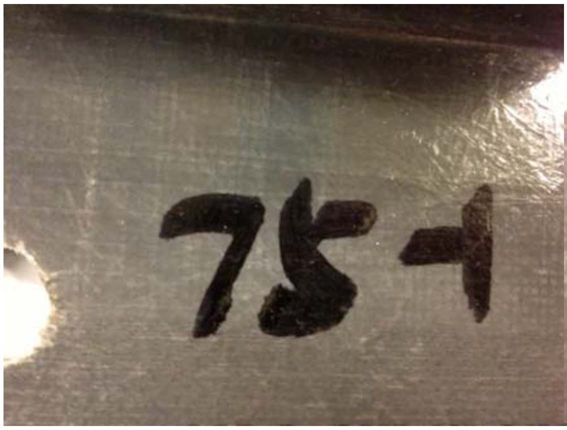

75% Load Level Damage

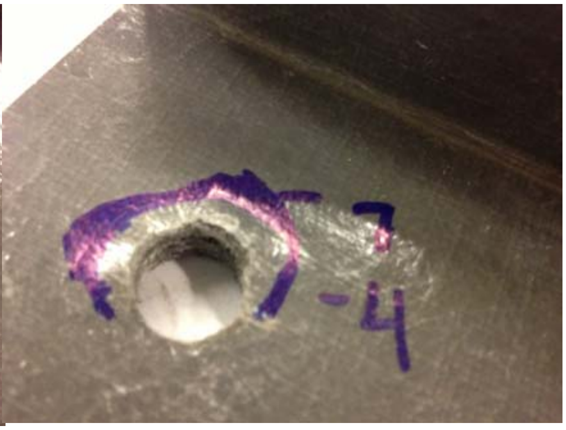

75% Load Level Damage

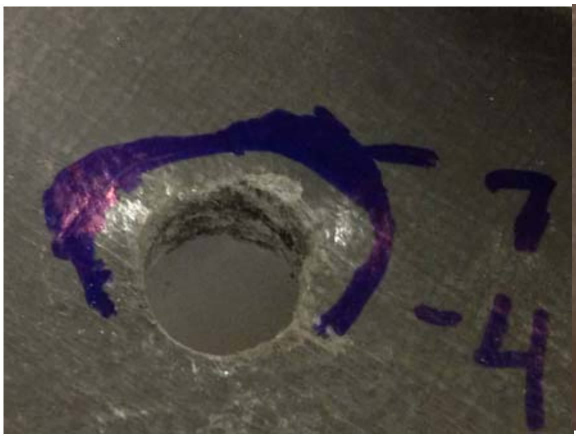

75% Load Level Damage

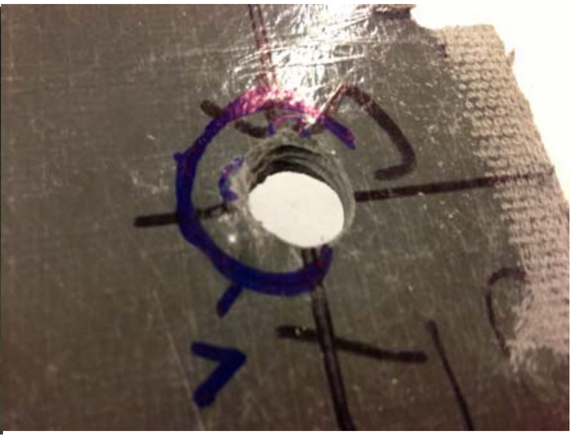

75% Load Level Damage

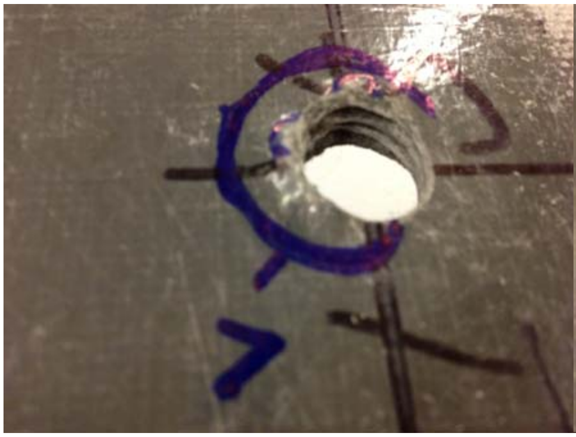

75% Load Level Damage

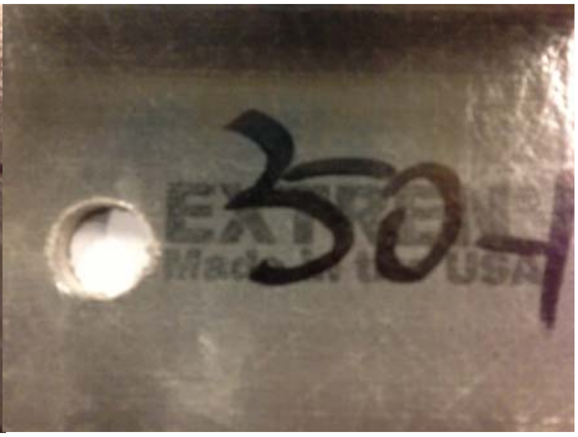

50% Load Level Damage

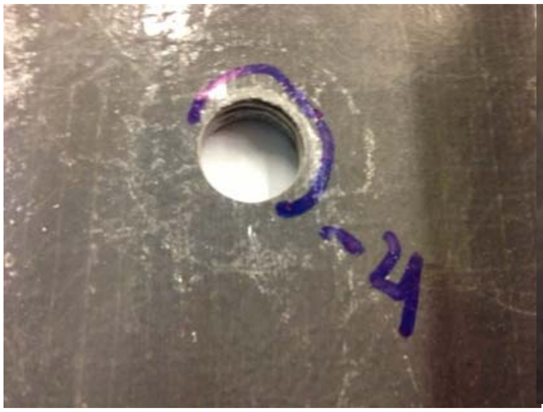

50% Load Level Damage

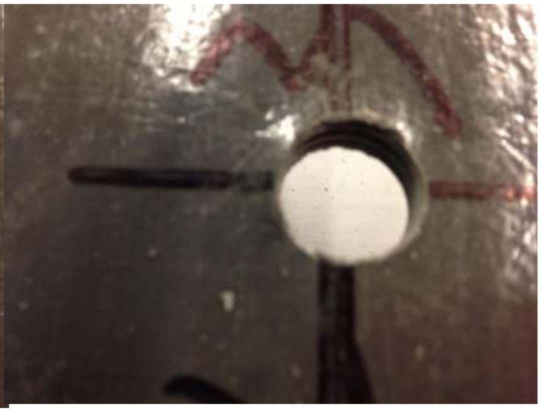

50% Load Level Damage

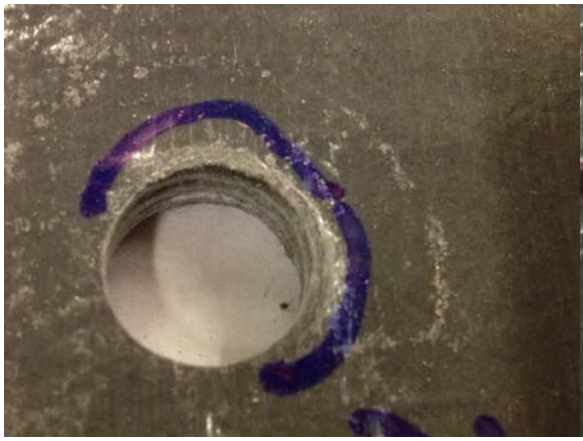

50% Load Level Damage

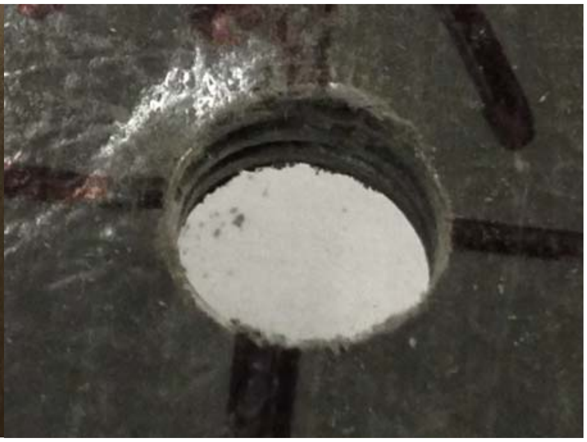

50% Load Level Damage

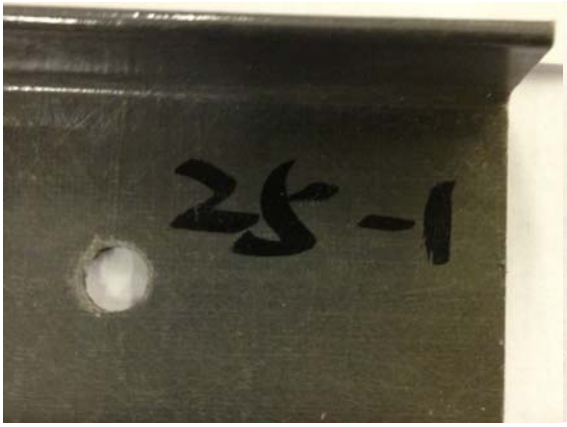

25% Load Level Damage

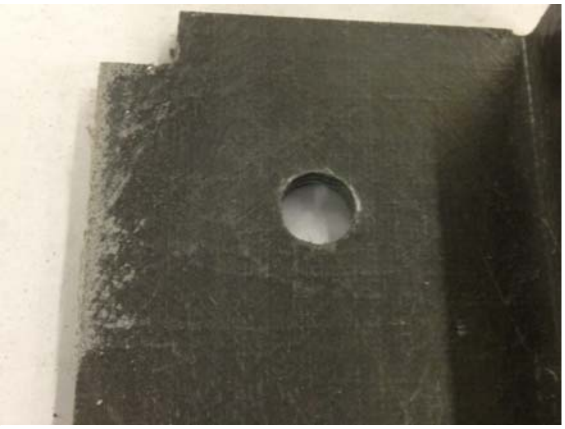

25% Load Level Damage

25% Load Level Damage

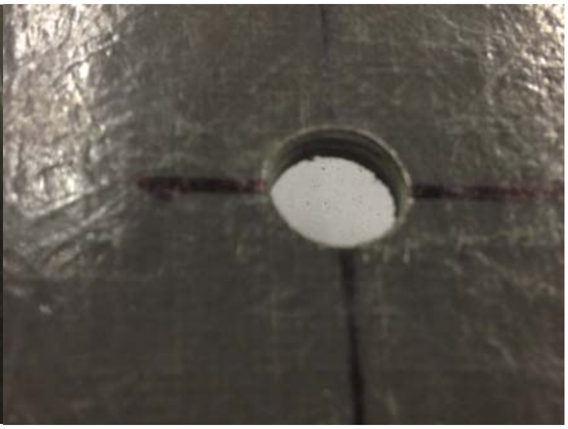

25% Load Level Damage

Appendix F. Phase III Testing Photos – Damage From Multi Directional Cyclic Loading

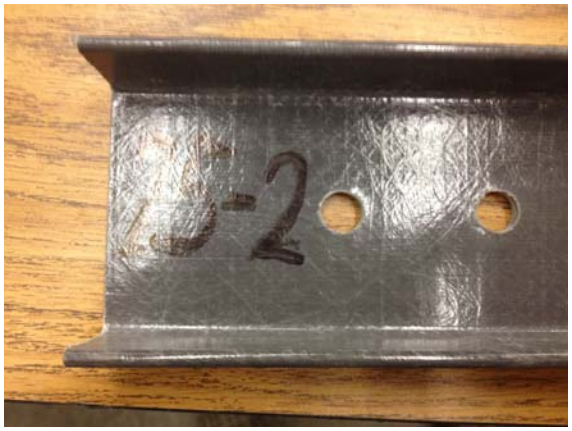

25% Load Level Damage

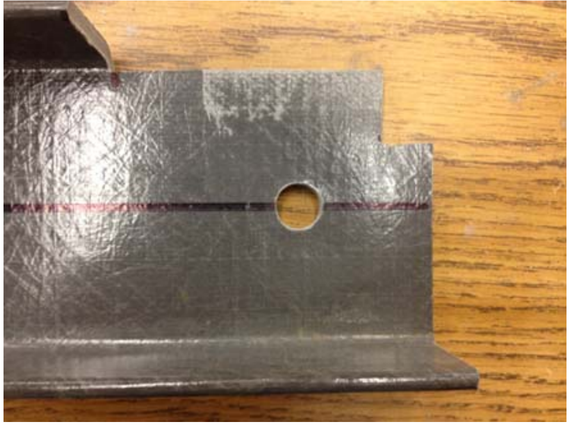

25% Load Level Damage

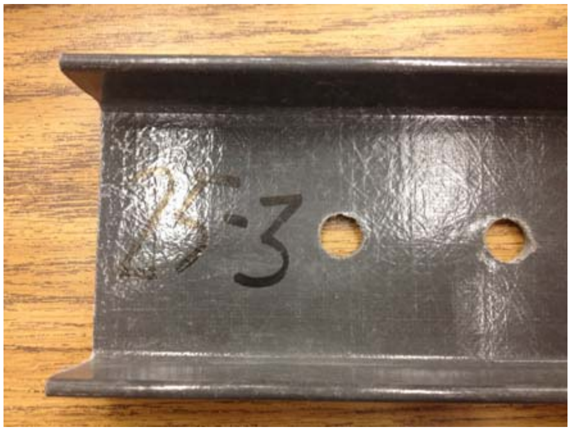

25% Load Level Damage

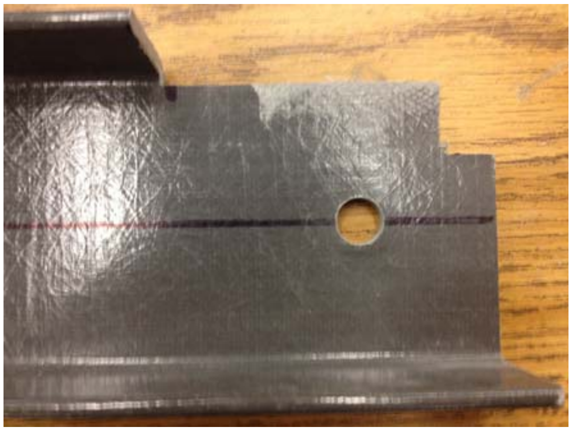

25% Load Level Damage

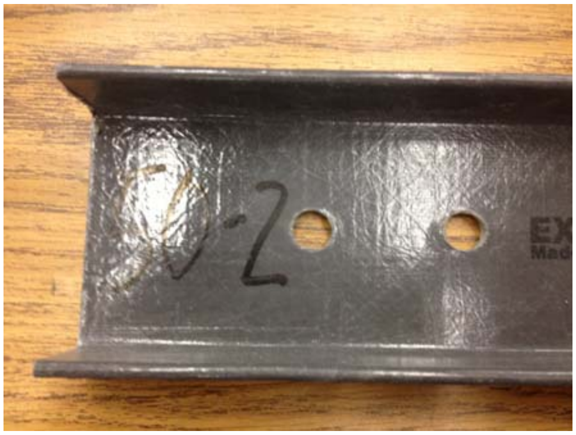

50% Load Level Damage

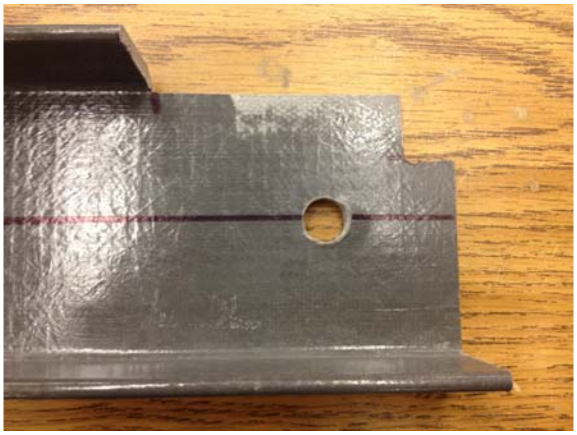

50% Load Level Damage

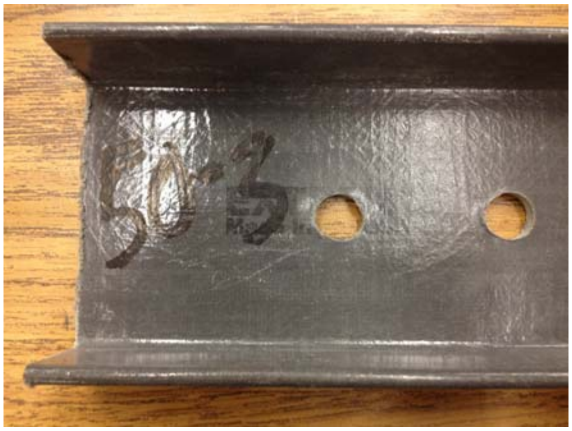

50% Load Level Damage

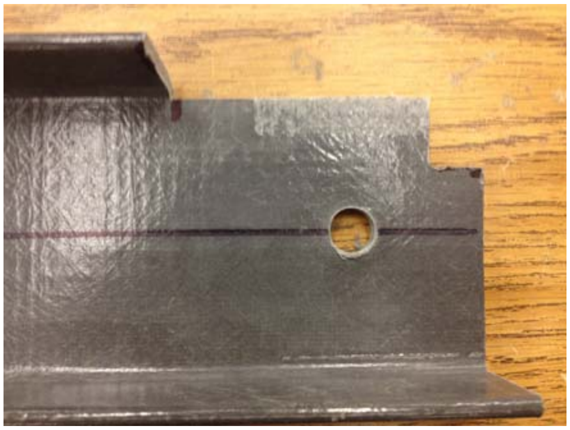

50% Load Level Damage

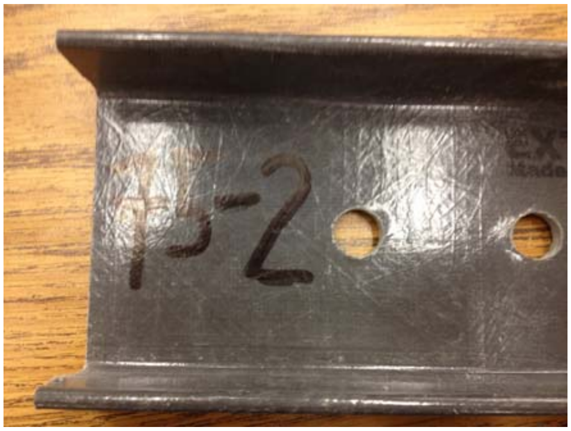

75% Load Level Damage

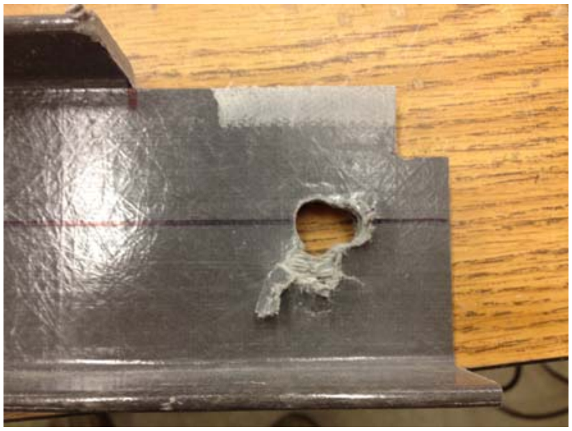

75% Load Level Damage

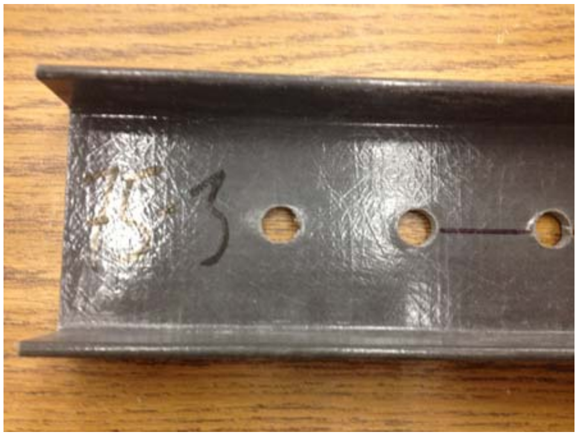

75% Load Level Damage

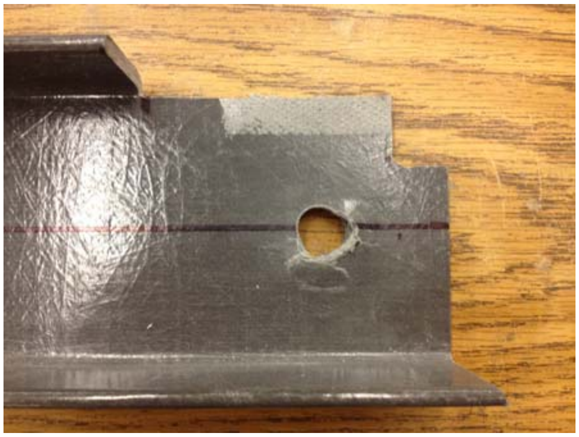

75% Load Level Damage

Appendix G. Phase III Testing Failure Photos

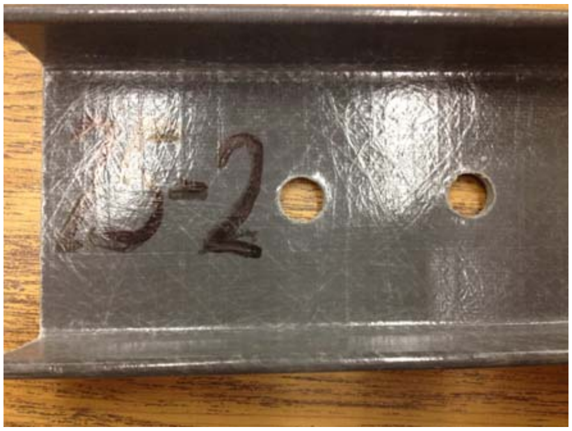

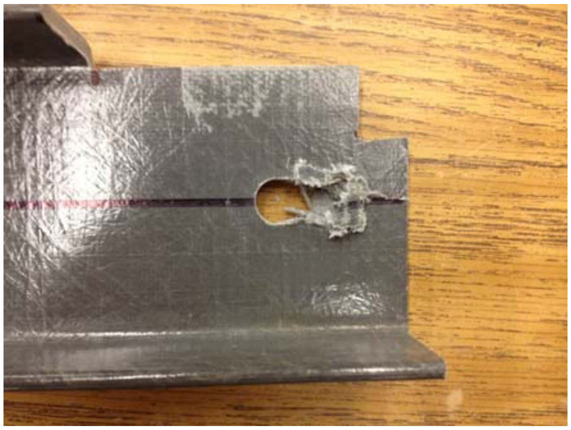

25% Load Level Failure

25% Load Level Failure

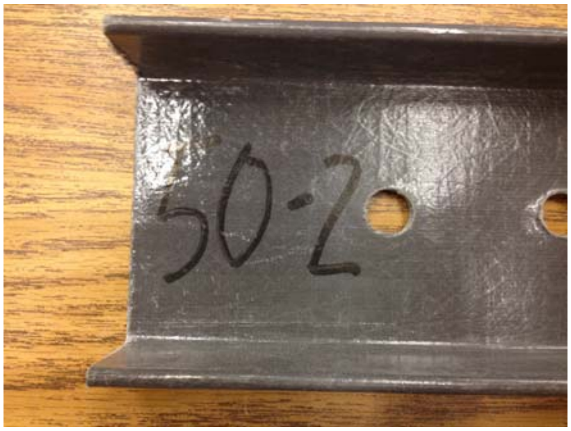

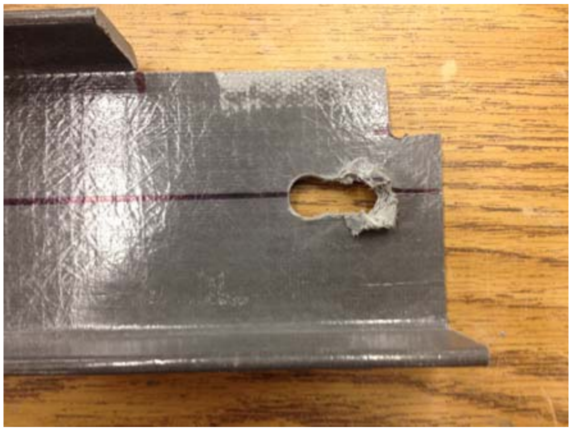

50% Load Level Failure

50% Load Level Failure

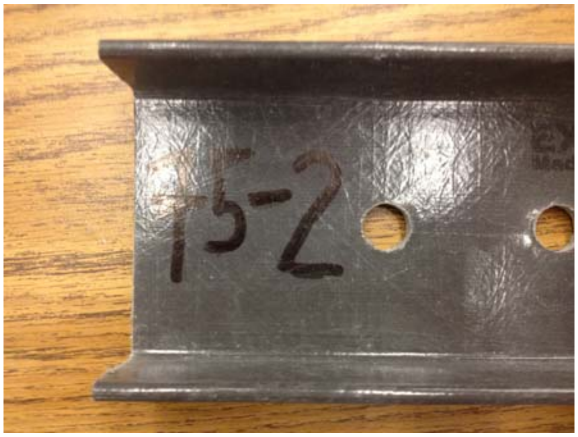

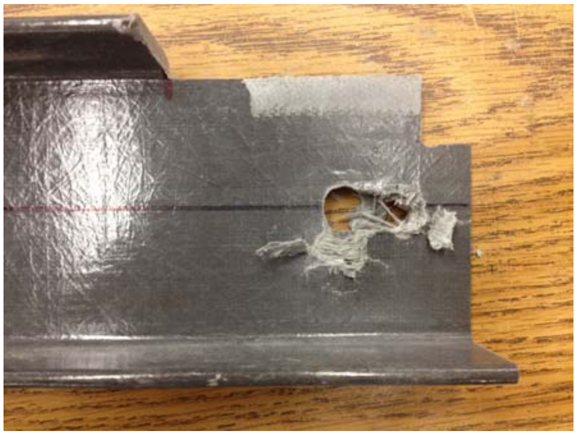

75% Load Level Failure

75% Load Level Failure

REFERENCES

Bank, L. (2006). *Composites for Construction*. John Wiley and Sons, Inc., Hoboken, New Jersey.

Barker, R.M., and Puckett, J.A. (1997). *Design of Highway Bridges based on AASHTO LRFD Bridge Design Specifications*. New York, NY, John Wiley & Sons, Inc.

Collins, T.A. (1977). "The Strength of Bolted Joints in Multi-Directional CFRP Laminates." *Composites,* 8(1), 43-55.

Collins, T.A. (1982). "On the Bearing Strength of Carbon Fibre-Reinforced Plastic Laminates." *Composites,* 13(3), 241-252.

Collins, T.A. (1987). "Experimentally Determined Strength of Mechanically Fastened Joints." *Joining of Fibre-reinforced Plastics,* ed. Matthews, F.L., Elsevier.

Deng, Q. (2004). *Three-Point Bending Fatigue Life for Unidirectional GFRP Beams.* Phd Dissertation, Southern Illinois University, Carbondale.

Devroye, L. (1986). *Non-Uniform Random Variate Generation.* New York, NY, Springer-Verlag.

Duthinh, D. (2000). *Connections of Fiber-Reinforced Polymer (FRP) Structural Members: A Review of the State of the Art,* Gaithersburg, MD, National Institute of Science and Technology.

GangaRao, V.S., and Nagaraj, V. (1997). "Static Behavior of Pultruded GFRP Beams." *J. Compos. Constr.,* 1, 120-129.

Garbo, S.P. and Ogonowski, J.M. (1981). AFWAL-TR-81-3041 Vol.1.

Godwin, E.W., Matthews, F.L. and Kilty, P.F. (1982). "Strength of Multi-Bolt Joints in GFP." *Composites,* 13(3), 268-272.

Hart-Smith, L.J. (1980). "Mechanically-Fastened Joints for Advanced Composites – Phenomenological Considerations and Simple Analyses." *Fibrous Composites in Structural Design,* ed. E. M. Lenoe, D.W. Oplinger and J.J. Burke, Plenum Press, New York.

Hassan, N., Mohamedien, M., and Rizkalla, S. (1997). "Multibolted Joints for GFRP Structural Members." *ASCE Journal of Composites for Construction,* 1, 3-9.

Ireman, T. (1998). "Three-Dimensional Stress Analysis of a Bolted Single-Lap Composite Joint.", *Composite Structures,* 43, 195-216.

Jones, R.M. (1975). *Mechanics of Composite Materials.* Hemisphere Publishing Corp., Bristol, Pa.

Kermanidis, T., Labeas, G., Tserpes, K.I., and Pantelakis, S. (2000). "Finite Element Modeling of Damage Accumulation in Bolted Composite Joints Under Incremental Tensile Loading." *European Congress on Computational Methods in Applied Sciences and Engineering, Barcelona,* 11-14.

Larsen, E.B. (2007). *Pressure Bag Molding: Manufacturing, Mechanical Testing, Non-Destructive Evaluation, and Analysis.* Master's Thesis, Montana State University, Bozeman.

Peimann, L.G. (1991). "Strength, Modulus of Elasticity, and Bond of Deformed FRP Rods." *Adv. Composites Mat. In Civ. Engrg. Struct., Proc., of the Specialty Conf., Mat. Engrg. Div.,* ASCE, 99-110.

Potter, R.T. (1978). "On the Mechanism of Tensile Fracture in Notched FRP." *Proc. R. Soc. London,* A361, 325-341.

Quinn, W.J. and Matthews, F.L. (1977). "Effect of Stacking Sequence on the Pin-Bearing Strength in Glass Fibre-Reinforced Plastics." *J. Composite Materials,* 11, 139-145.

Saadatmanesh, H., and Ehsani, M.R. (1991). "R/C Beams Strengthened with GFRP Plates: Experimental Study." *J. of Str. Engrg., ASCE,* 117(10), 3417-3433.

Shivakumar, K.N. and Crews, J.H. (1982). Tech. Memo 83268, Jan., NASA, Langley, Va., USA.

Shokrieh, M.M., Lessard, L.B. and Poon, C. (1996). "Three-Dimensional Progressive Failure Analysis of Pin/Bolt Loaded Composite Laminates." *Paper presented at the 83rd Meeting of the AGARD SMP on "Bolted Joints in Polymeric Composites", Florence, Italy.*

Tibbets, A. (2008). *Durable Fiber Reinforced Polymer Connections for Precast Concrete Structures.* Master's Thesis, University of Wisconsin, Madison.

Tsai, S., and Wu, E. (1971). "A General Theory of Strength of Anisotropic Materials." *Journal of Composite Materials,* 5, 58-80.

Kim, Y.J, Yoshitake, I., and Yang, M. (2013). "A Predictive Investigation Associated with Design Recommendations for CFRP-Confined Concrete in Aggressive Service Environments." *Construction and Building Materials,* 43, 69-79.